Carbon 201 (2023) 679–702

Contents lists available at ScienceDirect

Carbon

journal homepage: www.elsevier.com/locate/carbon

Advances of graphene-based aerogels and their modifications in lithium-sulfur batteries

Fail Sultanov [a,b], Almagul Mentbayeva [a,b,**], Sandugash Kalybekkyzy [a,b], Azhar Zhaisanova [a], Seung-Taek Myung [c,***], Zhumabay Bakenov [a,b,*]

[a] Department of Chemical and Materials Engineering, Nazarbayev University, Kabanbay Batyr Ave. 53, Astana, 010000, Kazakhstan
[b] National Laboratory Astana, Nazarbayev University, Kabanbay Batyr Ave. 53, Astana, 010000, Kazakhstan
[c] Department of Nano Technology and Advanced Materials Engineering, Sejong University, Gunjadong, Gwangjin-gu, Seoul, 05006, South Korea

ARTICLE INFO

Keywords:
Lithium-sulfur battery
Graphene aerogel
Charge capacity
Metal oxides and sulfides
Shuttle effect

ABSTRACT

Lithium-sulfur (Li–S) batteries are the current focus of attention as candidates for next-generation energy storage systems due to their high energy density, low cost and environmental friendliness. However, their commercialization is hampered by various issues, including poor electrical conductivity of sulfur and its reduction products, low utilization of active material, limited sulfur loading and severe lithium polysulfides (LiPSs) shuttling effect. To solve these problems, various 0D, 1D and 2D nanostructured carbon materials with developed surface morphology, electrochemical stability and electrical conductivity have been examined for immobilizing sulfur, mitigating its volume variation and enhancing its electrochemical kinetics. Here we review the recent progress in design and fabrication of carbon-based sulfur hosts, free-standing cathodes, interlayers and functional separators for Li–S batteries using 3D graphene networks presented by graphene aerogels (GAs). The main characteristics of GAs and their synthesis routes are overviewed first. Further, the fabrication of both conventional slurry-casted cathodes and binder and current collector-free self-supporting sulfur composite cathodes based on pure and modified GAs acting as highly porous matrix for sulfur are discussed. In-depth analysis of the mechanisms of electrochemical reactions depending on the modifier type are provided. The advances of modified GAs in the design and preparation of interlayers and functional separators for Li–S batteries are deliberated as well. Finally, the conclusion and perspectives for future development of 3D nanostructured carbons for Li–S battery technology are offered.

1. Introduction

The rechargeable Li-ion batteries (LIBs) have dominated the market for three decades in view of their high energy density, low self-discharge rate and long lifetime [1–3]. Nowadays charge storage capacity and energy density of LIBs are reaching their theoretical value, which is not enough to satisfy the performance demands of emerging portable electronics, advanced electric vehicles and other large-scale devices [4,5]. In search for other battery technologies with higher energy density and lower price, the attention of research community has focused on lithium-sulfur (Li–S) batteries, which have theoretical capacity of 1675 mAh g^{-1} and energy density of 2600 Wh kg^{-1} [6]. The advantage of using sulfur is also explained by its nontoxicity, abundance and low-cost.

The conventional Li–S cell consists of sulfur-based positive electrode, separator, liquid organic electrolyte and Li metal anode. The operating mechanism of Li–S batteries relies on a reversible redox reaction of sulfur, which has two electrons per one sulfur atom. During the discharge process, sulfur stepwise reduces to lithium sulfide, which includes complex structural and compositional evolutions. First, elemental sulfur is reduced to a long chain Li_2S_8, which is further reduced to Li_2S_6 and Li_2S_4 short chains. Then under liquid-solid two-phase reaction Li_2S_4 is reduced to solid Li_2S with further reduction to Li_2S. In the charge process, the Li_2S is reversibly oxidized into elemental sulfur in course of the lithium polysulfides (LiPSs) formation [6–9].

Regardless the advantages, for commercial application of Li–S batteries some inevitable challenges need to be solved. For instance,

* Corresponding author. Department of Chemical and Materials Engineering, Nazarbayev University, Kabanbay Batyr Ave. 53, Astana, 010000, Kazakhstan.
** Corresponding author. Department of Chemical and Materials Engineering, Nazarbayev University, Kabanbay Batyr Ave. 53, Astana, 010000, Kazakhstan.
*** Corresponding author.
E-mail addresses: almagul.mentbayeva@nu.edu.kz (A. Mentbayeva), smyung@sejong.ac.kr (S.-T. Myung), zbakenov@nu.edu.kz (Z. Bakenov).

https://doi.org/10.1016/j.carbon.2022.09.069
Received 5 July 2022; Received in revised form 22 September 2022; Accepted 25 September 2022
Available online 28 September 2022

naturally sulfur is a poor conductor (5×10^{-30} S cm^{-1}) with insulating discharge products (Li_2S_2 or Li_2S), which together result in the increase of battery resistance and low electrochemical performance. In addition, the density difference of Li_2S and sulfur (1.66 and 2.07 g cm^{-3}, respectively) leads to the increase in the volume of about 80% during conversion of sulfur to Li_2S [10–12]. Large volume expansion results in the damage of electrode's structure, fast capacity fading and the other issues related to the safety [13–16]. What is more, the produced LiPSs are highly soluble in organic electrolyte, which results in so-called "shuttle" effect. The dissolution of LiPSs in the electrolyte and their shuttle contributes to an irreversible sulfur lost, leading to a rapid capacity decay and low Coulombic efficiency of the cell. At the same time, insoluble Li_2S_2 and Li_2S can also deposit on the surface of a negative electrode, promoting the loss in active material, increase of polarization, lower Coulombic efficiency and cycling stability [17–20].

To overcome these issues, the mixing of sulfur with carbonaceous materials has become of a great interest after the pioneering work by Nazar's group in which the mesoporous carbon (CMK-3) was applied as a sulfur host for Li–S batteries [21]. Inspired by this, a variety of nano-carbons, such as carbon spheres [22], mesoporous carbon [23,24], graphene [25,26], CNTs [27] and carbon nanofibers [28–30] were examined as a sulfur host. However, the low polarity of carbon with weak affinity to polar LiPSs resulted in ineffective suppression of the shuttle effect, leading to insufficient cycling stability of the batteries [31]. Further, the functionalization and heteroatom doping of carbon materials were reported to be beneficial for improving their ability to chemically adsorb the LiPSs [32–34]. Additionally, due to their intrinsic capability for LiPSs adsorption, polar metal oxides [35–39], metal sulfides [40–43], metal nitrides [44–46], metal phosphides [47] and metal carbides [48] were utilized as a host for sulfur. However, the poor electronic and ionic conductivities of these polar metallic compounds resulted in low rate performance and low sulfur utilization.

A number of research articles have been published on the use of graphene aerogels (GAs) and their various modifications in Li–S batteries. GAs were utilized as a host for sulfur, support for free-standing cathodes, interlayers and separator modifiers demonstrating that their 3D interconnected meso- and microporous structure is of advantage due to such remarkable properties as lightweight, high specific surface area, outstanding mechanical characteristics and high electrical conductivity. Aerogels represent a class of porous materials in which the liquid phase is replaced by gaseous using specific drying methods [49,50]. GAs are composed of graphene sheets acting as a major building blocks to form 3D highly porous intimately linked network with high specific surface area and pore volume, and good thermal and electrical conductivity [51–54]. This surface can serve as a matrix for uniform sulfur immobilization with increased sulfur amount, suppressing the LiPSs shuttle effect and buffering the cell's volume expansion during continuous cycling.

Despite such advantages of the use of GAs in Li–S batteries and numerous works published, the literature survey shows that there are no review articles in this direction. Considering tremendous efforts and active research for progress in the Li–S battery technology, a systematic comparison of methods and materials, and analysis of the state of the art in this field is required. This encouraged us to work on the current review, which outlines the major developments in using GAs and their modifications (heteroatom-doping, CNTs and porous carbons, metal-containing compounds and other components addition) both in constructing conductive host for sulfur using conventional slurry-casting method and in the design of free-standing sulfur containing cathodes with no binder and without use of a current collector. Moreover, the features of using modified GAs in creation of interlayers and functional separators for Li–S batteries are also presented (Fig. 1). Finally, the summary and future perspectives of development of Li–S batteries and the promises of GAs utilization in their design are offered.

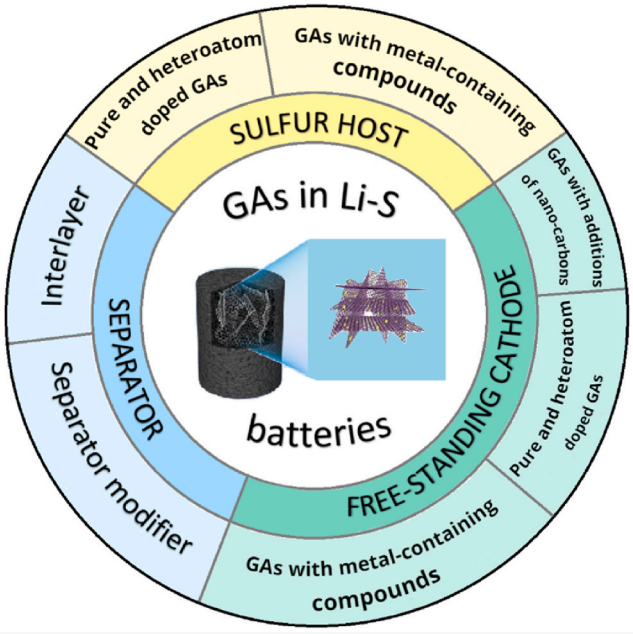

Fig. 1. Schematic illustration of the GAs modifications used in Li–S batteries.

2. Synthesis and characterization of GAs

Graphene composed of flat monolayers of carbon packed in the 2D hexagonal lattice with sp^2 hybridization attracts much attention since 2004 owing to its superior mechanical, thermal and electrical properties [55]. It is recognized as the lightest and thinnest known material with a zero bandgap, ultrahigh Young's modulus and flexibility, optical transmittance of around 98% and high theoretical surface area (2630 m^2/g) [56]. Owing to its unique properties graphene found application in various fields, including electronics [57], photonics [58], energy storage and conversion [59], sensors [60], bio-application [61], microwave adsorption [62,63], catalysis [64], photo-catalysis [65] and environment [66]. Graphene is recognized as an excellent material for preparation of cathodes for Li–S batteries providing high surface area, porous and electrically conductive matrix for immobilization of large sulfur amount and suppression of the LiPSs shuttle effect due to physical and chemical interaction with LiPSs [67]. However, despite the undeniable advantages of using 2D graphene in Li–S battery technology, researchers are still concerned about low trapping ability of the 2D graphene sheets to LiPSs due to its open structure, agglomeration tendency resulting in reduction of the specific surface area and dielectric constant and increase in the interface polarization and π-electron stacking on the basal plane which is not electrochemically active, thus making charge transfer not favorable [68]. In order to exploit all properties of graphene to a larger extent the attention was paid to convert 2D structure of graphene into 3D. The gelation ability of GO made it promising material to be used as an unique molecular building block toward the construction of macroscopic 3D monoliths widely recognized as GAs, expanding the graphene's application [69–72].

GAs are presented by a 3D structure composed of graphene sheets with porosity of up to 99.8%. They integrate the outstanding properties of discrete graphene sheets with the unique properties of porous materials, such as high specific surface area, ultra-light weight, hierarchical microporous structure, excellent mechanical properties and electrical conductivity [73]. The major point in fabrication of the GAs is the choice of the applied approach for drying rGO based hydrogels to achieve porous 3D network without structural collapse. Conventionally, two major techniques are used: freeze-drying and drying in supercritical CO_2. As reported, by varying rGO hydrogel drying methods different type of porosity could be obtained in the resulting aerogel. For instance,

during supercritical CO_2 drying the higher amount of macropores are formed, while freeze-drying leads to formation of aerogels's pronounced mesoporosity [74].

A number of review articles [50,56,63,69,75,76] were published to date discussing the major characteristics and synthesis methods for GAs. Despite on that, in this section of the review article the most common and efficient techniques for GAs preparation are briefly outlined and discussed. Hydrothermal synthesis is recognized as one of the promising technique for GAs preparation which is mainly based on the interaction of chemicals in sealed systems in aqueous state at the temperature above 120 °C and pressure above 1 atm through physical-chemical processes. During hydrothermal synthesis a range of chemicals can be used to modify the structure and chemical composition of the aerogel. Xu et al. [77] first developed one step hydrothermal process to form self-assembled graphene based hydrogel (Fig. 2 a-c). As revealed, the GO concentration is an important factor affecting morphology and other properties of GAs. They demonstrated that at lower concentrations of GO (2 mg ml^{-1}) the resulting aerogel exhibited strong mechanical properties, electrical conductivity, thermal stability and high specific capacity. Wan et al. [78] investigated the effects of different reducing agents (ammonia, ethylenediamine (EDA) and vitamin C), hydrothermal temperatures and reaction time on the density, specific surface area, mechanical properties and morphology of the fabricated GAs. As a result, GAs reduced by ammonia exhibited the lowest density and highest specific surface area, but reveals the worst mechanical characteristics (Fig. 2 d). GAs reduced by vitamin C delivered the strongest hydrophobicity due to elimination of the hydrophilic functional groups under influence of temperature. With the increase in the hydrothermal reaction time, the GO reduction degree increases leading to strong hydrophobicity, high elastic modulus and improved electrical conductivity of GAs.

Compared to hydrothermal method the chemical reduction method is conventionally conducted at lower temperature (below 100 °C) and under atmospheric pressure. Chemical reduction is usually conducted with the use of various reducing agents such as $NaHSO_3$ [79], ethylene diamine tetraacetic acid (EDTA) [80], ethylenediamine (EDA) [81], ascorbic acid [82], hexamethylenetetramine (HMTA) [83], hydrogen iodide (HI) [84], etc. With the reaction temperature of 80 °C under atmospheric conditions, sheets of GO are reduced with improvement of the hydrophobicity and π-π interaction between them. As a result of the synergistic effect of aggregation and steric hindrance of graphene sheets 3D graphene hydrogel can be formed. The self-assembly process can be controlled by tuning the concentration of the GO and reducing agents dispersed in solution. Yan et al. [85] demonstrated the preparation of

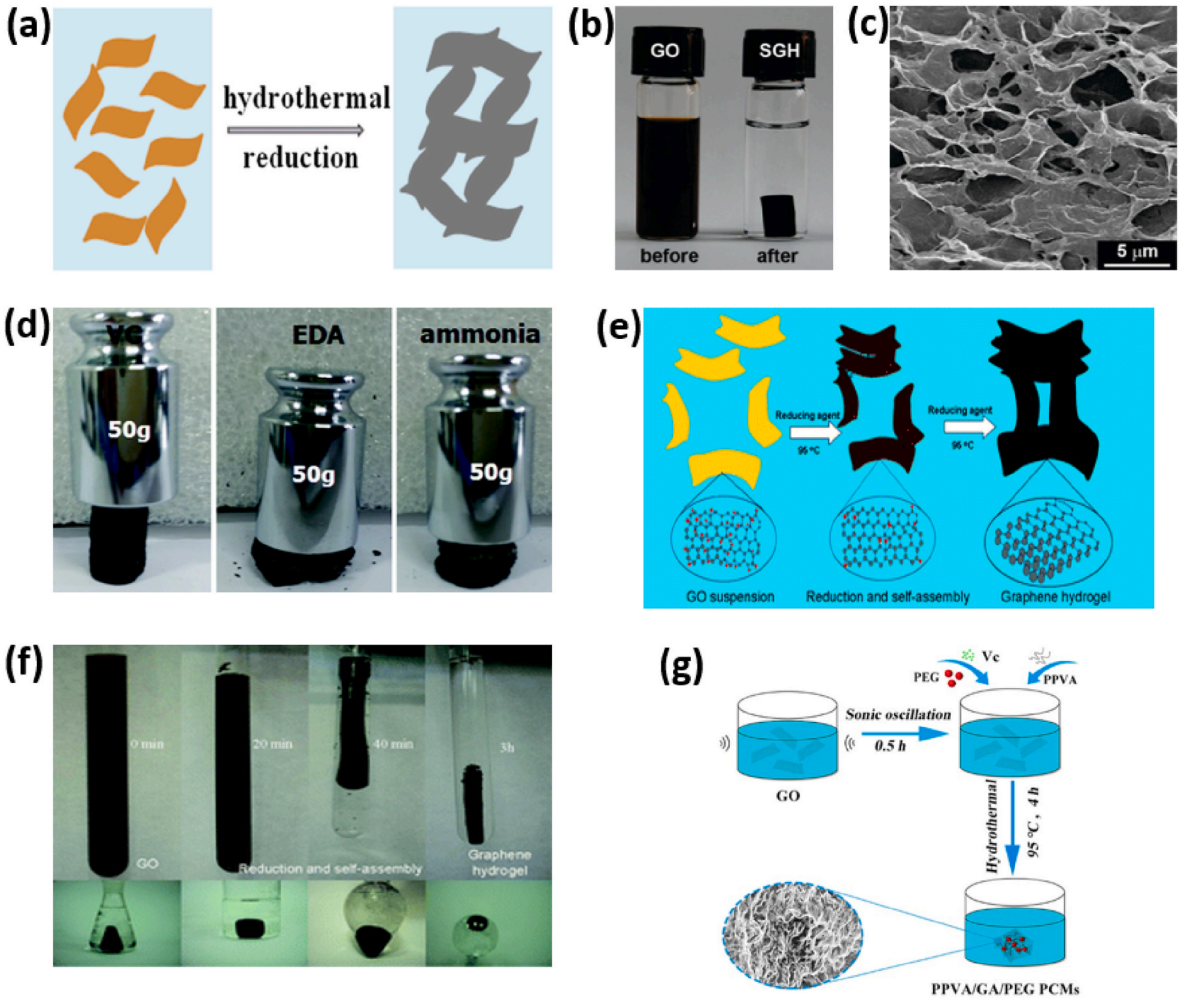

Fig. 2. (a) Mechanism of hydrothermal GAs formation, (b) Photographs of a 2 mg/mL homogeneous GO aqueous dispersion before and after hydrothermal reduction at 180 °C for 12 h, (c) SEM images of GAs microstructure. Reprinted with permission from [77], Copyright ACS Publications 2010. (d) The mechanical strength of the prepared GAs. Reprinted with permission from [78], Copyright RSC 2016. (e) The proposed self-assembly mechanism for graphene hydrogel formation during the chemical reduction of GO in an aqueous suspension. (f) The formation process of the graphene hydrogel from an aqueous GO suspension (1.5 mg ml^{-1}) via a one-step self-assembly of graphene. Reprinted with permission from [85], RSC Publishing 2011. (g) Scheme of fabrication GAs with PVA via cross-linking method. Reprinted with permission from [86], Copyright Elsevier 2019.

GAs by simple mild chemical reaction at 95 °C under atmospheric pressure using $NaHSO_3$, Na_2S, vitamin C, HI and hydroquinone as chemical reducers for GO (Fig. 2 e). The resulting 3D graphene-based architectures demonstrated low density, strong mechanical properties, thermal stability, high electrical conductivity and high specific capacitance. What is more, the shape of the GAs can be simply controlled by the type of the reactor in which the chemical reduction of GO is performed (Fig. 2 f).

A severe collapse or deformation of 3D porous network of GA may happen since the sheets of graphene in its structure are linked by weak electrostatic interaction, hydrogen bonding and π-π interaction. In this regard, chemical cross-linking can significantly improve the mechanical stability of GAs through formation of a strong covalent bonds. In cross-linking method two well-known approaches are widely used: hydrogen bonding and multi-valent metal ions utilization. In hydrogen bonding based cross-linking technology several cross-linkers are widely applied: hydroxyl-containing PVA [86] (Fig. 2 g), oxygen containing hydroxypropyl cellulose [87], polyethylene oxide [88], and nitrogen functional groups containing compounds (EDA, polyamines) [88]. These materials create hydrogen bonds and provide stronger bonding force within the gelation process. The multi-valent metal ions approach involves the use of metal ions (for ex. Ca^{2+}, Mg^{2+}, Cu^{2+}, Pb^{2+}, Cr^{3+}, Fe^{3+}) which improve the GO gelation process by a bonding force [89]. Additionally, the sol-gel method allows to obtain stronger bonding between GO sheets due to formation of covalent bonds during polymerization. Generally, sol-gel method includes the following steps: hydrolysis, condensation and polymerization of monomers with formation of chains with their further growth, agglomeration of the polymer structures and formation the networks. This method was applied for the first time by Worsley et al. [90]. They used resorcinol and formaldehyde with sodium carbonate added to the GO dispersion to fabricate GA. The resulting GA exhibited improved electrical conductivity, large surface area and pore volume.

3D printing is a technology for directly fabrication 3D structures by stacking layers of materials in order. GAs fabricated by 3D printing achieve controllable porous structure and mass production. For GA 3D printing the GO dispersion of a specific viscosity is used which is usually achieved by addition of polymers and SiO_2 [91]. Zhang et al. [92] fabricated GA by combining 3D printing and freeze-casting approach. The aqueous GO ink was ejected and freeze-cast into the designed 3D structures. The fabricated lightweight 3D printed GA presented superelastic properties and high electrical conductivity. In its turn 3D printing is divided to direct print writing and stereolitography.

The other approaches for GAs fabrication belong to the so-called template methods which include chemical vapor deposition, template-directed self-assembly and reduction, ice-template method, bubble template-method, etc. Despite on a such variety of the GAs synthesis methods, the literature survey on the utilization of GAs in Li–S battery demonstrated that hydrothermal, chemical reduction, cross-linking and sol-gel methods are more preferred since they are relatively fast and low-cost and do not require specific equipment. These methods allow to obtain the modified GAs with developed surface area, tuned porosity, improved mechanical characteristics and superior electrical conductivity in one step process. The fabricated by these methods GAs are able to provide highly conductive network for charge transfer in sulfur cathodes, flexible space for accommodation of volume expansion during continuous cycling and highly porous morphology to immobilize sulfur and its species.

3. GAs as a host material and free-standing cathodes

3.1. Pure GAs

3D structure of GAs is recognized as an efficient sulfur host since it is able to provide highly conductive network for the transfer of charge with a flexible and porous structure to accommodate the volume expansion of the Li–S cell during cycling and to immobilize and physically capture the LiPSs. Inspired by this, Zhou et al. [93] demonstrated the preparation of S@FD-rGO composite by thermal heating a mixture of sulfur and GO via one-step solid-state method. According to the presented XPS analysis, the S@FD-rGO composite displayed five major peaks, corresponding to C–C/C=O (284.6 eV), C–S (285.4 eV), C–O (286.4 eV), C=O (287.1 eV) and O–C=O (289 eV) bonding [94]. As revealed, the sample was characterized by 71.9% amount of C–C and C–S bonding. The successful sulfur loading to GA network was confirmed by the presence of S $2p_{3/2}$ peak at 163.7 eV, corresponding to the chemical bonding between them (Fig. 3 a) [94]. Additional peaks at 164.3 and 165.5 eV were attributed to the S–O bonding. The slurry-casted on Al foil cathode delivered the initial discharge capacity of 792 mAh g^{-1} with further increase to 880 mAh g^{-1} until the 3rd cycle at 180 mA g^{-1}. After 200 cycles it maintained the capacity of 384 mAh g^{-1}. Despite the moderate electrochemical characteristics, this early study was important to demonstrate the promise of using GAs as a flexible and electrically conductive matrix for sulfur immobilization due to the strong interaction of sulfur and rGO, which is beneficial for reduction of the cell's volume expansion during cycling and eventually decrease the sulfur aggregation. Further Zhang et al. [95] demonstrated that 3D rGO in the form of aerogel exhibits significantly improved discharge capacity and cycling stability compared to the regular 2D sulfur loaded rGO (Fig. 3 b). The 3D spherical carbon layers in 3D-S-rGO cathode are able to accommodate higher amounts of sulfur and Li ions and buffer the cell's volume expansion/shrinkage caused by Li intercalation/deintercalation during cycling, thus protecting the structural integrity of the cathode (Fig. 3 c). As a result, the slurry-casted 3D-S-rGO cathode delivered high initial discharge capacity of 1140 mAh g^{-1} at 0.2C and maintained 790 mAh g^{-1} after 200 cycles at the sulfur content of 75.8%.

Currently, the requirements for flexibility, low thickness and lightweight of cathodes for Li–S batteries have increased [96]. The conventional cathodes obtained by slurry-casting method include the use of metal current collector, which is usually aluminum foil, and binders, which together contribute to the final weight and the total price of the battery. The exclusion of binder in cathodes is favorable, since it is not an active material and may cause pore blocking, thus decreasing the electric conductivity [97]. Therefore, the formation of free-standing cathodes without binders and collectors is of a great interest. Free-standing cathodes are mainly fabricated from carbon foams [98], GAs [99], carbon nanotube paper [100] and carbon nanofibers [101]. The advantages of using GAs as a matrix for free-standing sulfur-based cathodes are mainly attributed to their outstanding mechanical properties, hierarchical porous structure with micro- meso- and macropores and the ability to be modified by various additives during the one-stage hydrothermal synthesis [102,103]. In this regard, Jiang et al. [104] have demonstrated the facile one step synthesis of self-supporting electrode based on GA and S. The GA-S composite was hydrothermally obtained by mixing the GO suspension with S/CS_2 solution, which was then heated to 120, 150 and 180 °C for 12 h. As revealed, the GA/S composite heated at 180 °C demonstrated the uniformly dispersed sulfur particles of 5 nm in size over graphene matrix. The formation of a nanometer sized sulfur crystals with low degree of aggregation is caused by the synergistic effect of existing oxygen-containing groups on the GO sheets, which play a major role in sulfur immobilization and prevention of the formation of its larger sized particles, while the high temperature favors the higher amount of sulfur-oxygen-containing functional bonding, which was confirmed by the much stronger C–O–S bonding of sulfur and graphene prepared at high temperature. The GA-S-180 delivered the initial discharge capacity of 1351.3 mAh g^{-1} at 100 mA g^{-1} and specific capacity of 716.2 mAh g^{-1} after 50 cycles at 100 mA g^{-1}.

Li et al. [105] demonstrated the preparation of GA with immobilized sulfur particles by a modified two-step hydrothermal reduction and freeze-drying methods. Opposite to [104], the researchers [105] used $Na_2S_2O_3$ as a source for sulfur which was immobilized into the GAs

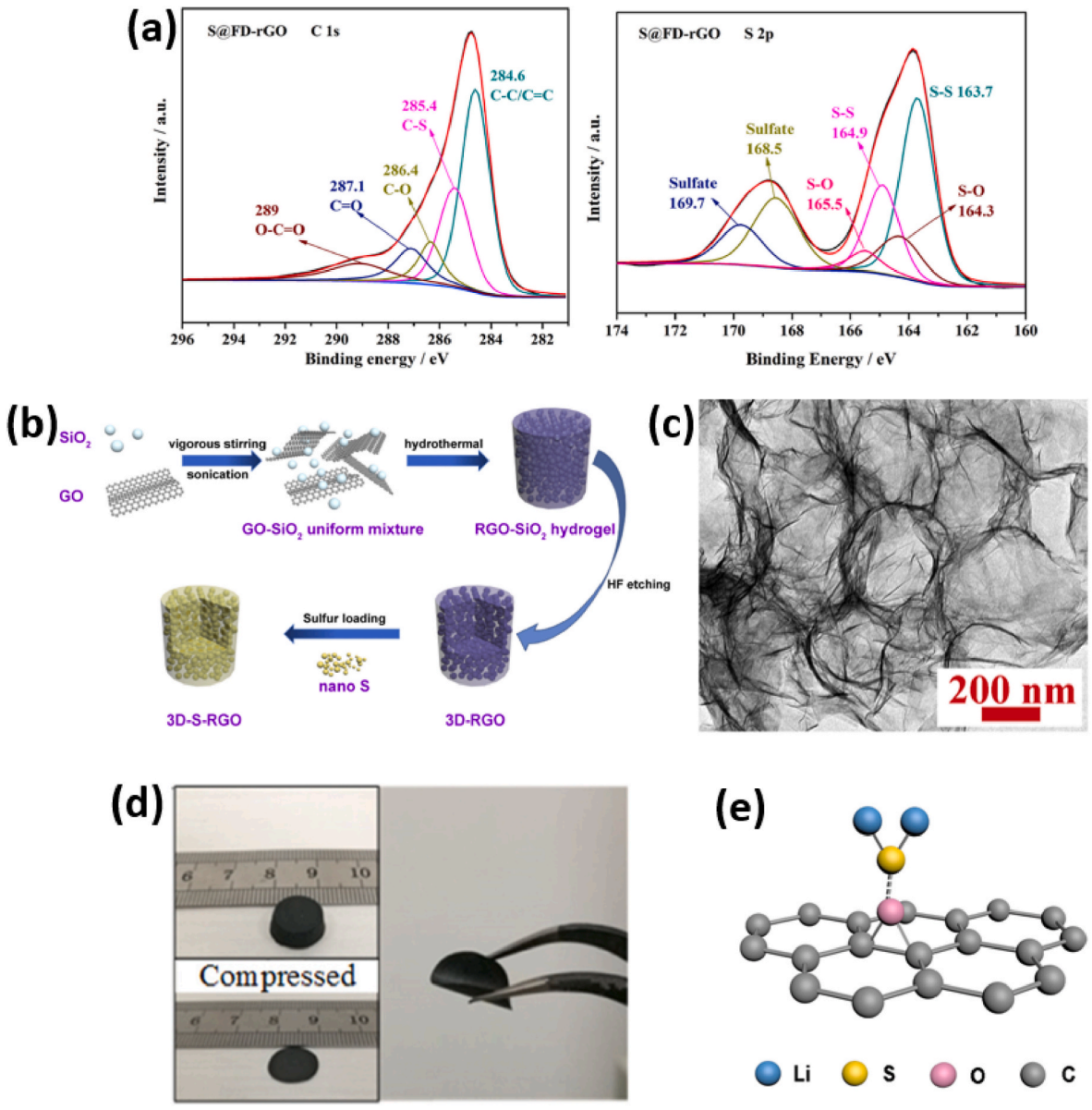

Fig. 3. (a) C 1 s and S 2p XPS spectra of S@FD-rGO. Reprinted with permission from [93], Copyright Elsevier 2016. (b) Schematic illustration for the synthesis of 3D-S-RGO, (c) TEM image of 3D-rGO aerogel. Reprinted with permission from [95], Copyright Elsevier 2018. (d) Digital images of the flexible S/GA cathode. Reprinted with permission from [105], Copyright Elsevier 2018. (e) Schematic illustrating a C–O–S chemical bond interaction between Li_2S and epoxide groups of graphene. Reprinted with permission from [106], Copyright Elsevier 2018.

structure to form a free-standing cathode (Fig. 3 d). In general, the specific amounts of GO and $Na_2S_2O_3$ were dispersed in DI water with addition of 1 M HCl and reducing agent (ascorbic acid), heated at 95 °C for 30 min with the following cooling the dispersion and reheated one more time for next 5 h. The careful control of the reduction time and temperature, as well as applying the ice-casting approach resulted in pronounced microporosity of the resulting S/GA sample. The GA provided tunable electrically conductive porous network which is favorable for more uniform dispersion of sulfur and reaching the higher sulfur loading. Moreover, the GA's folded structure operated as a coating shield for sulfur particles that hinder the LiPSs dissolution. Correspondingly, the specific capacity of higher than 1100 mAh g^{-1} and areal capacity of more than 3 mAh cm^{-2} were delivered by the S/GA free-standing cathode, while the reversible capacity was found to be more than 500 mAh g^{-1} after 60 cycles at 0.1C at 62% sulfur content and 2.5 mg cm^{-2} areal sulfur loading.

The approach of using the dissolved LiPSs as a catholyte instead of solid sulfur for homogeneous sulfur deposition on a carbon matrix is also widely applied in Li–S battery technology [107,108]. The use of catholyte is favorable for increasing the loading and facilitating the electrolyte diffusion rate [109]. Li_2S_n (n = 6, 8) is widely used as a catholyte due to many reasons, among which are less lithium dendrite formation, higher Coulombic efficiency [110] and rate capability [111] and complete sulfur utilization [112]. As reported [113,114], the dissolved LiPSs provide both the active material and Li conductance in electrolyte medium. Considering that, Cavallo et al. [115] proposed the mild GO reduction using L-ascorbic acid catalyzed with HCl during GA hydrothermal synthesis with further Li_2S_8 catholyte deposition on the separator and as-prepared rGA disc accounting 3.26 mg cm^{-2} overall areal sulfur loading. The mesoporous GA/S demonstrated the areal capacity of 3.4 mAh cm^{-2} with retention of 85% over 350 cycles. The achieved excellent electrochemical performance is mainly associated with the high specific surface area and porous structure of reduced GAs, which grant the larger catholyte uptake and intensify the reversible

electrochemical reaction with fast kinetics. The rGO surface oxygens act as a LiPSs interaction points, reducing the shuttle effect, while the presence of dissolved LiPSs in the electrolyte buffers their migration from rGO and provides Li^+ conduction.

Application of Li_2S with a theoretical capacity of 1166 mAh g^{-1} as a cathode material in Li–S batteries is also a promising strategy for improvement of electrochemical performance. As known, Li_2S exists in a maximum volume state compared to sulfur-based cathode excluding the issues related to cell's volume expansion during long-term cycling. However, Li_2S has a poor electrical and ionic conductivities encouraging scientists to design the composite based on Li_2S with various conductive additives [116,117]. The literature survey revealed that most of the studies on preparation of Li_2S/carbon composites are based on simple physical mixing of Li_2S with carbon [118–120]. Consequently, the resulting particle size of Li_2S is too large and their distribution is not homogeneous, together leading to a large barrier during initial charge and severe shuttle effect. A high potential barrier (about 1.0 V) appears during initial charging which is ascribed to the direct conversion of Li_2S to sulfur [121]. Evidently, the reduction of the Li_2S particle size and improvement of its uniform distribution over electrically conductive carbonaceous network is rather efficient approach to lower the potential barrier [122,123]. Additionally, Li_2S particles with decreased size are able to more effectively bond to graphene surface and therefore more significant suppress the shuttle effect. With this in mind, Wang et al. [106] have demonstrated the chemical in-situ lithiation of hydrothermally prepared nano-S/GA composite with the use of lithium triethylborohydride in tetrahydrofuran as lithium source. The in-situ lithiated Li_2S/GA sample is characterized by porous structure with 10 nm L_2S particles which are homogeneously distributed over graphene surface. As a result of chemical lithiation, the C–O–S chemical bonding is retained between Li_2S and graphene, and large amount of H_2 released during the synthesis generated the numerous pores in the GA structure. This provided the increased surface area and high rate of lithium ions transport, as well as the higher accommodation of Li_2S particles, thus more efficiently alleviating the shuttle effect. Therefore, the initial discharge capacity of in-situ lithiated free-standing nano-Li_2S/GA reached 838.5 mAh g^{-1} at 0.1C and after 100 cycles it reduced to 462.8 mAh g^{-1} with a capacity retention rate of 55.2%. Comparingly, these values for ex-situ lithiated Li_2S/GA were 760.2 mAh g^{-1} and 182.0 mAh g^{-1}, respectively (23.9% of capacity retention).

In summary, the lightweight, porous and electrically conductive structure of GAs serves as an excellent matrix for fabrication of sulfur-based cathodes with high sulfur loading and strong confining of LiPSs due to tailored microporosity. The synergistic effect of existing pores and high conductive paths facilitate the electrochemical reaction between Li ions and sulfur species. The intrinsic surface polar oxygen groups of GO minimize the LiPSs shuttle effect and stabilize the cycling capacity of cathodes. Sulfur can be immobilized into the GA in one step during their hydrothermal synthesis, as well as by other approaches, like dissolving sulfur in CS_2 or other organic solvents, via chemical precipitation of sulfur using $Na_2S_2O_3$ as a source or by using catholytes or Li_2S. Moreover, the outstanding mechanical properties of GAs allow to fabricate frees-standing cathodes for Li–S batteries which is a promising alternative to the conventional slurry-casted cathodes.

3.2. Heteroatom doped GAs

Doping of graphene by heteroatoms is an efficient technique to design the structures capable of trapping LiPSs and improve the chemical binding of sulfur and its species to the carbon host, which is vital for elimination of shuttle effect [124–129]. To ensure the strong binding of carbon host to LiPSs, the requirement for Lewis base interaction with the Lewis acidic LiPSs can be fulfilled by the existence of lone pair electron of the doping atom. The doping atom's electronegativity must be higher than that for carbon atom to provide a constant dipole moment at the local doping site. In order to facilitate the electrostatic dipole-dipole interaction over the Li-doping atom bond, the atomic radii of the dopant atom should be small enough to pair with Li. Additionally, the bond between atoms of carbon and dopant must be stable enough to avoid the irreversible reaction with Li_2S_4. The doping atom should form a π-bond with a conjugated system and be capable of accepting the additional charge from the π-electrons [130]. Considering that, among the various carbon dopants (N, O, B, F, S, P, Cl) nitrogen (N) atom is known to be a more promising to suppress the LiPSs shuttle effect due to abundant extra pair of electrons. These electrons allow nitrogen atom to act as an electron-rich donor playing a role of a Lewis-base sites interacting with the terminal atoms of Li in LiPSs via dipole-dipole electrostatic forces. In addition, N-doping is also favorable for improvement of carbon's surface polarity, wettability and electrical conductivity [131–133]. As literature survey reveals, ammonium persulfate, thiourea, hydrazine hydrate, and organic amines are widely used for GAs nitrogen doping [33,134,135]. Kang et al. [136] demonstrated that ethylenediamine (EDA) can be used both as a nitrogen source and a structural modifier for rGO based hydrogels, which further acted as a conductive network for sulfur immobilization (Fig. 4 a). They demonstrated that significant amount of loaded sulfur (77 wt%) remained in the NGAs pores, providing open channels for electrolyte access and minimizing the sulfur volume changes during charge/discharge cycling. As reported, the NGA-S composites delivered a high initial discharge capacity of 1258 mAh g^{-1} at 0.1C, which remained 1077 mAh g^{-1} after 75 cycles. Further, Cheng et al. [137] have synthesized 3D porous nitrogen doped graphene (3D-PNG) by hydrothermal method using urea as a source of nitrogen and self-removable template for optimized pore structure (Fig. 4 b). The electrodes based on 3D-PNG/S exhibited higher utilization of sulfur with the initial discharge capacity of 1311 mAh g^{-1} at 0.2C and outstanding cycling stability of 714 mAh g^{-1} at 1.5 mA cm^{-1} after 400 cycles for a sample with 4 mg cm^{-2} areal sulfur loading. The outstanding electrochemical performance of N-doped GAs can be explained by the multiscale (micro and nano) well-designed structure with high specific surface area and improved polarity affording the excellent ability to deliver electrons. 3D interconnected macropores also act as an effective reservoir for electrolyte and ion transport channels, thus promoting the rapid ion transfer within composite electrolyte, while graphene surface ensures sulfur deposition and formation of self-supporting structure. In addition, N-doping along with the GA's high surface area and graphene wrapped nanopore structure create a synergistic effect of LiPSs confining under the action of chemical adsorption and physical trapping (Fig. 4 c).

Jia et al. [138] conducted a comprehensive research on the influence of the nature of N-dopants for GAs on the electrochemical performance of GA-based sulfur cathodes. EDA, urea and ammonia were studied as sources of nitrogen during hydrothermal synthesis of GAs. Based on the results of N 1s XPS analysis (Fig. 4 d), three major peaks were observed for the N-doped GAs: pyrrolic-N (399.7–399.9 eV), pyridinic-N (398.5–398.7 eV) and graphitic-N peak (401.1–401.6 eV) [139]. The proportion of the pyrrolic-N and pyridinic-N peaks for the aerogel reduced by EDA was much higher than that for aerogels reduced with urea and ammonia, which resulted in its better electrochemical performance. The sulfur/aerogel cathode reduced by EDA delivered 1210.7 mAh g^{-1} initial discharge capacity at 0.1C and retained 876.4 mAh g^{-1} after 50 cycles, while the sample reduced with ammonia delivered capacities of 1104.7 mAh g^{-1} and 537.9 mAh g^{-1}, respectively. An improved electrochemical performance of NGA/S reduced with EDA is mainly attributed to the uniform nitrogen distribution and higher proportion of pyridinic-N, which has a stronger binding energy to LiPSs. As known, pyridinic-N is a nitrogen atom that substitutes one carbon atom in graphene hexagonal ring at the edge and forms chemical bonds with two carbon atoms, contributing a pair of orphan electrons, which have a strong binding to LiPSs [140]. Additionally, the use of nano-sulfur with increased area of contact with a carbon-based matrix and electrolyte resulted in a significant improvement of the charge transport, lithium ion diffusion, as well as the active material utilization and rate

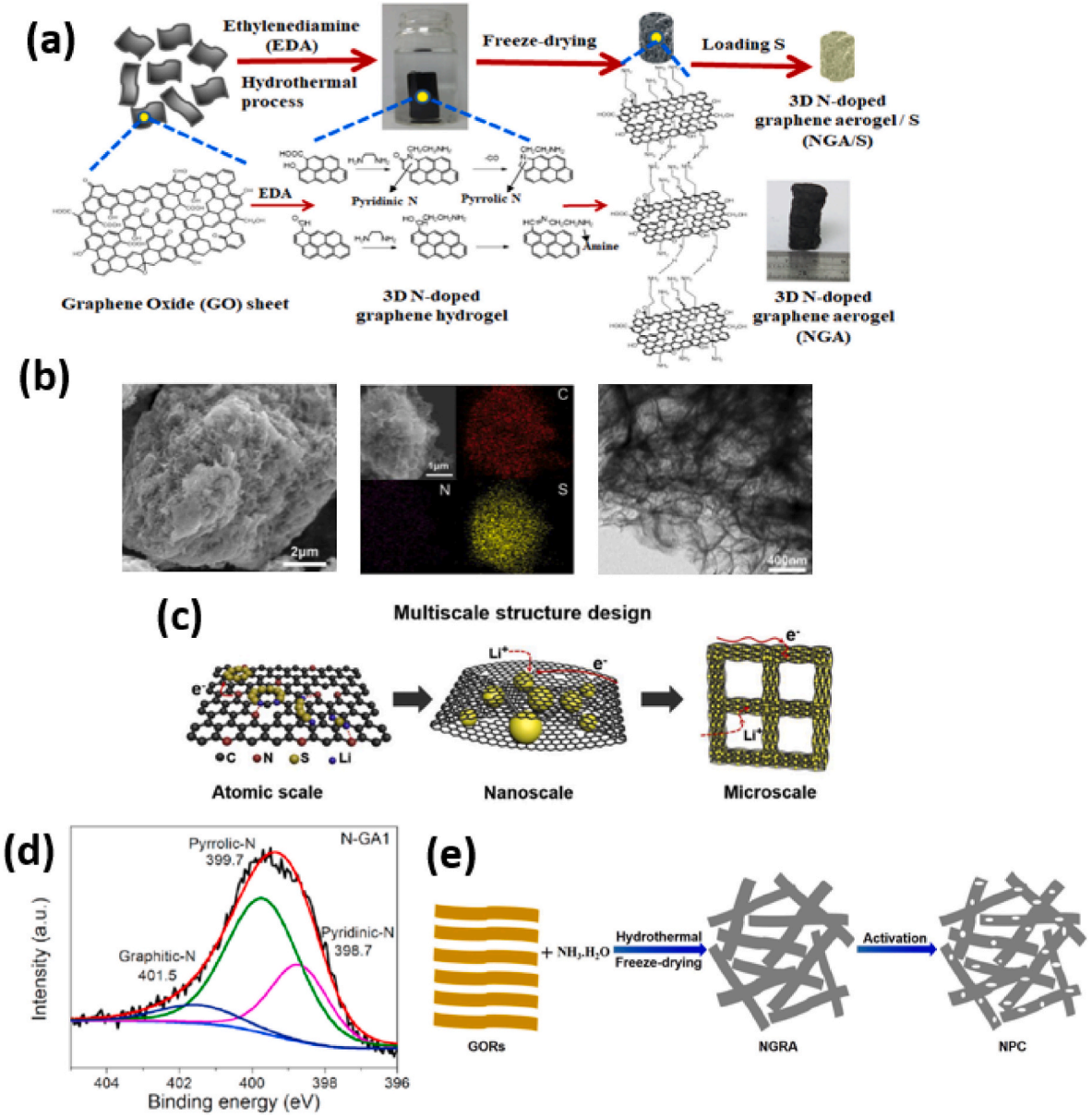

Fig. 4. (a) Schematic of synthesis steps for NGA/S composite and possible EDA reaction pathways for nitrogen doping. Reprinted with permission from [136], Copyright Elsevier 2018. (b) Energy-dispersive X-ray spectroscopy maps of C, N and S in the 3D-PNG/S nanocomposite and related TEM image, (c) Schematic illustration of the multiscale structure design of 3D-PNG as sulfur host material. Reprinted with permission from [137], Copyright Elsevier 2019. (d) The N 1s XPS spectrum of the NGA. Reprinted with permission from [138] Copyright Elsevier 2021. (e) Illustration of the preparation processes of NPC. Reprinted with permission from [141], Copyright Elsevier 2019.

performance. The coating of sulfur with graphene can inhibit the shuttle effect, enhance cell's stability and increase the sulfur loading. Interestingly, Zhou et al. [141] demonstrated the opposite approach of using N-doped graphene nanoribbon aerogel (NGRA) as a source for preparation of nanostructured porous carbon (NPC) under physical CO_2 activation (Fig. 4 e) [142,143]. The as-obtained hierarchically porous NPC with large surface area (1380 $m^2\ g^{-1}$) and sponge-like morphology acted as a host material for Li–S battery. The superior electrochemical performance of S/NPC is commonly explained by the abundant pores in carbon host, acting as reservoirs for LiPSs, preventing their diffusion to anode side, thus suppressing the shuttle effect and enhancing the cell's cycling stability. In addition, N-based functional groups positively affect electrochemical performance as a result of extraordinary binding capability to LiPSs [144].

Boron (B) doping of graphene is another prospective technique to achieve the desired electrochemical performance and stability of GA/S cathodes. As known, B-doped carbon has a higher electrical conductivity than the pristine one, and while being doped to the carbon's framework boron atom is positively polarized, which may result in its stronger chemisorption with a negatively charged sulfur species [145]. Xie et al. [146] demonstrated the advantage of using boron-doped GAs (BGA) as a porous network for anchoring sulfur and LiPSs. Boric acid was used as a source of boron and reducing agent during hydrothermal synthesis of BGAs. According to the XPS analysis (Fig. 5 a), boron atoms were doped into graphene via $-BC_2O$, $-BCO_2$, and $-BC_3$ bonding. Positively polarized boron-doped GA demonstrated the higher binding energy to sulfur compared to pristine GA and N-doped GA, indicating that electron density of sulfur was partly distributed over its surface. The BGA cathode with 59 wt% loaded sulfur delivered the initial discharge capacity of 1290 mAh g^{-1} at 0.2C, which slightly decreased to 994 mAh g^{-1} after 100 cycles. Manthiram et al. [103] predicted that electron binding energy for B-doped GA of 1.99–2.17 eV is greater than those for O and N

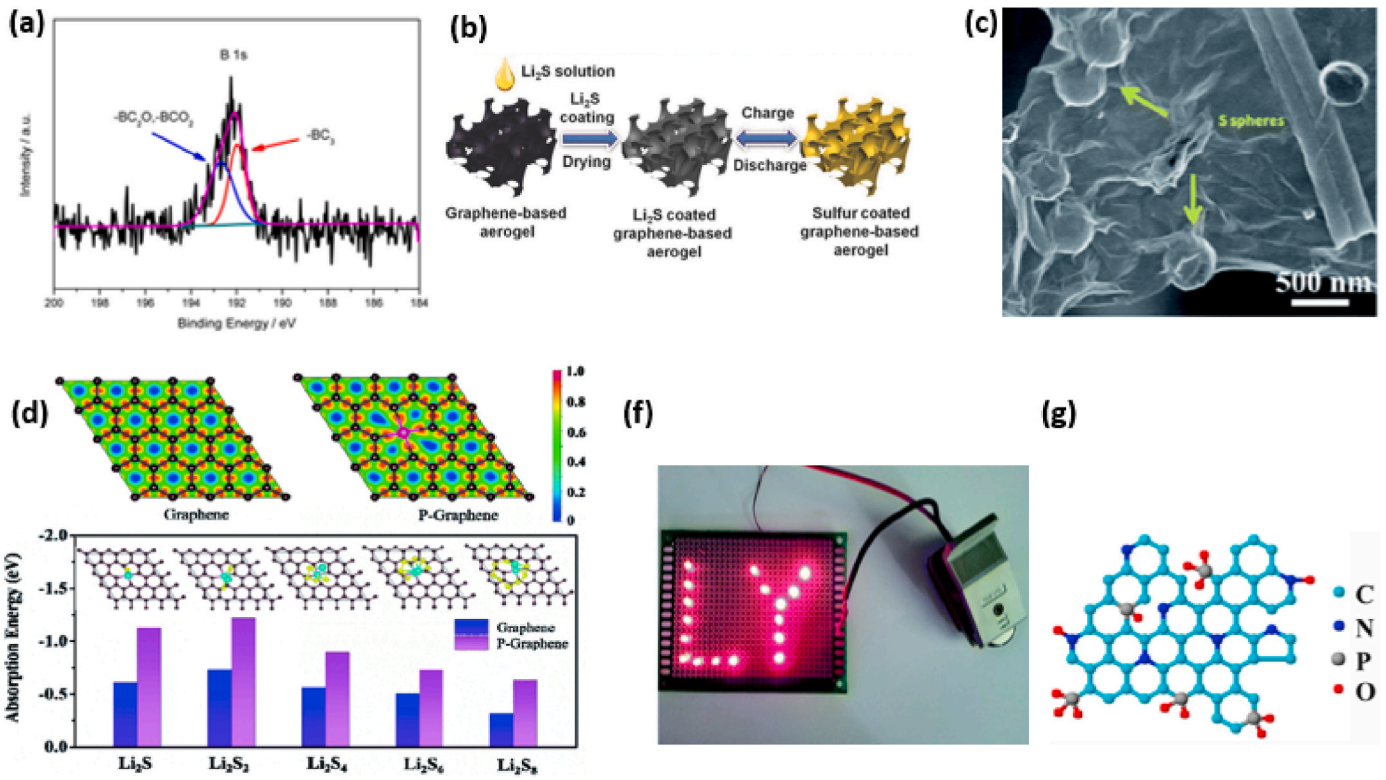

Fig. 5. (a) B 1s peak of XPS spectrum of BGA. Reprinted with permission from [146], Copyright ACS Publications 2015. (b) Illustrations of the Li_2S coating process and the in situ charge/discharge process of the graphene-based electrode. Reprinted with permission from [103], Wiley Online Library Copyright 2015. (c) SEM image shows the sulfur spheres wrapped with the P-doped graphene sheets, (d) The electron localization function patterns of graphene and P-graphene (the column chart compares the adsorption energy of LiPSs on graphene/P-graphene. The brown, purple, yellow and blue spheres denote C, P, S and Li atoms, respectively), (f) Series of LED lights can be lit up using a coin Li–S cell with the PGCNF/S cathode. Reprinted with permission from [153], RSC Publishing Copyright, 2020. (g) Schematic chemical structure of the dual N and P co-doped GA. Reprinted with permission from [154], Copyright Elsevier 2019.

sites, which can be ascribed by the contribution of additional covalent-like bonding between S and B. Additionally, the B atom is substantially protruded towards S atom due to B–S bonding interaction. Even a small amount of B atoms (1.1 atom%) improves the cycling stability of the B-doped cathodes due to the strong binding of Li_2S and B doping species. The synergistic effect of GA network, Li_2S and nitrogen or boron doping resulted in promoting rapid electron and ion transfer by creation of a shortened ion/electron transport pathways, decreasing the energy barrier and improvement of the affinity between nonpolar graphene and polar LiPSs (Fig. 5 b). Consequently, the Li_2S/N-doped GA and Li_2S/B-doped GA free-standing cathodes exhibited the initial specific capacities of 801 and 720 mAh g^{-1} at 0.3C and after 100 cycles it retained 635 and 532 mAh g^{-1}, respectively. The discharge capacities of 561 and 487 mAh g^{-1} for Li_2S/N-doped GA and 528 and 395 mAh g^{-1} for Li_2S/B-doped GA were observed at 1 C and 2 C, respectively.

Phosphorus (P) doping of graphene is also an effective solution to improve its overall electrical conductivity and fabricate more developed porous structure that provide large specific surface area to load higher amounts of sulfur [147]. Based on previous works it is commonly accepted that pyrrolic-N is characterized by a stronger adsorption capability to Li_2S_8 among other two types of N (graphitic, pyridinic) [148]. However, according to the DFT calculations reported in [147], -P-O is characterized by even stronger adsorption energy to LiPSs. For instance, -P-O demonstrates the stronger adsorption behavior towards Li_2S_8 with a higher adsorption energy (−1.390) compared to graphitic-N (−0.567), pyridinic-N (−0.839) and pyrrolic-N (−0.940). This can be explained by the larger radius of P atom compared to N and C atoms. The P atom doped into graphene with a larger radius creates a longer C and P atoms bond distance, which results in decrease of overlapping the p_z orbitals and decrease of the π-bonding [149]. This promotes appearance of graphene buckling (1.28 Å) in the vertical direction. The P-doped region exhibits the sp^2 and sp^3 orbital hybridization features [150] and the buckled graphene with a partial sp^3 bonding can improve their interaction [151,152]. When it comes to the top of –P-O functional group, the puckering and polarization become even stronger than that for pure P-doped sample, which greatly improves the interaction between Li_2S_8 and graphene. Tan et al. [153] demonstrated that P-doped graphene/carbon nanofiber/sulfur spheres (PGCNF/S) composite aerogel with 85% sulfur content can efficiently suppress the shuttle effect due to sulfur spheres physical wrapping with the fabricated network and chemical interfacial interactions (Fig. 5 c). The PGCNF/S free-standing cathode delivered a high specific capacity of 1360 mAh g^{-1} and long-term cycling stability up to 600 cycles at 0.5C with 83% capacity retaining. Even though graphene has a uniform charge density distribution, the electrons in P-doped graphene are more localized around P atoms which is also promoted by the higher amount of valence electrons of P atoms compared to C atoms. In other words, -P-C bonding electrons are more localized compared to -C-C bond electrons. The polarity of graphene also increases with the increment in P atoms, which further enhances the overall electron localization. Furthermore, the values of adsorption energy of Li_2S_n on P-graphene (−1.127 for Li_2S, −1.219 for Li_2S_2, -0.892 for Li_2S_4, -0.724 for Li_2S_6 and -0.631 for Li_2S_8) are much higher than those for Li_2S_n on pristine graphene (Fig. 5 d, f). Further, Ren et al. [154] demonstrated that the dual N and P co-doping 3D graphene (PGCNF/S) can be a promising solution for improvement of the electrochemical performance of sulfur-based cathodes. Benefitting from the pyridinic-N (397.74 eV), pyrrolic-N (399.79 eV), graphitic-N (400.95 eV), oxidized-N (402.28 eV), as well as P–C (130.4 eV) and P–O (132.8 eV) bonding in the composite, they could demonstrate the synergistic effect of anchoring the dissolved LiPSs via Li_2S_n–N bonding

due to excellent interaction between electrophilic Li^+ and electronegative N atoms. Additionally, P atoms covalently bonded to C and O atoms could form an electron-rich regions on the porous substrate producing abundant active sites to enhance the surface affinity to LiPSs (Fig. 5 g). All this resulted in excellent dual N, P co-doped sulfur cathode's electrochemical performance, in particular, the initial discharge capacity of 1420 mAh g^{-1} at 0.1C with a reversible capacity of 503 mAh g^{-1} after 500 cycles at 1 C was observed.

To sum up, heteroatom doping of GAs is a quite promising technique to improve the electrochemical performance of the sulfur-based cathodes. N-doping is one of the major and simplest approach to enhance the electroconductivity, polarity and chemical binding of graphene to LiPSs in course of formation pyridinic-N, pyrrolic-N, graphitic-N and oxidized-N bonding. What is more, there is a multiple choice of the investigated substances which can act as an efficient nitrogen source. The only issue related to the N-doping approach is to achieve the homogeneous distribution of the N atoms over graphene's surface and increase the proportion of the pyridinic-N, which has a stronger binding ability to LiPSs. Boron doping is another efficient technique to improve the electrochemical performance of the GA/S based cathodes in view of formation of $-BC_2O$, $-BCO_2$, and $-BC_3$ bonds which make the graphene positively polarized. As shown, even the small amount of B atoms doped to graphene (less than 1.5%) may result in better cycling stability of the Li–S battery in course of the strong binding of Li_2S and B doped species due to the contribution of the additional covalent-like bonding between S and B. The formation of the -P-O and –P-C bonding, which have a higher adsorption energy to Li_2S_8 compared to N-based species, makes the P doping an alternative efficient technique to achieve the excellent electrochemical performance of GA/S cathodes. The -P-C bonding electrons are more localized which promotes the increase of the graphene polarity and overall electron localization, producing higher amount of abundant active sites to interact with sulfur and its species. Finally, dual co-doping of the graphene with the listed heteroatoms can be a promising technique to utilize the benefits from both types of dopants and achieve the desired electrochemical performance of the Li–S batteries.

3.3. GAs with additions of nano-carbons

3D carbonaceous conductive materials such as CNT-based sponges [155], carbon-based aerogels [156], 3D carbon papers [157], etc. are widely used as a carrier for liquid-type catholytes. Among those CNTs are promising candidates as a sulfur host material due to their large specific surface area, high electrical conductivity, unique fabric morphology and the ability to form a 3D porous conductive network [155,158]. However, the optimization of the catholyte's concentration and catholyte to carbon ratio is still an issue. In this regard, Li et al. [159] reported the approach for synthesis of 3D NrGO/CNT based hybrid aerogel, which acts as a conductive scaffold for L_2S_6 catholyte deposition (Fig. 6 a). The advantage of the NrGO/CNT based hybrid aerogel over CNT sponge is the ability of the first to accommodate a

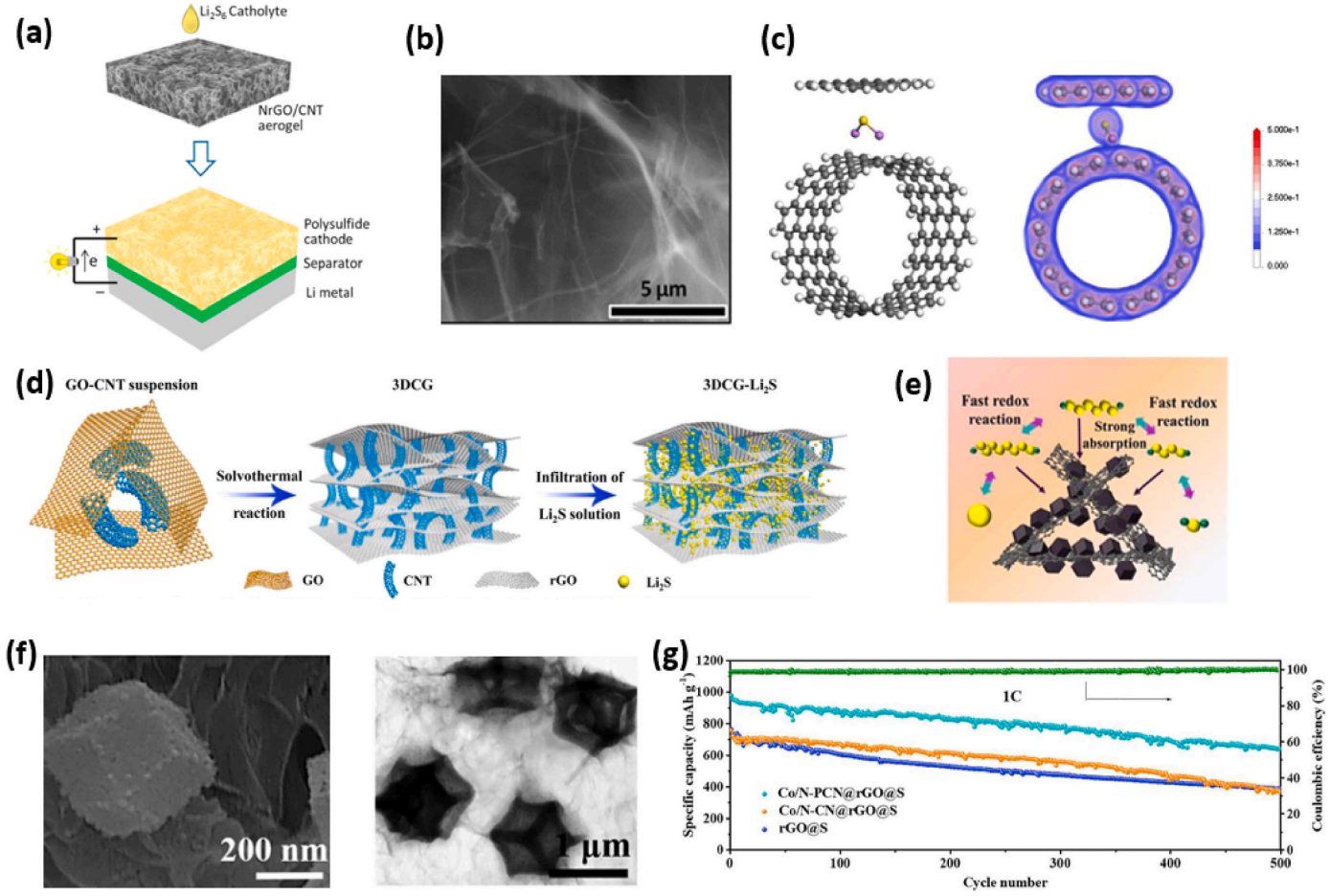

Fig. 6. (a) A scheme of the Li/polysulfide battery with 3D graphene aerogel as the host for Li_2S_6 catholyte in the cathode. Reprinted with permission from [159], Copyright Elsevier 2016. (b) SEM image of GA/CNT@S aerogel. Reprinted with permission from [156], Copyright Elsevier 2019. (c) Predicted optimized configurations (left column) and electron density maps (right column) a Li_2S molecule intercalated into GA/CNT composite structure, (d) Synthetic procedure of the GA/CNT-Li_2S composite. Reprinted with permission from [160], Copyright ACS Publications 2016. (f) FESEM and TEM images of Co/N–PCN@rGO, (g) cycle performance at 1 C of Co/N–PCN@rGO@S, Co/N–CN@rGO@S and rGO@S composites electrodes, respectively. Reprinted with permission from [166], Copyright Elsevier 2020.

larger amount of catholyte, thus increasing the LiPSs loading and equivalent S/C ratio. Also an important role of CNTs in the composite is associated with the improvement of mechanical characteristics and flexibility of free-standing cathode's due to strengthening effect of CNTs ribs, as well as the creation of additional active sites to improve the overall N-doping of the composite and enhance the electric conductivity which together resulted in superior electrochemical performance of the battery. The resulting NrGO/CNT aerogel-based free-standing cathode exhibited low overpotential, high value of specific discharge capacity of 1150 mAh g^{-1} at 0.25C, 0.11% decay rate over 400 cycles and high rate capability of 767 mAh g^{-1} at 2 C. Additionally, Gómez-Urbano et al. [156] presented a comprehensive research on the investigation of the effect of thermal reduction of GO and addition of CNTs on the electrochemical performance of the GA/CNT@S cathode (Fig. 6 b). The main outcomes of the research is that incorporation of only 2 wt% of CNTs greatly improves the specific capacity and its retention compared to the CNT free samples. Simultaneously, the thermal reduction of GO resulted in adequate electrochemical performance of the GA/S cathode. The GA/CNT@S and rGO@S free-standing cathodes delivered sufficient capacity retention between 20th and 100th cycle with a capacity loss of 7.7% and 17.1%, respectively. Moreover, the reversible capacity of higher than 500 mAh g^{-1} at 0.1C after 100 cycles was delivered by the both types of cathodes at 4.0 mg cm^{-2} areal sulfur loading. Further He et al. [160] demonstrated the preparation of well-designed GA/CNT -Li_2S free-standing cathodes by solvothermal reaction and liquid infiltration-evaporation coating (Fig. 6 d). The introduction of CNTs resulted in formation of developed mesoporous structure compared to pristine GA which is more beneficial for providing abundant accessible active sites for hosting Li_2S. As a result, the highly porous structure of CNT/GA composite provided larger loading of Li_2S (81.4%) and abundant reaction sites, facilitating the charge transfer and electrolyte penetration. Mesopores in the composite can trap the dissolved LiPSs suppressing the shuttle effect, while larger pores provide the efficient charge transfer and electrolyte penetration, resulting in high utilization of Li_2S. According to the theoretical calculations, the Li_2S exhibits larger interaction with graphene and CNTs combined together in the aerogel's structure (Fig. 6 c). The larger overlap of electron density between Li_2S and GA/CNT aerogel compared to Li_2S/graphene indicates that the charge transport of Li_2S is enhanced. Therefore, the resulting CNT/GA-Li_2S free-standing cathode delivered the initial specific capacity of 1052.1 mAh g^{-1} at 0.2C and retained 958.3 mAh g^{-1} after 300 cycles (0.02% per cycle of capacity decay). At the high 4 C rate the capacity of the sample was found to be 514 mAh g^{-1}.

Capacity retention of sulfur composite cathodes can be further improved by insuring better adhesion of sulfur to the surface of CNTs and graphene. As known, the active material tends to detach from CNTs and graphene during the continuous charge/discharge cycles, which can be explained by their flat surface and, as a consequence, the absence of geometric constraints for sulfur, leading to poor cycle stability. Porous carbon (PC) exhibits excellent confinement to sulfur and its species due to its intrinsic micro- and mesoporosity [161–164]. Yet due to its relatively high electrical conductivity, integration of PC with CNT or graphene was found to be rather effective approach to enhance the electrochemical performance of sulfur-based cathodes. Wang et al. [165] have demonstrated an approach for hydrothermal synthesis of rGO based aerogels on the surface of which the PC was anchored by using sucrose solution as a precursor. The promising electrochemical performance of PC/rGO/S composites is mainly attributed to high electrical conductivity of PC, its ability to load a large amount of sulfur and to decrease the shuttle effect via physical confinement. In addition, flexible 3D rGO and PC can act as an electrically conductive networks, which shorten the electron and Li-ion transfer path. As a result, the PC/rGO/S composites exhibited the initial discharge capacity of 1122 mAh g^{-1} at 1.0 A g^{-1} and maintained a capacity of 643 mAh g^{-1} after 100 cycles. Further Wang et al. [166] have reported the fabrication of the composite based on Co and N co-doped porous carbon nanocages on GA network (Co/N–PCN@rGO) by pyrolyzation and acid-leaching methods (Fig. 6 f). To investigate the mechanism of the interaction between Co/N–PCN@rGO and Li_2S_6 solution the XPS analysis was applied. As a result, two evident peaks at 784.4 and 402.4 eV were observed corresponding to Co–S and N–S bonding [167]. At the same time, apart from two prominent peaks at 163.8 and 165.1 eV corresponding to terminal and bridging sulfur atoms, two other peaks at 168.5 and 169.4 eV were observed in the S 2p XPS spectrum. These peaks confirm the formation of polythionate species resulted from the chemical reaction between Co and Li_2S_6 [168]. Additionally, cyclic voltammetry of the symmetric cell in Li_2S_6 electrolyte confirmed that Co/N–PCN@rGO composite exhibited higher redox current resulting in better catalytic activity towards LiPSs transformation. The Co/N–PCN@rGO@S free-standing cathode retained a capacity of 900 mAh g^{-1} after 100 cycles at 0.2C with the reversible capacity of 640 mAh g^{-1} after 500 cycles at 1 C (Fig. 6 g), which corresponds to 0.066% decay rate per cycle. The Co/N–PCN@rGO@S composite cathode also maintained the capacity of 762 mAh g^{-1} after 50 cycles at 0.2C at a higher sulfur loading (3.5 mg cm^{-2}). The achieved electrochemical performance of the Co/N–PCN@rGO@S cathode is mainly attributed to the prepared 3D conductive graphene framework supported Co, N co-doped porous carbon nanocages acting as an excellent LiPSs mediator capable to entrap the long-chain LiPSs and facilitate their redox reaction [169].

Overall, the preparation of the composites of GAs with nanostructured carbons is one of the efficient techniques to suppress the LiPSs shuttle effect and improve the electrochemical performance of the sulfur-based cathodes. The introduction of CNTs results in a significant improvement of the GAs based free-standing cathode's mechanical properties and flexibility, promotes the formation of a developed pore structure and enhances the overall electric conductivity. Addition of PC is also beneficial to improve the electrical conductivity of the composite cathode as well as to create additional sites for LiPSs binding and facilitating their redox reaction.

3.4. GAs with metal-containing compounds

Due to their intrinsic oxygen rich surface structure metal oxides have strong affinity to LiPSs species and the reported spectroscopic investigations demonstrated excellent chemical interactions between them [170,171]. However, metal oxides have insufficient surface area to host a large sulfur amount, low electrical conductivity and exhibit poor electrochemical performance as a sulfur host [172]. The idea of decorating 3D highly porous carbonaceous materials with metal oxides is promising in course of possible achieving their synergistic effect, in which GAs with high surface area and excellent electrical conductivity act as a porous matrix for sulfur immobilization while metal oxides are responsible for additional sites for chemical interaction with sulfur and its species.

Titanium oxide (TiO_2) is known as the one of the most promising metal oxide to improve the chemical entrapment for intermediate LiPSs and facilitate the redox reaction kinetics. Wang et al. [173] proposed the use of TiO_2 nanoplatelets with high percentage of (001) facets anchored on graphene walls as a chemical adsorber of generated LiPSs (Fig. 7 a). Nanoplatelets with the side length of about 50 nm and 5 nm thickness were formed and further utilized to fabricate the S@TiO_2@GA composite (55.2%, 10.3% and 34.5%, respectively (Fig. 7 b)). The well-matching of TiO_2 (001) nanoplatelets with graphene (002) nanosheets attributed to their consecutive orientation improved the ion/-electron transfer, sulfur loading capability, ability to capture the soluble sulfurous species by both physical adsorption and chemical bonding (Ti–S), which resulted in a high initial discharge capacity of S@TiO_2@GA composite of 1404 mAh g^{-1} and 905 mAh g^{-1} after 100 cycles at 0.2C (for comparison these values for S@GA sample were 810 mAh g^{-1} and 495 mAh g^{-1}, respectively). Chen et al. [174] have proposed a strategy for preparing self-supporting and electrically conductive polar TiO-G/S film with 3D porous structure. TiO_2 nanotubes were

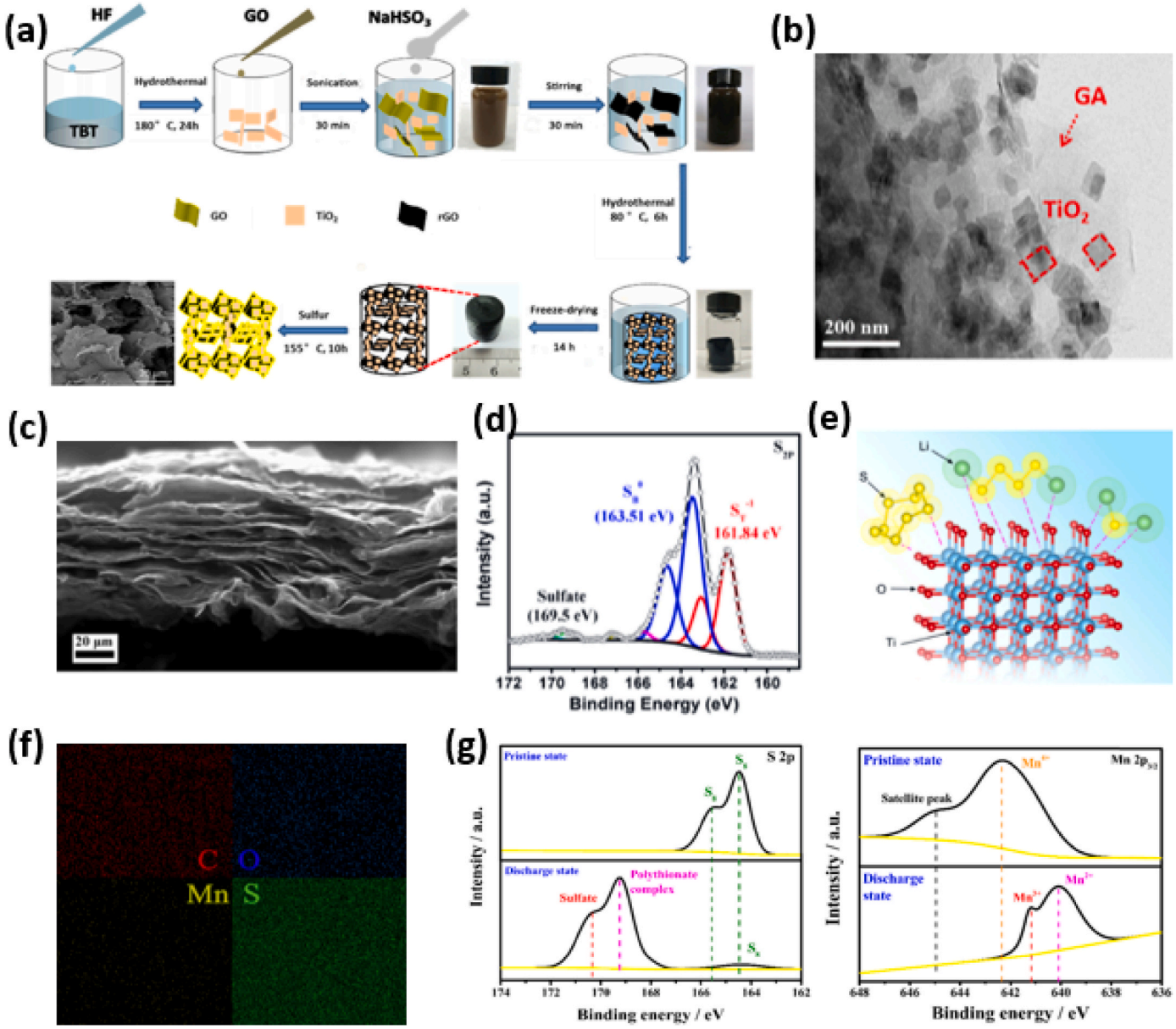

Fig. 7. (a) Schematic illustration of preparation process of S@TiO_2@GA, (b) TEM image of S@TiO_2@GA. Reprinted with permission from [173], Copyright Elsevier 2020. (c) Cross-sectional SEM image of TiO-G/S composite, (d) High-resolution S 2p spectra of TiO-G/Li_2S_6, (e) Demonstration of the chemical interaction between TiO and sulfur species. Reprinted with permission from [174], Copyright Elsevier 2018. (f) Elemental mapping of C, O, Mn and S of MGPP@S, (g) XPS spectra of MGPP@S composite (S 2p - left, Mn $2p_{3/2}$ –right). Reprinted with permission from [177], Copyright Elsevier 2019.

thermally transformed to ultrafine TiO nanoparticles and the graphene surface acted as a supporting substrate to prevent their aggregation (Fig. 7 c). This homogeneous distribution of TiO nanoparticles over 3D graphene structure played a crucial role in chemical adsorbing LiPSs and accelerating the redox reaction during charge-discharge process. The TiO and LiPSs binding mechanism is mainly explained by existence of the abundant low coordinated Ti sites with unsaturated chemical binding capable of chemical interacting with sulfur species (Fig. 7 d, e). As reported in [175], TiO is characterized by a strong chemical adsorption energy to LiPSs in course of the formation of both Ti–S and Li–O bonds. Consequently, the TiO-G/S delivered an initial discharge capacity of 1350 mAh g^{-1} at 0.1C and 832 mAh g^{-1} at 2 C. Moreover, at areal sulfur loading of 5.2 mg cm^{-1} the sample demonstrated areal capacity of 3.2 mAh cm^{-2} after 200 cycles at 0.2C.

Complex ternary hybrid electrodes can be constructed by development of GAs composites with PC, metal oxides and metal sulfides, and possible additions of various polymers. In fact, carbon plays a role of a major host material which provides physical spaces and electric pathways for active sulfurous species, while metal oxides are responsible for secondary host to decrease the loss of sulfur in view of their strong affinity to LiPSs. GAs are able to provide a physical support due to existence of interconnected space in highly porous electrically conductive 3D network with strong mechanical properties. Wang et al. [176] reported that the introduction of glucose to TiO_2/GA acting both as a cross-linker and a dispersing agent is rather favorable to increase its specific surface area and optimize the pore size distribution, leading to enhanced adsorption of soluble LiPSs. Authors speculate that glucose precursor was transformed into oligosaccharide and aromatic compounds and after nucleation and growth their molecules were cross-linked at high temperature forming spherical carbon with functional groups. These spherical carbon particles might be interconnected with graphene, playing a role in increase of the porosity of aerogel

during synthesis by cooperative dispersion. As a result of this glucose modification, the sample TiO_2/GA with the content of 15.3 wt% of 5–10 nm in size TiO_2 particles and 60 wt% of sulfur exhibited the initial discharge capacity of 1011 mAh g^{-1} at 2 C with a 100% Coulombic efficiency over 500 cycles. Tan et al. [177] proposed a composite of GA with manganese oxide (MnO_2) nanoparticles and co-polymer based on polyvinylpyrrolidone/polyvinylalcohol (PVP/PVA). The nanoparticles of MnO_2 were distributed over the graphene sheets and acted as a robust material for chemisorption of LiPSs (Fig. 7 f). The mechanism of chemical transformations of sulfur and Mn during cycling was

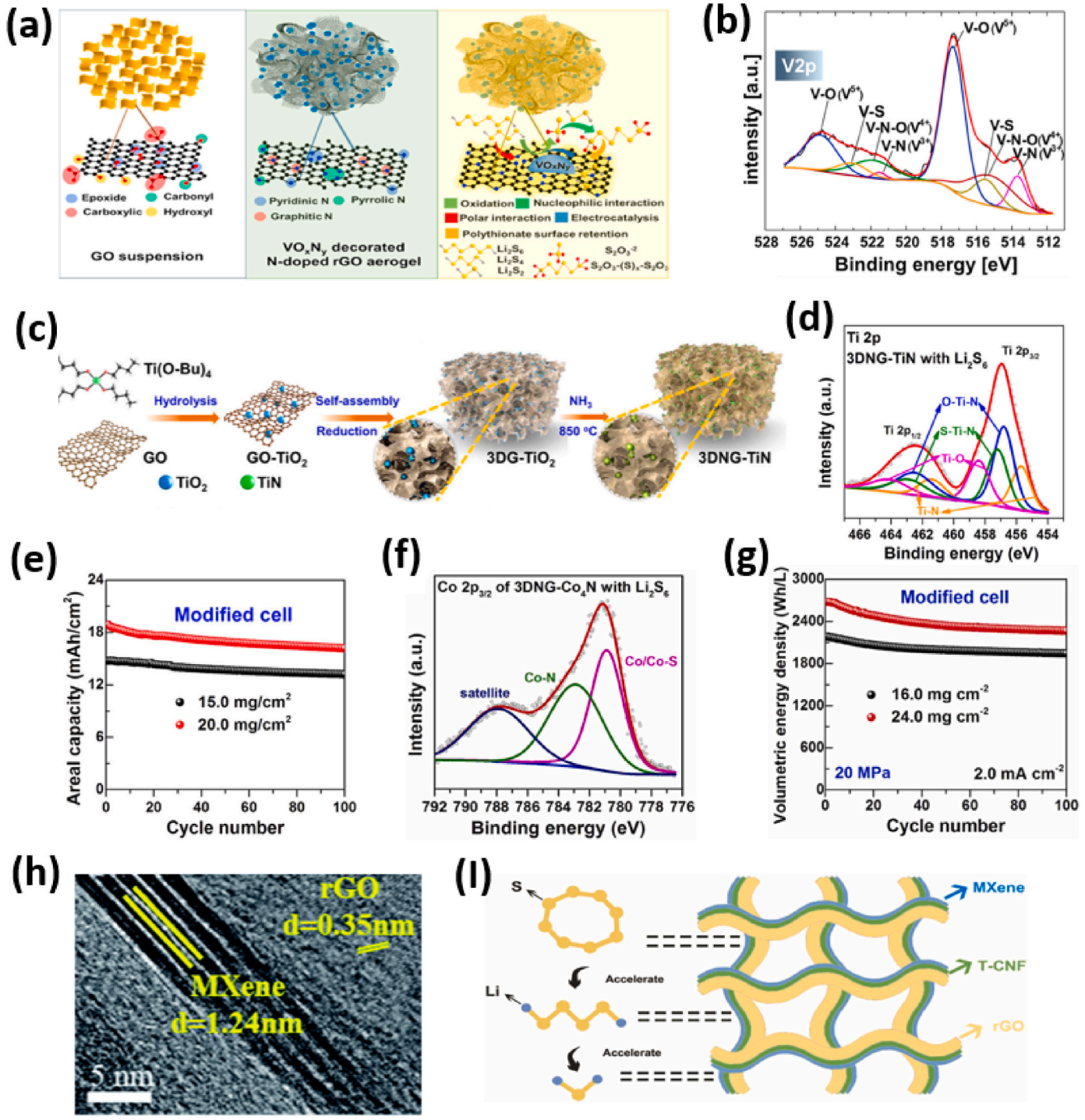

Fig. 8. (a) Schematic sketching of the study that outlines from material synthesis to interaction mechanism of VONNG aerogel as a prospective host material for sulfur cathodes, (b) XPS analysis of LiPSs interacted VONNG matrix (b) O1s spectrum, VONNG (bottom) vs. absorbed. Reprinted with permission from [191], Copyright Elsevier 2020. (c) Schematic of the 3DNG–TiN composite prepared via a three-step process of hydrolysis–self-assembly–nitridation, (d) Ti 2p XPS spectrum of the 3DNG–TiN composite with Li_2S_6 absorbed, (e) Cycling performance of modified cells with ultrahigh sulfur loadings of 15.0 and 20.0 mg cm^{-2} at 2.0 mA/cm^2. Reprinted with permission from [198], Copyright ACS Publications 2021. (f) Co $2p_{3/2}$ XPS spectra of 3DNG-Co_4N with Li_2S_6 adsorption, (g) The volumetric energy density of 3DNG-Co_4N/S cathodes with a modified separator. Reprinted with permission from [200], Copyright Elsevier 2022. (h) HRTEM images of the $Ti_3C_2T_x$ MXene/GA. Reprinted with permission from [206], Copyright RSC Publishing 2019. (f) The illustration of GA/T-CNF/MXene aerogel electrode enhancing the kinetic reaction rate of lithium-sulfur battery. Reprinted with permission from [211], Copyright Elsevier 2022.

investigated by XPS, according to which sulfur in the pristine MGPP@S is in the form of S_8 (S $2p_{3/2}$ (164.4 eV) and S $2p_{1/2}$ (165.5 eV) states of S–S bonding) [79], while in the discharged state MGPP@S contained more polythionate complex (169.2 eV) in course of reaction of long-chain LiPSs and metal oxide [179]. At the same time, the pristine MGPP@S demonstrated a Mn^{4+} characteristic peak at 642.3 eV and after discharge to 2.0 V, Mn^{4+} was reduced to Mn^{3+} (641.2 eV) and Mn^{2+} (640.1 eV (Fig. 7 g), [180]. The co-existence of polytionate and reduced Mn ions confirmed the redox reaction between LiPSs and MnO_2. Additionally, a flexible grid based on hydrogen bonded PVA and PVP is responsible for physical and chemical trapping of sulfur. As known, PVP has a strong affinity to Li_2S and intermediate LiPSs [181,182], while PVA is able to integrate with PVP by creation of flexible grid with excellent tensile strength [183,184]. As a result, the ternary composite cathode based on GA with MnO_2, PVP/PVA and sulfur (MGPP@S) exhibited the rate performance of 1492, 1054, 833, 659 mAh g^{-1} at 0.1C, 0.2C, 0.5C and 1 C, respectively. The capacity of 755 mAh g^{-1} was demonstrated by the hybrid electrode at 0.2C after 250 cycles; the capacity fading of only 0.06% per cycle during 500 cycles at 1 C was observed. Yang et al. [185] combined GA with lanthanum oxide (La_2O_3) by a one-step hydrothermal treatment followed by sulfur immobilization (rGO@La_2O_3@S). The role of La_2O_3 microboards in the composite was to form a matrix for loading active sulfur species and trap LiPSs chemically, suppressing the shuttle effect [186–188]. The resulting 3D porous rGO@La_2O_3 matrix was able to effectively compensate the cell's volumetric expansion during charge-discharge cycling. The rGO@La_2O_3@S sample with 18.9 wt% of La_2O_3 microboards and 69.13 wt% of sulfur demonstrated the initial discharge capacity of 1227.4 mAh g^{-1} with its decrease to 1181.4 mAh g^{-1} at the second cycle at 0.2C.

Vanadium oxide (V_2O_5) [168,189] and vanadium nitride (VN) [46,190] are also known as the materials with a good affinity to LiPSs, which may result in prolonging the lifetime of Li–S batteries. Vanadium oxide is a strong catalytic redox converter for LiPSs, while vanadium nitride is characterized by a pronounced binding to LiPSs, rapid transfer of electrons and high electrocatalytic activity. Zubair et al. [191] proposed an approach for preparation of N-doped rGO-based aerogel/vanadium oxynitride composite (VONNG) by using the powder of V_2O_5 as a precursor (Fig. 8 a). As a result, the fabricated VO_xN_y heterostructure can exploit the individual characteristics of VO_x and VN at the contact between V–O and V–N bonds with enhance of binding ability to LiPSs and their rapid electrocatalytic conversion. In particular, the observed peak at 531.62 eV in O1s spectrum of VONNG corresponds to O–S bonding indicating the conversion of LiPSs into oxidized state in the form of thiosulfate [192]. Two peaks for V2p region at 515.25 eV in $V2p_{3/2}$ band and 521.33 eV in $V2p_{1/2}$ band refer to binding energies of V–S interaction and reduction of VO_xN_y (Fig. 8 b) [193,194]. This demonstrate that LiPSs have a strong binding to vanadium of VO_xN_y nanoparticles, while the surface reduction of VON is ascribed to the LiPSs oxidation. Moreover, VO_xN_y is capable to offer a redox potential window vs. Li/Li^+ higher than that of 2.4 V of LiPSs conversion. The assembled cells using VONNG/S as a cathode is characterized by initial discharge capacity of 1400 mAh g^{-1} and 1250 mAh g^{-1} at 0.05C and 0.1C, respectively, and the reverse capacity of 700 mAh g^{-1} at 0.2C after 200 cycles. The capacity loss was lower than 0.05% per cycle over 850 cycles with Coulombic efficiency close to 99% even at 5 C [191].

Recently the highly conductive titanium nitride (TiN) received much attention because of N–S and Ti–S bonds formation which can act both as catalytic and anchoring sites for LiPSs [195–197]. Cheng et al. [198] demonstrated the approach for fabrication of 3D free-standing electrode based on N-doped GA and TiN (3DNG–TiN), Fig. 8 c). The electrode's scaffold presented by GA provided fast channels for charge transfer and enough space to immobilize sulfur. Simultaneously, even a small amount of TiN particles (4.8 wt%) could remarkably enhance the adsorption ability and reaction kinetics of LiPSs and effectively suppress the LiPSs shuttling effect. The strong chemisorption of 3DNG–TiN to LiPSs is mainly ascribed by the appearance of S–Ti–N bond (457.2/462.9 eV) in the Ti 2p XPS spectrum resulted from TiN-polysulfides interaction [199] (Fig. 8 d). The prepared free-standing cathode delivered 1046.7 mAh g^{-1} after 100 cycles at 2.0 mA cm^{-2} with 10 mg cm^{-2} areal sulfur loading and even when the sulfur loading was increased to 20 mg cm^{-2} the cathode still exhibited a high capacity of 18.9 mAh cm^{-2} after 100 cycles at 2.0 mA cm^{-2} with the use of 3DNG–TiN modified separator (Fig. 8 e). Further Cheng et al. [200] reported the preparation of 3D free-standing cathode based on N-doped GA and Co_4N nanoparticles (3DNG-Co_4N). Similar to 3DNG–TiN [198], the 3DNG-Co_4N@S cathode delivered a superior electrochemical performance which is mainly explained by the strong adsorption of cobalt nitride (Co_4N) nanoparticles towards LiPSs. The XPS measurement of 3DNG-Co_4N composite after saturation with Li_2S_6 demonstrated the decrease in the percentage of C–N bond from 68.3% to 63.4% due to formation of Co–S bond, which is usually formed in course of interaction of Co_4N with LiPSs [201] (Fig. 8 f). Also the formation of highly active electrocatalyst (CoS_x) is able to promote the redox reaction kinetics of LiPSs and their stronger anchoring, thus suppressing the shuttle effect which results in better electrochemical performance and cycling stability of the Li–S cell. At the high areal sulfur loading of 24 mg cm^{-2} the cell consisting of developed cathode (3DNG-Co_4N@S) and modified separator (3DNG-Co_4N) delivered the volumetric energy density of 2678.1 Wh L^{-1} at 2.0 mA cm^{-2} (Fig. 8 g).

MXenes composed of early transition metal carbides, nitrides or carbonitrides are recognized as the brand-new 2D materials for energy storage application [202–205]. They are fabricated by extracting "A" layers from the MAX phases, in which M is an early transition metal, A is IIIA or IVA group elements and X is a carbon or nitrogen atom. However, the utilization of pristine MXenes in Li–S batteries is hindered by their restacking tendency and low specific surface area. Song et al. [206] have demonstrated the preparation of 3D porous $Ti_3C_2T_x$ MXene/GA composite by simple mixing GO/vitamin C and MXene suspensions, followed by the hydrothermal treatment and subsequent freeze-drying. The formed $Ti_3C_2T_x$ MXene/GA composites acted as a free-standing LiPSs reservoir for Li_2S_6 catholyte with developed surface morphology and low aggregation (Fig. 8 h). The $Ti_3C_2T_x$ MXene/GA-30 (30 wt% of MXene) sample exhibited the high discharge capacity of 771 mAh g^{-1} at 2 C with a reversible capacity of 685 mAh g^{-1}after 200 cycles. Additionally, at higher sulfur loading of 6.0 mg cm^{-2}, the $Ti_3C_2T_x$ MXene/GA-30 demonstrated the discharge capacity of 879 mAh g^{-1} at 0.1C after 30 cycles, corresponding to 5.27 mAh cm^{-2} areal capacity, which is higher than that for previously reported MXene-based hosts for sulfur [207–210]. As reported, the mechanism of interaction of MXene/GA-30 with sulfur species is mainly ascribed by the formation of S–Ti–C bonding upon cycling [207] confirming the strong adsorption of LiPSs by the composite cathode. The appearance of two Ti 2p peaks at 456.2 and 465.1 eV in the XPS spectrum of the MXene/GA-30@S can be assigned to S–Ti–C bonding indicating that MXene is able to provide reasonable electronic conductivity and effectively trap LiPSs during long-term cycling. Such an excellent performance of $Ti_3C_2T_x$ MXene/GA-30 can be attributed to the synergistic effect of 2D polar surfaces of GO and MXene, which provide strong chemical interaction and adsorption sites for sulfur species, significantly alleviating the shuttle effect. Superior conductivity of MXene provides the fast transfer of electrons and increase the redox reaction kinetics, while the 3D porous structure of GAs facilitates diffusion of ions and better accommodates sulfur and its species decreasing the volume expansion. Further Liu et al. [211] proposed a strategy by combining the GAs with Tempo-oxidized cellulose nanofibers (T-CNF) and MXenes (GA/T-CNF/MXene) with the aim to obtain a composite free-standing cathode with improved mechanical characteristics and flexibility. T-CNF acted as a reinforcing agent to support GA uniformly coated with MXene due to its high aspect ratio and abundant carboxyl groups. The polar groups such as COO- carried by CNF and –OH, –F, –O carried by MXene could greatly improve the adsorption of LiPSs, while the uniform porous structure of GA promoted homogeneous distribution of sulfur in

the electrode material and enhance the redox kinetic of LiPSs (Fig. 8 i). As a result, the fabricated composite cathode delivered the high initial discharge capacity of 1470 mAh g^{-1} at 0.1C and excellent rate capability of 744 mAh g^{-1} at 5 C.

In recent years metal sulfides started to arrow interest of researchers due to their ability to improve the electrochemical performance of Li–S batteries [212–214]. Like metal oxides, metal sulfides can promote a strong interaction with polar LiPSs and create more active sites for their redox reactions during cycling, which is explained by an existence of conductive matrix and charge transfer through its structure. However, similar to metal oxides, most of the pristine metal sulfides exhibit low electronic conductivity, which has an adverse effect on redox property of the captured Li_2S_x, eventually leading to decrease in sulfur utilization [215]. Taking this into account, Li et al. [216] proposed an approach of combining the N/S co-doped GA with polar manganese sulfide (MnS) nanocrystals via hydrothermal method with subsequent separate annealing of the resulting MNSG-aerogels in N_2 medium at 900, 750 and 600 °C (denoted as MNSG-900, MNSG-750, MNSG-600, respectively). The long-term cycling performance at 0.2C of the S/MNSG-900 aerogel delivered the initial specific discharge capacity of 1284 mAh g^{-1} with further decrease to 817 mAh g^{-1} after 200 cycles. For comparison, for the samples S/MNSG-750 and S/MNSG-600 the values of discharge capacity after 200 cycles were found to be 728 mAh g^{-1} and 641 mAh g^{-1}. The better electrochemical performance of S/MNSG-900 than that of S/MNSG-750 and S/MNSG-600 can be explained by the complete elimination of oxygen-containing groups on the graphene surface during the higher temperature processing [217] and the higher amount of polar MnS in the resulting composite. Authors suggest that the soft acid base interaction between Mn^{2+} cations and S^{2-}/S_2^{2-} anions provides the Mn atoms with higher density of valence electrons in sulfides than in oxides [218].

Li et al. [219] demonstrated perspectives of combining of 3D porous coral-like GAs with tungsten disulfide (WS_2) by in-situ hydrothermal process. Homogeneously distributed WS_2 polar particles act as a reaction sites to bond Li_2S_x via chemical interaction, thus decreasing the loss of active material; highly porous structure of GAs provides short diffusion pathways for Li^+ and a large specific surface area (Fig. 9 a). The restacking of GO layers during hydrothermal synthesis was also avoided with the use of WS_2. Based on DFT simulation, the adsorption energy of WS_2 with various sulfur species (−0.57, −0.46, −0.17, −0.15, −0.10 and −0.02 eV for Li_2S, Li_2S_2, Li_2S_4, Li_2S_6, Li_2S_8 and S_8, respectively (Fig. 9 b),) is highly dependent on the number of sulfur atoms in LiPSs.

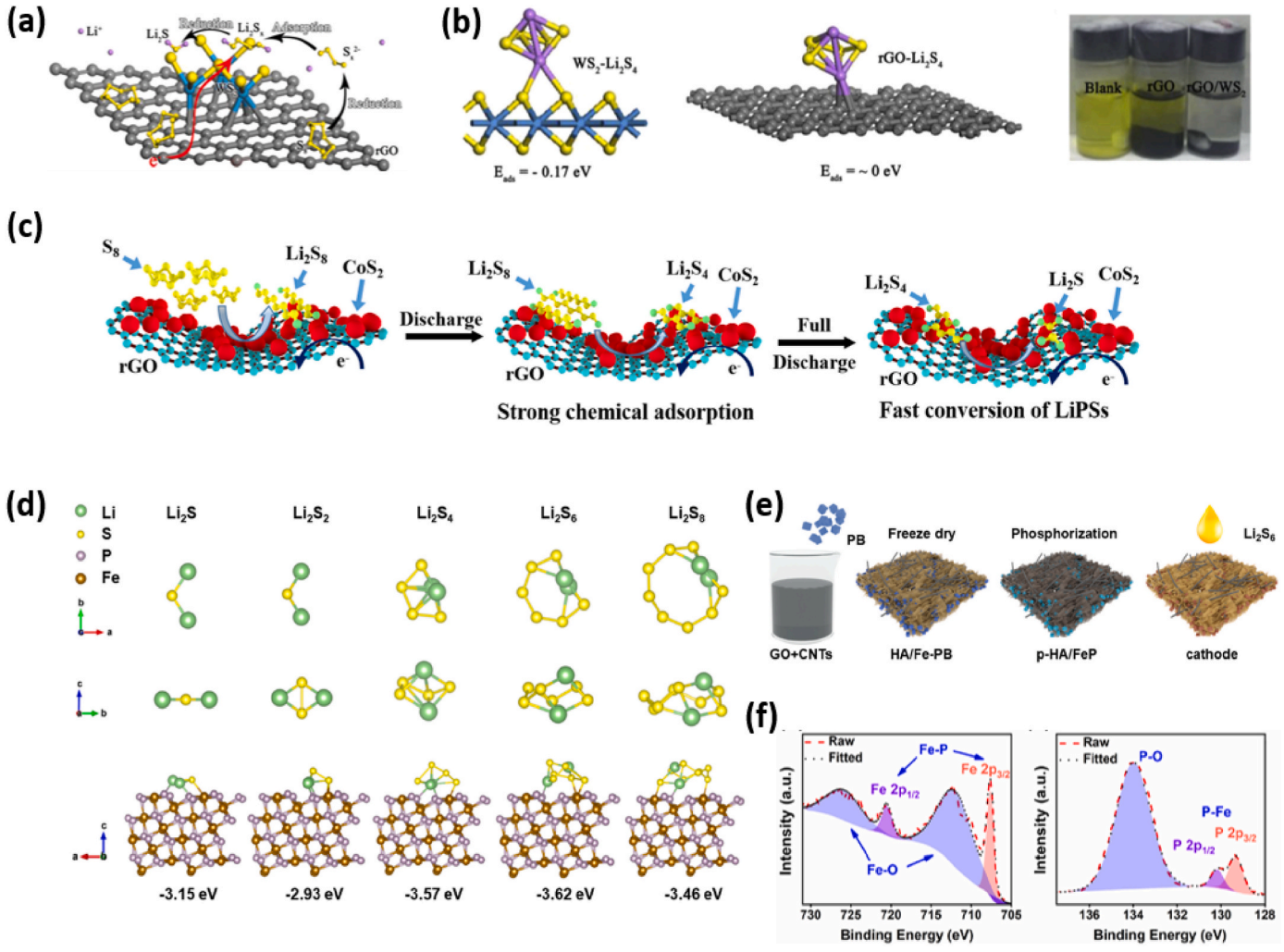

Fig. 9. (a) Schematic illustration on the rGO/WS_2–S hybrid electrode design to improve the performance of Li–S battery, (b) Schematic illustration on the interaction between Li_2S_4, WS_2 (001) and rGO (The blue, purple, yellow and black balls represents the W, Li, S and C atoms respectively) and digital photo of a Li_2S_4 absorption test result (Blank, rGO, rGO/WS_2 powder). Reprinted with permission from [219], Copyright Elsevier 2019. (c) Mechanism diagram of trapping and catalysis of LiPSs during discharge for CoS_2/rGO-30 aerogel cathode. Reprinted with permission from [225], Copyright Elsevier 2021. (d) Theoretical calculations on binding geometries and energies of polysulfides on the (111) plane of FeP, (e) Fabrication of hybrid rGO/CNTs aerogels embedding FeP nanocubes, (f) High-resolution XPS spectra of Fe 2p (left) and P 2p (right). Reprinted with permission from [229], Copyright Elsevier 2020. (A colour version of this figure can be viewed online.)

Therefore, it can be assumed that rGO/WS_2–S composite is able to enhance the sulfur utilization and improve the stability of the Li–S cell in course of its ability to effectively slow down the process of Li_2S_x dissolution. What is more, the superior catalytic nature of WS_2 increases the rate of Li_2S_x oxidation and reduction during charge/discharge cycles. Consequently, the obtained rGO/WS_2–S composite exhibited the initial discharge capacity of 1531 mAh g^{-1} at 0.05C with high sulfur utilization of 91.6% and the Coulombic efficiency of ~100%. The cell demonstrated a higher reversible capacity of 504 mAh g^{-1} at 1 C after 500 cycles with a low capacity decay (0.086% per cycle).

2D layered transition metal sulfides are attractive due to their large specific surface area, ability to adsorb and accelerate the conversion of Li_2S_n. Molybdenum disulfide (MoS_2) layered nanosheets adsorb sulfur species and catalyze the redox reaction, possessing the perspective in their utilization as a Li–S battery multi-functional electrocatalyst [220–222]. However, their main disadvantage are aggregation and low conductivity, which restricts their utilization as sulfur support [223]. In this regard, Hou et al. [224] have recently demonstrated the one-step hydrothermal synthesis of self-supporting 3D GAs and MoS_2 nanoporous spheres based (S@MoS_2@GA) sulfur cathode. The uniform anchoring MoS_2 on the GAs leads to strong chemisorption of Li_2S_n which is due to Li–S bonds formation and acceleration of the sulfur redox reactions. As a result, the S@MoS_2@GA multi-functional electrocatalyst exhibited the discharge capacity of 565 mAh g^{-1} after 200 cycles at 0.2C and a reversible capacity of 324 mAh g^{-1} after 500 cycles at 1 C with a capacity decay of 0.054% per cycle. The preparation of trapping-catalyst host material for sulfur-based on rGO/CoS_2 composite aerogel was demonstrated in [225]. During hydrothermal synthesis, the in-situ growth of cobalt disulfide (CoS_2) nanoparticles is promoted by interaction of Co^{2+} with surface functional groups of GO, resulting in their uniform distribution over GA sheets [226]. The formed CoS_2/rGO-30 composite aerogel demonstrated the initial discharge capacity of 1457 mAh g^{-1} at 0.2C and after 200 cycles it remained 1132 mAh g^{-1}. With increase in sulfur loading up to 6.37 mg cm^{-2} (84.7% of sulfur content), the rGO/CoS_2 aerogel cathode still delivered the discharge capacity of 897 mAh g^{-1} at 0.1C and areal capacity of 5.7 mAh cm^{-2}, which is higher than the areal capacity of current LIBs (4 mAh cm^{-2}). The superior electrochemical performance of rGO/CoS_2@S aerogel based cathode is mainly explained by synergistic effect of CoS_2 nanoparticles deposited on graphene layers, which effectively trap and catalyze LiPSs (Fig. 9 c). In particular, symmetric cell investigations demonstrated that CoS_2/rGO@S sample has two obvious redox peaks at −0.42 V (reduction of S_8 to LiPSs) and at 0.38 V (reverse oxidation of LiPSs to S_8), while for rGO aerogel the values of these peaks were −0.71 V and 0.97 V, respectively. The current density of rGO aerogel is lower than that for CoS_2/rGO and the potential gap between the anodic and cathodic peaks is higher than that for CoS_2/rGO composite confirming that the catalysis of CoS_2 nanoparticles in aerogels is beneficial to improve the electrochemical conversion kinetics of LiPSs.

Metal phosphides are known as an efficient LiPSs mediator in Li–S batteries owing to their high electric conductivity, electrocatalytic properties and strong binding with LiPs [47,227]. Huang et al. [228] demonstrated that Fe_3O_4/rGO/CNTs composite with a strong phosphorization exhibited strong chemical bonding towards LiPSs and catalytic capability to expedite their conversion. Chen et al. [229] reported the perspective of introducing iron phosphide (FeP) nanocubes anchoring materials derived from MOFs into the structure of rGO/CNT aerogel for further improvement of Li–S batteries electrochemical performance (Fig. 9 e). Based on DFT results, the LiPSs clusters are subjected to structural distortions on the highly polarized FeP surfaces and are chemically bonded via Fe–S and Li–P bonding. According to the calculations, the binding energies of Li_2S, Li_2S_2, Li_2S_4, Li_2S_6, and Li_2S_8 on FeP are −3.15, −2.93, −3.57, −3.62, and −3.46 eV, respectively, indicating exothermic adsorption reactions (Fig. 9 d). This demonstrate that LiPSs can be easily anchored and stabilized on FeP (111). The XPS investigation demonstrated the presence of both phosphides and oxidized species in Fe 2p spectrum at 707.6 and 720.5 eV corresponding to the $2p_{3/2}$ and $2p_{1/2}$ peaks of Fe–P, and those at 712.4 and 726.5 eV attributed to the Fe–O species. Phosphorus species are identified at 134.0 eV (P–O) and at 129.3 and 130.2 eV (P–Fe), respectively for $2p_{3/2}$ and $2p_{1/2}$ in the P 2p spectrum (Fig. 9 f). This all confirms that the natural oxidation layer on the transition metal phosphides is beneficial for promoting the LiPSs binding [230]. As a result of synergistic effect of electrically conductive rGO/CNTs based aerogel network and FeP nanocubes anchoring material, the composite free-standing cathode exhibited a cycling capacity of 1312.3 mAh g^{-1} at 0.2C with a decay of 0.037% per cycle over 500 cycles. At the maximum areal sulfur loading of 9.6 mg cm^{-2} the cell cycled over 50 times with the high areal capacity of 8.5 mAh cm^{2-}.

Generally, there is a large choice of metal-containing additives to GAs to improve the electrochemical performance and cycling stability of the GA/S based cathodes. Among them the most widely known ones are metal oxide and metal sulfide particles, which can create additional abundant sites for LiPSs anchoring and improve their redox reaction in course of formation bonds with stronger energy adsorption to LiPSs. However, these materials are characterized by poor ionic/electronic conductivities and tend to agglomerate during cathode's preparation. Metal nitrides and phosphides are also beneficial to Li–S batteries technology in course of their electrical conductivity, electrocatalytic properties and intrinsic ability to chemically trap LiPSs via formation of specific bonds (V–N, S–Ti–N, P–O etc.) and soft acid based interactions between metal cations and sulfur anions. The combination of two 2D materials – graphene and MXene is also promising technique. MXene with functional groups on its surface increases the polarity of carbon and improves the adsorption of LiPSs. The formation of S–Ti–C bonding indicates that MXene is able to provide good electronic conductivity and effectively bind LiPSs during long-term cycling which results in a significant improvement of the Li–S battery's electrochemical performance and cycling stability.

Table 1 demonstrates the reported results on the electrochemical characteristics of the pure and modified GA@S cathodes with the highest areal sulfur loading. As known, high sulfur loading is important for the high energy density Li–S batteries. The porous 3D structure of GAs provides the reliable space for accommodation of large sulfur amount, improves the stability of cathodes and promotes the charge transfer. As can be seen from Table 1, the sulfur content in the GAs matrices ranges from 60 up to 90% and the highest areal sulfur loading was observed as 24 mg cm^{-2}. This is mainly attributed to the major characteristics of GAs such as high specific surface area, developed porosity with suitable pore size, electrical conductivity and physical confinement to LiPSs, as well as the possibility of their modification during synthesis which may result in both, chemical attraction of LiPSs and their catalytic conversion. Also, GAs are a promising material for free-standing cathodes preparation. These 3D nanoarchitectures are lightweight, electrically conductive and highly porous with enough space to accommodate high sulfur amount. Free-standing cathodes are promising alternative to slurry-casted cathodes. Conventionally, to achieve the higher sulfur loading in the slurry-casted cathodes the increase in the electrode's thickness is required which may reduce the kinetics of lithium ions and electrons transportation. This procedure is completely eliminated in the case of free-standing cathodes. What is more, the possibility of using GAs as an interlayer and separator modifier is also beneficial for fabrication of high sulfur loading cathodes with improved electrochemical performance and cycling stability. For instance, the modified cell (3DNG–TiN@S as cathode and 3DNG–TiN as separator modifier) delivered areal capacity of 18.9 mAh cm^{-2} with 85% retention after 100 cycles at 2.0 mA cm^{-2} at 20 mg cm^{-2} areal sulfur loading [198] which is a promising result compared to the previously reported.

Table 1
The electrochemical characteristics of high areal sulfur loading cathodes with modified GAs.

Description	S content, wt %/areal sulfur loading, mg cm^2	Initial capacity, mAh g^{-1}	Rate performance, mAh g^{-1}	Final capacity, mAh g^{-1}	The highest areal sulfur loading/ corresponding electrochemical performance	Ref.
GA (slurry-casted)	75.8/2.5	1140 (0.2C)	Around 600 (3 C)	790 with 69% retention after 200 cycles at 0.2C	–	[95]
N-doped GA (slurry-casted)	77.3/1.2	1258 (0.1C)	340 (2 C)	1077 with 86% retention after 75 cycles at 0.1C	–	[136]
3D-PNG (slurry-casted)	72.5/1.8	840 (2 C)	580 (3 C)	554 with 66% retention after 800 cycles at 2 C	4.0 mg cm^{-2}/1003 mAh g^{-1} with 70% retention after 400 cycles at 1.5 mA cm^{-2}	[137]
GA-S-180 (free-standing)	73.7/5.0	1351.3 (100 mA g^{-1})	517.9 (1 A g^{-1})	517.9 with 38% retention after 50 cycles at 100 mA g^{-1}	–	[104]
PGCNF/S (free-standing)	85/15.8	1360 (0.1C)	834 (5 C)	1028 with 83% retention after 600 cycles at 0.5C	–	[153]
NrGO/CNT (free-standing)	60/6.0	1150 (0.25C)	767 (2 C)	610 with 55.5% retention after 400 cycles at 0.5C	–	[159]
TiO-G/S (free-standing)	65/1.0	1350 (0.1C)	832 (2 C)	455 with 55% retention after 200 cycles at 2 C	5.2/786 mAh g^{-1} with 77% retention after 300 cycles at 0.2C	[174]
3DNG–TiN (free-standing)	85.0/10	990.5 (1.0 mA/cm^2)	636.8 (7.0 mA/ cm^2)	897 with 90% retention after 50 cycles at 1.0 mA/ cm^2	20.0/18.9 mAh cm^{-2} with 85% retention after 100 cycles at 2.0 mA cm^{-2} (used modified separator)	[198]
$Ti_3C_2T_x$ MXene/GA (free-standing)	45/1.57	1270 (0.1C)	977 (1 C)	596 with 63% retention after 500 cycles at 1 C	6.0/879 mAh g^{-1} after 30 cycles at 0.1C	[206]
CoS_2/GA (free-standing)	53.0/1.27	1457 (0.2C)	1156 (2 C)	1001 with 82% retention after 400 cycles at 1 C	6.37/897 mAh g^{-1} with 89% retention after 60 cycles at 0.1C	[225]
MoS_2/GA (free-standing)	88.4/-	688 (0.2C)	206 (5 C)	324 with 73% retention after 500 cycles at 1 C	–	[224]
3DNG-Co_4N (free-standing)	86.6/8.0	1027 (1.0 mA cm^{-2})	659 (5 mA cm^{-2})	938 with 91% capacity retention after 100 cycles at 1.0 mA cm^{-2}	24.0/21.8 mAh cm^{-2} (initial) at 2.0 mA cm^{-2}	[200]
rGO/CNTs aerogels embedding FeP nanocubes (free-standing)	60/-	1312 (0.2C)	647 (2 C)	–	9.6/8.5 mAh cm^{-2} after 50 cycles at 0.2C	[229]
GA–CNFs–Ni separator	90/1.5	1338 (0.1C)	631 (2C)	620 with 71% retention after 500 cycles at 1.25C	10.0/5.5 mAh cm^{-2} after 60 cycles at 0.1C	[231]

4. GAs as interlayers and separator modifier in Li–S batteries

In addition to the importance of developing effective host materials for Li–S batteries, much of the attention of scientists is focused on the design of separators. Separator is one of the core components of Li–S batteries, which major function is to ensure the electrical isolation between cathode and anode to avert the internal short-circuit and to provide the Li ions diffusion pathway [232,233]. Commonly used commercial separators (polypropylene, polyethylene) are characterized by the large pores, nonconductive surface, hydrophobicity and are not suitable for superior electrochemical performance and stability of Li–S batteries [232]. Separators for Li–S cell should satisfy some additional requirements such as LiPSs trapping ability, improvement of electrical conductivity for complete utilization of sulfur, enhancement of sulfur species conversion kinetics and anode protection [234–237]. GAs and their composites with good electrical conductivity, existing functional groups, adjustable pores and high specific surface area can be a promising material for separator modification. Based on the character of interactions between LiPSs species and modified separator, its trapping ability can be categorized into physical and chemical LiPSs anchoring and electrostatically LiPSs rejection.

The strategy for creation of the dual-trapping system using modified GAs both as a sulfur host and separator modifier to effectively suppress the shuttle effect in Li–S batteries was implemented by Tan et al. [238]. GAs decorated with MnO_2 (MG) and I/N-co-doped GAs (ING) were synthesized via hydrothermal treatment and subsequent freeze-drying and used as Celgard 2400 separator modifier and host for sulfur, respectively (Fig. 10 a). The MG@Sep is able to trap the S_x^{2-} anions via strong Mn-S_x interaction, which was confirmed by the XPS investigation by the presence of the peak at 640.6 eV corresponding to Mn^{2+} detected after cycling. This peak verify the redox reaction between MnO_2 and LiPSs. Moreover, the MG@Sep is capable of seizing S_x^{2-} to avoid the LiPSs diffusion to anode side. MG@Sep separator with its hierarchically porous structure can easily immobilize the sulfur species by both, physical and chemical adsorption [177]. The initial discharge capacity of 1499 mAh g^{-1} at 0.2C was exhibited by MG@Sep + ING/S cell. 902 mAh g^{-1} was retained by MG@Sep + ING/S cell after 200 cycles with Coulombic efficiency over 99%. The combined use of ING/S cathode and MG/Sep separator, acting as an efficient sulfurous species immobilizer and shuttle effect suppresser, respectively, enabled Li–S batteries to demonstrate large initial discharge capacity and durable cycle stability. Moreover, after 200 cycles no sulfurous species were detected on the anode (Fig. 10 b). Zhang et al. [231] reported the modification of the commercial separator with 3D graphene aerogel–CNF–Ni (GA-CNFs-Ni) composite composed of herringbone structured CNFs grown in the GA's structure. This composite demonstrated the ability to serve both as physical LiPSs trapping barrier and a conductive network to reactivate the captured materials. Polar Ni nanoparticles served as chemical adsorbents for long-chain LiPSs with their further transformation to short-chain LiPSs in course of their strong electrocatalytic activity, thus improving the rate performance (Fig. 10 c, d). The calculated binding energies of Ni with S_8, Li_2S, Li_2S_2, Li_2S_4, Li_2S_6, and Li_2S_8 are −6.27, −4.15, −5.39, −6.52, −9.10, and −9.04 eV, respectively, suggesting the strong chemisorption effect of Ni to LiPSs (Fig. 10 e). The solid sulfur species (Li_2S and Li_2S_2) were further deposited on herringbone CNF's surface with gaps and defects enlarging the abundant reaction sites among the electron, electrolyte and sulfur species ensuring the stable operation of the cathode. Additionally, the 3D plane-to line network composed of GAs and CNFs provides more channels and contacts for electrolyte infiltration and transportation of Li ions, which improves the electrochemical performance of the cathode at higher sulfur loading. The resulting cell with the modified separator delivered 900 mAh g^{-1} after 90 cycles at 0.2C (sulfur loading was 5 mg cm^{-2}, 90 wt%) and excellent rate capability of 580 mAh g^{-1} at 1 C. At 10 mg cm^{-2} areal

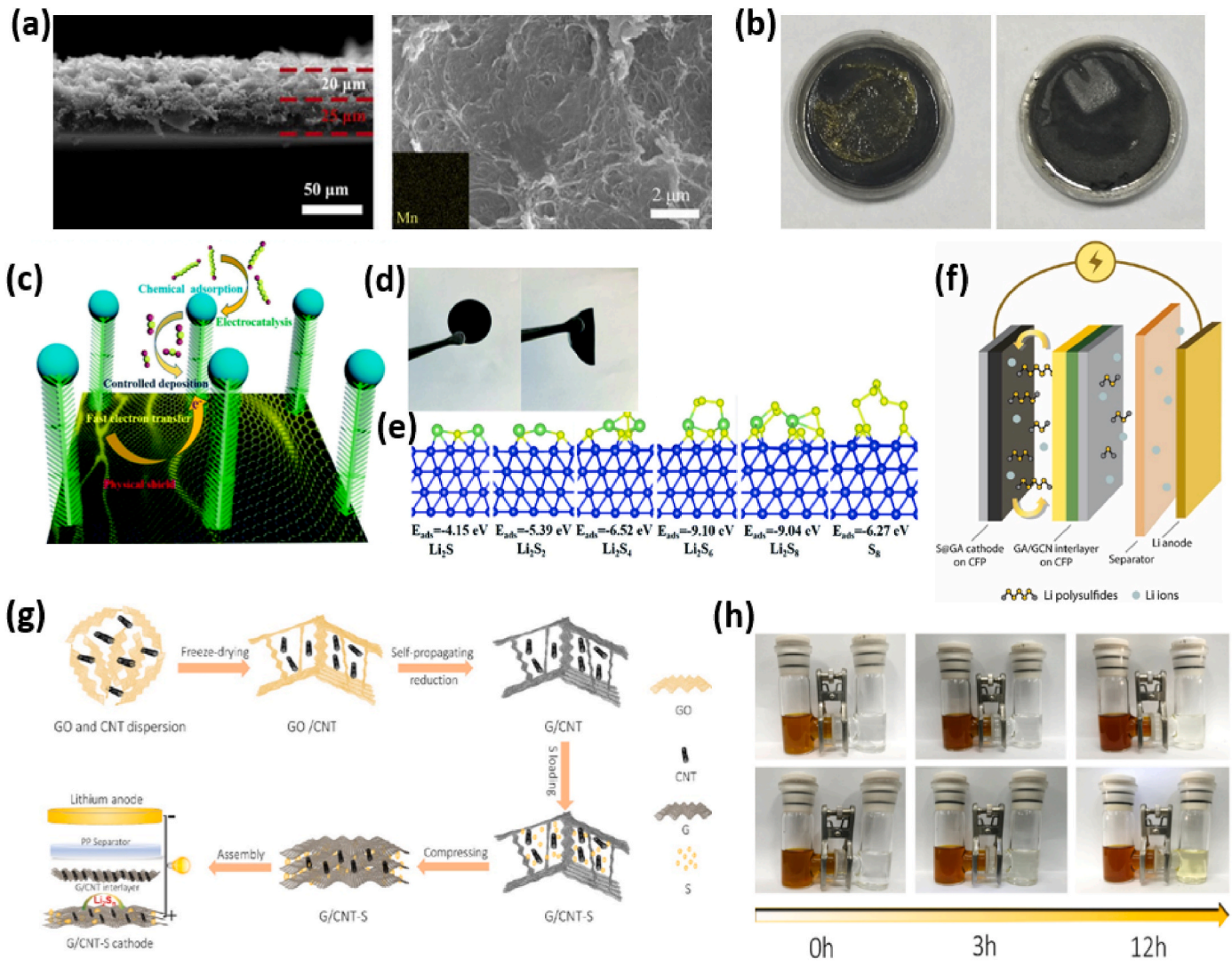

Fig. 10. (a) SEM images of cross-section and top view of MG@Sep, (b) Photographs of Li anode for Non@Sep + ING/S (left) and MG@Sep + ING/S (right) cells after 200 cycles at 0.2C. Reprinted with permission from [238], Copyright Elsevier 2020. (c) Schematic illustration of the synergistic effects of the GA–CNFs–Ni hybrids in Li–S cells, (d) Optical GA–CNFs–Ni coated separator, (e) Theoretical structure configurations and binding energies between the (111) planes of Ni and various sulfur species (S_8 and S_x^{2-}, $1 \leq x \leq 8$). Reprinted with permission from [231], Copyright RSC Publishing 2018. (f) A schematic of a lithium sulfur battery with the S@GA cathode and the GA/GCN interlayer produced by a layer-by-layer coating method where the GCN is the top layer and the GA is the bottom layer coated on the CFP substrate. Reprinted with permission from [246], Copyright Elsevier 2018. (g) Schematic of the synthesis of G/CNT-S//G/CNT cathode integrated G/CNT-S host with G/CNT interlayer for Li–S batteries, (h) Polysulfide permeation measurements for G/CNT/PP (top) and individual PP (bottom) separators during the course of polysulfide diffusion from Li_2S_6/THF solution (left side) to pure THF (right side) of the U-shaped glass cell. Reprinted with permission from [249], Copyright Elsevier 2019.

sulfur loading the electrode exhibited stable areal capacity of 5.5 mAh cm^{-2} at 0.1C after 60 cycles with electrolyte/sulfur ratio of 6 μL mg^{-1}.

The interlayer is a self-supporting film between the separator and electrode [239]. Various materials, such as Nafion membranes [240], porous carbons [15,241], CNTs [242], GO [243], and metal oxides [244] have been applied to design functional interlayers. However, each of them has drawbacks: nonpolar surface of carbon nanomaterials resulting in a weak affinity to LiPSs, while metal oxides are generally not stable during charge-discharge cycling. To overcome these issues, researchers found that 3D structure of GAs with various modifications has stronger physical and chemical sulfur trapping ability and they are more favorable for electron transfer kinetics compared to 2D and 1D carbon nanomaterials [171,177,245]. The combination of GA as a sulfur host and interlayer based on nitrogen rich graphitic carbon nitride (GCN) was proposed by Wutthiprom et al. [246]. GA acting as a host for sulfur was synthesized under hydrazine (N_2H_4) reduction with the subsequent freeze-drying. The interlayer was constructed from the carbon fiber paper (CFP) substrate, surface of which was coated with GA and GCN (Fig. 10 f). As a result, the cell with bare S@GA demonstrated the specific capacity of 819 mAh g^{-1} at 0.1C, while S@GA cathode with GA/GCN-based interlayer exhibited 1138 mAh g^{-1}. At higher 1 C rate the S@GA with GA/GCN interlayer demonstrated almost 100% Coulombic efficiency with 0.056% capacity fading per cycle after 800 cycles. In addition, the ex-situ XPS analysis of GA/GCN interlayer demonstrated the existence of chemical bonds with sulfur species on its surface, which indicates its strong LiPSs absorption. Further, Tan et al. [220] reported the preparation of rGO@MoS_2 interlayer applied on the commercial Celgard 2400 separator. It was confirmed that the rGO layers acted as a physical barrier for LiPSs shuttle and provided the conductive network, while MoS_2 was responsible for chemical adsorption to LiPSs and catalyzed the transformation of long-chain LiPSs to short-chain acting as a lithium conductor [247,248]. As a result, the cell with rGO/MoS_2 coated separator exhibited the initial capacity of 1121 mAh g^{-1} at 0.2C and after 200 cycles it retained 671 mAh g^{-1} (60%

capacity retention). Shi et al. [249] developed free-standing integrated G/CNT-S@G/CNT composite, in which G/CNT-S acted as cathode and G/CNT as an interlayer, both in the form of GAs with CNTs (Fig. 10 g). To confirm the importance of G/CNT interlayer the electrochemical properties of the integrated G/CNT-S@G/CNT and G/CNT-S (interlayer free) cathodes were investigated. G/CNT-S@G/CNT displayed the initial discharge capacity of 1286 mAh g^{-1} at 0.2C, while this value for G/CNT-S was found to be 1047 mAh g^{-1}. When increasing the current density, higher capacities of 990 mAh g^{-1} at 0.5C (12th cycle), 732 mAh g^{-1} at 1 C (22nd cycle), and 493 mAh g^{-1} at 2 C (32nd cycle) were achieved, in comparison with G/CNT-S (736 mAh g^{-1} at 0.5C (12th cycle), 484 mAh g^{-1} at 1 C (22nd cycle), and 269 mAh g^{-1} at 2 C (32nd cycle)). Such an outstanding electrochemical parameters are mainly attributed to synergistic effect of CNTs and graphene network, which provides porous structure, fast ionic and electronic transfer, high sulfur loading and utilization, as well as mechanical flexibility. The attached interlayer is beneficial to suppress the LiPSs shuttle effect by chemical and physical adsorption, which was also confirmed by the visualized permeation test of 0.1 M of Li_2S_6 tetrahydrofuran (THF) solution and theoretical calculations of the adsorption energies between fabricated interlayer and Li_2S_6 molecules (Fig. 10 h).

To sum up, GAs and their modified forms demonstrate their promise as excellent materials for fabrication of interlayers and modification of separators. Owing to their porous structure, ability to homogeneously disperse various additives and flexibility they can be easily coated to commercial separator without affecting its mechanical properties. These functional coatings are rather beneficial to improve the hydrophilicity of separator's surface, improve its interaction with electrolyte and create an additional physical barrier for LiPSs physical and chemical capturing. Porous and flexible interlayers based on GAs and their modified forms are also promising to improve the electrochemical performance of the Li–S batteries in course of formation of an additional self-supporting functional layer, which greatly suppress the diffusion of LiPSs by chemical interaction, physical blocking and catalytic oxidation of sulfur species, leading to enhanced capacity and cycling performance [239].

5. Summary and perspective

This review outlines recent research breakthroughs on GAs and their modified forms (heteroatom-doped GAs, GAs with CNTs and porous carbons and metal-containing compounds) for application in Li–S cell as a functional sulfur host, free-standing cathode, interlayer and separator modifier. As reported in previous analysis [169], despite superior specific capacity of sulfur, the Li–S technology can compete with LIBs after reaching the following characteristics: sulfur content higher than 75 wt %, the minimal value of capacity 900 mAh g^{-1} and areal sulfur loading more than 5 mg cm^{-2}. The achievement of these properties will allow to create the Li–S pouch cell with specific energy of 350 Wh kg^{-1}. The use of 3D structured GA of high surface area with additional modifications resulted in formation of highly porous framework for uniform sulfur deposition, which is capable to reduce the LiPSs shuttle effect and volumetric expansion of cell, enhance the overall electrical conductivity of the electrode and facilitate the electrochemical reaction. The main advantage of GAs is the simplicity of their doping and fabricating composites during one-staged hydrothermal synthesis. As revealed, doping GAs with heteroatoms, additions of metal-containing compounds are the effective solutions to enhance their polarity and electrical conductivity and create the additional sites for LiPSs chemical adsorption. The comprehensive study demonstrated that GAs and their modified forms are excellent candidates for a sulfur host with extremely large areal sulfur loading up to ~24 mg cm^{-2}, resulting in a tremendous areal capacity of around 21.8 mAh cm^{-2}, which is higher than that for commercial LIBs (3.0 mAh cm^{-2}). Also, the use of GAs-based porous structure opens a wide opportunity for the development of free-standing electrodes with excellent flexibility and high sulfur content excluding the inactive components such as binders and current collectors. Addition of CNTs to GA is favorable to improve the flexibility of free-standing cathodes and increase the catholyte uptake. Finally, modified GAs can serve as a free-standing interlayer or separator modifier, thus effectively suppressing the LiPSs shuttle effect, improving cathode's conductivity, as well as facilitating the sulfur species conversion rate.

Despite the great progress in Li–S battery technology, there are still several issues need to be solved for its further advancement:

1. To achieve the high capacity and long-term stability, the systematic research should be devoted to the control and optimization of the surface morphology and pore size of carbon host materials, including GAs, to increase both the areal sulfur loading (mg cm^{-2}) and sulfur content (%), which are not linearly dependent. The average areal sulfur loading in carbon-based host materials more often do not exceed 4 mg cm^{-2} with the sulfur content lower than 75% due to their disordered, poorly developed and non-polar structure. The construction of 3D porous architecture with large specific surface area is essential to accomplish high sulfur loading and high sulfur content. The increase in amount of loaded sulfur leads to increase in the Li–S cell's areal capacity, which is the key parameter to open them for industrial application;
2. Conductivity of graphene is often balanced by a number of functional groups and heteroatoms, which are responsible for effective LiPSs adsorbing. To achieve simultaneously high conductivity and high LiPSs adsorption it is necessary to develop novel or optimize the existing composites based on GAs with heteroatom doping, addition of metal oxides, metal sulfides, metal nitrides, metal phosphides, MXenes, MOFs-derived nanoparticles, etc., increasing the surface polarity along with other factors enhancing a weak bonding energy between pristine graphene and LiPSs. Literature survey revealed, that N-doping is the most widely used technique to improve the polarity and electrical conductivity of carbon. However, there are other options like boron and phosphorus doping of carbon which could significantly improve its affinity to LiPSs even at a relatively small content of doped atoms and improve the cell's electrochemical performance and cycling stability. A small number of the research articles devoted to this field must encourage scientists to focus their attention on this direction in future research;
3. To increase the amount of sulfur loading and improve its utilization ratio, the research should be continued on the development of methods for preparation of 3D free-standing cathodes. In this direction, GAs have already proved to be excellent substrates for high sulfur loading with excellent flexibility, absence of binder, which leads to increase in the amount of active material, not blocking the pores of the carbon matrix and the possibility of their utilization directly without current collectors, decreasing the cell's total weight;
4. A small number of works devoted to the use of GAs as an interlayers and separator modifiers for Li–S batteries must encourage scientists to continue the research in this direction. The optimized surface morphology, layer thickness, pore size, ion selectivity, lightweight and additional LiPSs trapping ability of interlayers or modified separators should be considered to design advanced Li–S batteries. In addition, an intense research should be also focused on modifying Li anode to avoid dendrites formation during charge-discharge cycling. Using flexible graphene acting as an artificial SEI to shield the Li anode is one of the promising solutions to eliminate side reactions;
5. Despite the fact that GAs are widely used in Li–S batteries, the mechanism of their interaction with sulfur compounds has not been sufficiently investigated. It is vital to use the existing computational methods, like DFT, quantum/molecular mechanics, molecular dynamics, etc., as well as more advanced in-situ characterization techniques for the design of Li–S batteries with improved energy density and cycling stability.

Overall, GAs and their modified forms offer a great potential to develop each functional constituent for an advanced Li–S battery. On the

cathode side, they encapsulate sulfur, improve the electronic and ionic conductivities and physically and chemically bond the LiPSs preventing their shuttle. GAs are also able to serve as an effective physical barrier to eliminate the shuttle effect when used as both separator modifier and interlayer. Further research should be focused on expanding application of graphene and its derivatives on other parts of Li–S batteries, including separator, electrolyte and anode. To achieve the cell with outstanding electrochemical performance it is necessary to holistically improve each of its parts.

Author role statement

Fail Sultanov: Conceptualization, Writing – original draft, Writing – review & editing; Almagul Mentbayeva: Conceptualization, Supervision, Writing – review & editing; Sandugash Kalybekkyzy: Writing – original draft; Azhar Zhaisanova: Writing – original draft; Seung-Taek Myung: Writing – review & editing, Resources; Zhumabay Bakenov: Conceptualization, Writing – review & editing, Supervision, Funding acquisition.

Declaration of competing interest

The authors declare that they have no known competing financial interests or personal relationships that could have appeared to influence the work reported in this paper.

Data availability

Data will be made available on request.

Acknowledgement

This work was supported by the research grant #51763/ПЦФ-МЦРОАП РК-19 from the Ministry of Digital Development, Innovation and Aerospace Industry of the Republic of Kazakhstan.

References

[1] N. Mahmood, C. Zhang, Y. Hou, Nickel sulfide/nitrogen-doped graphene composites: phase-controlled synthesis and high performance anode materials for lithium ion batteries, Small 9 (2013) 1321–1328, https://doi.org/10.1002/smll.201203032.
[2] A. Manthiram, X. Yu, S. Wang, Lithium battery chemistries enabled by solid-state electrolytes, Nat. Rev. Mater. 2 (2017), 16103, https://doi.org/10.1038/natrevmats.2016.103.
[3] J. Meng, H. Guo, C. Niu, Y. Zhao, L. Xu, Q. Li, L. Mai, Advances in structure and property optimizations of battery electrode materials, Joule 1 (2017) 522–547, https://doi.org/10.1016/j.joule.2017.08.001.
[4] Z.-L. Xu, X. Liu, Y. Luo, L. Zhou, J.-K. Kim, Nanosilicon anodes for high performance rechargeable batteries, Prog. Mater. Sci. 90 (2017) 1–44, https://doi.org/10.1016/j.pmatsci.2017.07.003.
[5] N. Tolganbek, Y. Yerkinbekova, S. Kalybekkyzy, Z. Bakenov, A. Mentbayeva, Current state of high voltage olivine structured LiMPO4 cathode materials for energy storage applications: a review, J. Alloys Compd. 882 (2021), 160774, https://doi.org/10.1016/j.jallcom.2021.160774.
[6] L. Ma, K.E. Hendrickson, S. Wei, L.A. Archer, Nanomaterials: science and applications in the lithium–sulfur battery, Nano Today 10 (2015) 315–338, https://doi.org/10.1016/j.nantod.2015.04.011.
[7] Z.-L. Xu, J.-K. Kim, K. Kang, Carbon nanomaterials for advanced lithium sulfur batteries, Nano Today 19 (2018) 84–107, https://doi.org/10.1016/j.nantod.2018.02.006.
[8] Y. Yang, G. Zheng, Y. Cui, Nanostructured sulfur cathodes, Chem. Soc. Rev. 42 (2013) 3018, https://doi.org/10.1039/c2cs35256g.
[9] Y.-X. Yin, S. Xin, Y.-G. Guo, L.-J. Wan, Lithium-sulfur batteries: electrochemistry, materials, and prospects, Angew. Chem. Int. Ed. 52 (2013) 13186–13200, https://doi.org/10.1002/anie.201304762.
[10] R. Fang, S. Zhao, Z. Sun, D.-W. Wang, H.-M. Cheng, F. Li, More reliable lithium-sulfur batteries: status, solutions and prospects, Adv. Mater. 29 (2017), 1606823, https://doi.org/10.1002/adma.201606823.
[11] W. Yang, W. Yang, A. Song, G. Sun, G. Shao, 3D interconnected porous carbon nanosheets/carbon nanotubes as a polysulfide reservoir for high performance lithium–sulfur batteries, Nanoscale 10 (2018) 816–824, https://doi.org/10.1039/C7NR06805K.
[12] K. Kumaresan, Y. Mikhaylik, R.E. White, A mathematical model for a lithium–sulfur cell, J. Electrochem. Soc. 155 (2008) A576, https://doi.org/10.1149/1.2937304.
[13] D.-W. Wang, Q. Zeng, G. Zhou, L. Yin, F. Li, H.-M. Cheng, I.R. Gentle, G.Q.M. Lu, Carbon–sulfur composites for Li–S batteries: status and prospects, J. Mater. Chem. A. 1 (2013) 9382, https://doi.org/10.1039/c3ta11045a.
[14] X. Ji, L.F. Nazar, Advances in Li–S batteries, J. Mater. Chem. 20 (2010) 9821, https://doi.org/10.1039/b925751a.
[15] Y.-S. Su, A. Manthiram, Lithium–sulphur batteries with a microporous carbon paper as a bifunctional interlayer, Nat. Commun. 3 (2012) 1166, https://doi.org/10.1038/ncomms2163.
[16] Y.V. Mikhaylik, J.R. Akridge, Low temperature performance of Li/S batteries, J. Electrochem. Soc. 150 (2003) A306, https://doi.org/10.1149/1.1545452.
[17] A.F. Hofmann, D.N. Fronczek, W.G. Bessler, Mechanistic modeling of polysulfide shuttle and capacity loss in lithium–sulfur batteries, J. Power Sources 259 (2014) 300–310, https://doi.org/10.1016/j.jpowsour.2014.02.082.
[18] S.-H. Chung, A. Manthiram, Carbonized eggshell membrane as a natural polysulfide reservoir for highly reversible Li-S batteries, Adv. Mater. 26 (2014) 1360–1365, https://doi.org/10.1002/adma.201304365.
[19] S.-H. Chung, A. Manthiram, Lithium–sulfur batteries with superior cycle stability by employing porous current collectors, Electrochim. Acta 107 (2013) 569–576, https://doi.org/10.1016/j.electacta.2013.06.034.
[20] J. Guo, Y. Xu, C. Wang, Sulfur-impregnated disordered carbon nanotubes cathode for lithium–sulfur batteries, Nano Lett. 11 (2011) 4288–4294, https://doi.org/10.1021/nl202297p.
[21] X. Ji, K.T. Lee, L.F. Nazar, A highly ordered nanostructured carbon–sulphur cathode for lithium–sulphur batteries, Nat. Mater. 8 (2009) 500–506, https://doi.org/10.1038/nmat2460.
[22] C. Zhang, H.B. Wu, C. Yuan, Z. Guo, X.W.D. Lou, Confining sulfur in double-shelled hollow carbon spheres for lithium-sulfur batteries, Angew. Chem. Int. Ed. 51 (2012) 9592–9595, https://doi.org/10.1002/anie.201205292.
[23] J. Zhang, C.-P. Yang, Y.-X. Yin, L.-J. Wan, Y.-G. Guo, Sulfur encapsulated in graphitic carbon nanocages for high-rate and long-cycle lithium-sulfur batteries, Adv. Mater. 28 (2016) 9539–9544, https://doi.org/10.1002/adma.201602913.
[24] Q. Zhu, Q. Zhao, Y. An, B. Anasori, H. Wang, B. Xu, Ultra-microporous carbons encapsulate small sulfur molecules for high performance lithium-sulfur battery, Nano Energy 33 (2017) 402–409, https://doi.org/10.1016/j.nanoen.2017.01.060.
[25] Z. Zhang, L.-L. Kong, S. Liu, G.-R. Li, X.-P. Gao, A high-efficiency sulfur/carbon composite based on 3D graphene Nanosheet@Carbon nanotube matrix as cathode for lithium-sulfur battery, Adv. Energy Mater. 7 (2017), 1602543, https://doi.org/10.1002/aenm.201602543.
[26] H. Wang, X. Yuan, G. Zeng, Y. Wu, Y. Liu, Q. Jiang, S. Gu, Three dimensional graphene based materials: synthesis and applications from energy storage and conversion to electrochemical sensor and environmental remediation, Adv. Colloid Interface Sci. 221 (2015) 41–59, https://doi.org/10.1016/j.cis.2015.04.005.
[27] L. Ma, H.L. Zhuang, S. Wei, K.E. Hendrickson, M.S. Kim, G. Cohn, R.G. Hennig, L. A. Archer, Enhanced Li–S batteries using amine-functionalized carbon nanotubes in the cathode, ACS Nano 10 (2016) 1050–1059, https://doi.org/10.1021/acsnano.5b06373.
[28] C. Zu, Y. Fu, A. Manthiram, Highly reversible Li/dissolved polysulfide batteries with binder-free carbon nanofiber electrodes, J. Mater. Chem. A. 1 (2013), 10362, https://doi.org/10.1039/c3ta11958k.
[29] R. Fang, S. Zhao, P. Hou, M. Cheng, S. Wang, H.-M. Cheng, C. Liu, F. Li, 3D interconnected electrode materials with ultrahigh areal sulfur loading for Li-S batteries, Adv. Mater. 28 (2016) 3374–3382, https://doi.org/10.1002/adma.201506014.
[30] S. Kalybekkyzy, A. Mentbayeva, Y. Yerkinbekova, N. Baikalov, M.V. Kahraman, Z. Bakenov, Electrospun 3D structured carbon current collector for Li/S batteries, Nanomaterials 10 (2020) 745, https://doi.org/10.3390/nano10040745.
[31] H.-J. Peng, Q. Zhang, Designing host materials for sulfur cathodes: from physical confinement to surface chemistry, Angew. Chem. Int. Ed. 54 (2015) 11018–11020, https://doi.org/10.1002/anie.201505444.
[32] D. Su, M. Cortie, G. Wang, Fabrication of N-doped graphene–carbon nanotube hybrids from prussian blue for lithium–sulfur batteries, Adv. Energy Mater. 7 (2017), 1602014, https://doi.org/10.1002/aenm.201602014.
[33] G. Zhou, E. Paek, G.S. Hwang, A. Manthiram, Long-life Li/polysulphide batteries with high sulphur loading enabled by lightweight three-dimensional nitrogen/sulphur-codoped graphene sponge, Nat. Commun. 6 (2015) 7760, https://doi.org/10.1038/ncomms8760.
[34] H. Yuan, W. Zhang, J. Wang, G. Zhou, Z. Zhuang, J. Luo, H. Huang, Y. Gan, C. Liang, Y. Xia, J. Zhang, X. Tao, Facilitation of sulfur evolution reaction by pyridinic nitrogen doped carbon nanoflakes for highly-stable lithium-sulfur batteries, Energy Storage Mater. 10 (2018) 1–9, https://doi.org/10.1016/j.ensm.2017.07.015.
[35] Z. Li, J. Zhang, B. Guan, D. Wang, L.-M. Liu, X.W. Lou, A sulfur host based on titanium monoxide@carbon hollow spheres for advanced lithium–sulfur batteries, Nat. Commun. 7 (2016), 13065, https://doi.org/10.1038/ncomms13065.
[36] L. Ma, R. Chen, G. Zhu, Y. Hu, Y. Wang, T. Chen, J. Liu, Z. Jin, Cerium oxide nanocrystal embedded bimodal micromesoporous nitrogen-rich carbon nanospheres as effective sulfur host for lithium–sulfur batteries, ACS Nano 11 (2017) 7274–7283, https://doi.org/10.1021/acsnano.7b03227.
[37] M. Xiang, H. Wu, H. Liu, J. Huang, Y. Zheng, L. Yang, P. Jing, Y. Zhang, S. Dou, H. Liu, A flexible 3D multifunctional MgO-decorated carbon Foam@CNTs hybrid as self-supported cathode for high-performance lithium-sulfur batteries, Adv. Funct. Mater. 27 (2017), 1702573, https://doi.org/10.1002/adfm.201702573.

[38] W. Xue, Q.-B. Yan, G. Xu, L. Suo, Y. Chen, C. Wang, C.-A. Wang, J. Li, Double-oxide sulfur host for advanced lithium-sulfur batteries, Nano Energy 38 (2017) 12–18, https://doi.org/10.1016/j.nanoen.2017.05.041.

[39] H. Li, J. Wang, Y. Zhang, Y. Wang, A. Mentbayeva, Z. Bakenov, Synthesis of carbon coated Fe3O4 grown on graphene as effective sulfur-host materials for advanced lithium/sulfur battery, J. Power Sources 437 (2019), 226901, https://doi.org/10.1016/j.jpowsour.2019.226901.

[40] Z. Xiao, Z. Yang, L. Zhang, H. Pan, R. Wang, Sandwich-type NbS $_2$ @S@I-doped graphene for high-sulfur-loaded, ultrahigh-rate, and long-life lithium–sulfur batteries, ACS Nano 11 (2017) 8488–8498, https://doi.org/10.1021/acsnano.7b04442.

[41] T. Chen, Z. Zhang, B. Cheng, R. Chen, Y. Hu, L. Ma, G. Zhu, J. Liu, Z. Jin, Self-templated formation of interlaced carbon nanotubes threaded hollow Co $_3$ S $_4$ nanoboxes for high-rate and heat-resistant lithium–sulfur batteries, J. Am. Chem. Soc. 139 (2017) 12710–12715, https://doi.org/10.1021/jacs.7b06973.

[42] T. Chen, L. Ma, B. Cheng, R. Chen, Y. Hu, G. Zhu, Y. Wang, J. Liang, Z. Tie, J. Liu, Z. Jin, Metallic and polar Co 9 S 8 inlaid carbon hollow nanopolyhedra as efficient polysulfide mediator for lithium−sulfur batteries, Nano Energy 38 (2017) 239–248, https://doi.org/10.1016/j.nanoen.2017.05.064.

[43] J. Pu, Z. Shen, J. Zheng, W. Wu, C. Zhu, Q. Zhou, H. Zhang, F. Pan, Multifunctional Co 3 S 4 @sulfur nanotubes for enhanced lithium-sulfur battery performance, Nano Energy 37 (2017) 7–14, https://doi.org/10.1016/j.nanoen.2017.05.009.

[44] D.-R. Deng, F. Xue, Y.-J. Jia, J.-C. Ye, C.-D. Bai, M.-S. Zheng, Q.-F. Dong, Co $_4$ N nanosheet assembled mesoporous sphere as a matrix for ultrahigh sulfur content lithium–sulfur batteries, ACS Nano 11 (2017) 6031–6039, https://doi.org/10.1021/acsnano.7b01945.

[45] X. Li, K. Ding, B. Gao, Q. Li, Y. Li, J. Fu, X. Zhang, P.K. Chu, K. Huo, Freestanding carbon encapsulated mesoporous vanadium nitride nanowires enable highly stable sulfur cathodes for lithium-sulfur batteries, Nano Energy 40 (2017) 655–662, https://doi.org/10.1016/j.nanoen.2017.09.018.

[46] Z. Sun, J. Zhang, L. Yin, G. Hu, R. Fang, H.-M. Cheng, F. Li, Conductive porous vanadium nitride/graphene composite as chemical anchor of polysulfides for lithium-sulfur batteries, Nat. Commun. 8 (2017), 14627, https://doi.org/10.1038/ncomms14627.

[47] H. Yuan, X. Chen, G. Zhou, W. Zhang, J. Luo, H. Huang, Y. Gan, C. Liang, Y. Xia, J. Zhang, J. Wang, X. Tao, Efficient activation of Li $_2$ S by transition metal phosphides nanoparticles for highly stable lithium–sulfur batteries, ACS Energy Lett. 2 (2017) 1711–1719, https://doi.org/10.1021/acsenergylett.7b00465.

[48] R. Fang, S. Zhao, Z. Sun, D.-W. Wang, R. Amal, S. Wang, H.-M. Cheng, F. Li, Polysulfide immobilization and conversion on a conductive polar MoC@MoOx material for lithium-sulfur batteries, Energy Storage Mater. 10 (2018) 56–61, https://doi.org/10.1016/j.ensm.2017.08.005.

[49] J. Xie, L. Niu, Y. Qiao, Y. Lei, G. Li, X. Zhang, P. Chen, The influence of the drying method on the microstructure and the compression behavior of graphene aerogel, Diam. Relat. Mater. 121 (2022), 108772, https://doi.org/10.1016/j.diamond.2021.108772.

[50] E. Garcia-Bordejé, A.M. Benito, W.K. Maser, Graphene aerogels via hydrothermal gelation of graphene oxide colloids: fine-tuning of its porous and chemical properties and catalytic applications, Adv. Colloid Interface Sci. 292 (2021), 102420, https://doi.org/10.1016/j.cis.2021.102420.

[51] W. Chen, P. Xiao, H. Chen, H. Zhang, Q. Zhang, Y. Chen, Polymeric graphene bulk materials with a 3D cross-linked monolithic graphene network, Adv. Mater. 31 (2019), 1802403, https://doi.org/10.1002/adma.201802403.

[52] J. Phiri, L.-S. Johansson, P. Gane, T. Maloney, A comparative study of mechanical, thermal and electrical properties of graphene-, graphene oxide- and reduced graphene oxide-doped microfibrillated cellulose nanocomposites, Compos. B Eng. 147 (2018) 104–113, https://doi.org/10.1016/j.compositesb.2018.04.018.

[53] X. Cao, J. Zhang, S. Chen, R.J. Varley, K. Pan, 1D/2D nanomaterials synergistic, compressible, and response rapidly 3D graphene aerogel for piezoresistive sensor, Adv. Funct. Mater. 30 (2020), 2003618, https://doi.org/10.1002/adfm.202003618.

[54] X. Song, Y. Chen, M. Rong, Z. Xie, T. Zhao, Y. Wang, X. Chen, O.S. Wolfbeis, A phytic acid induced super-amphiphilic multifunctional 3D graphene-based foam, Angew. Chem. Int. Ed. 55 (2016) 3936–3941, https://doi.org/10.1002/anie.201511064.

[55] S. Stankovich, D.A. Dikin, G.H.B. Dommett, K.M. Kohlhaas, E.J. Zimney, E. A. Stach, R.D. Piner, S.T. Nguyen, R.S. Ruoff, Graphene-based composite materials, Nature 442 (2006) 282–286, https://doi.org/10.1038/nature04969.

[56] G. Nassar, E. Daou, R. Najjar, M. Bassil, R. Habchi, A review on the current research on graphene-based aerogels and their applications, Carbon Trends 4 (2021), 100065, https://doi.org/10.1016/j.cartre.2021.100065.

[57] Y.Z.N. Htwe, M. Mariatti, Printed graphene and hybrid conductive inks for flexible, stretchable, and wearable electronics: progress, opportunities, and challenges, J. Sci. Adv. Mater. Devices. 7 (2022), 100435, https://doi.org/10.1016/j.jsamd.2022.100435.

[58] Z. Saleki, A.J. Majarshin, Y.-A. Luo, D.-L. Zhang, Spectral statistics of a 1D photonic crystal containing an anisotropic graphene-based hyperbolic metamaterial defect layer, Opt. Mater. 121 (2021), 111483, https://doi.org/10.1016/j.optmat.2021.111483.

[59] P. Yang, X. Yang, W. Liu, R. Guo, Z. Yao, Graphene-based electrocatalysts for advanced energy conversion, Green Energy Environ (2022), https://doi.org/10.1016/j.gee.2022.06.008. S2468025722001042.

[60] A. Nag, R.B.V.B. Simorangkir, D.R. Gawade, S. Nuthalapati, J.L. Buckley, B. O'Flynn, M.E. Altinsoy, S.C. Mukhopadhyay, Graphene-based wearable temperature sensors: a review, Mater. Des. 221 (2022), 110971, https://doi.org/10.1016/j.matdes.2022.110971.

[61] M. Azizi-Lalabadi, S.M. Jafari, Bio-nanocomposites of graphene with biopolymers; fabrication, properties, and applications, Adv. Colloid Interface Sci. 292 (2021), 102416, https://doi.org/10.1016/j.cis.2021.102416.

[62] F. Sultanov, C. Daulbayev, B. Bakbolat, O. Daulbayev, Advances of 3D graphene and its composites in the field of microwave absorption, Adv. Colloid Interface Sci. 285 (2020), 102281, https://doi.org/10.1016/j.cis.2020.102281.

[63] D. Zhi, T. Li, J. Li, H. Ren, F. Meng, A review of three-dimensional graphene-based aerogels: synthesis, structure and application for microwave absorption, Compos. B Eng. 211 (2021), https://doi.org/10.1016/j.compositesb.2021.108642.

[64] N. Talukder, Y. Wang, B.B. Nunna, E.S. Lee, Nitrogen-doped graphene nanomaterials for electrochemical catalysis/reactions: a review on chemical structures and stability, Carbon 185 (2021) 198–214, https://doi.org/10.1016/j.carbon.2021.09.025.

[65] Y.-H. Li, Z.-R. Tang, Y.-J. Xu, Multifunctional graphene-based composite photocatalysts oriented by multifaced roles of graphene in photocatalysis, Chin. J. Catal. 43 (2022) 708–730, https://doi.org/10.1016/S1872-2067(21)63871-8.

[66] N. Nirmala, V. Shriniti, K. Aasresha, J. Arun, K.P. Gopinath, S.S. Dawn, A. Sheeladevi, P. Priyadharsini, K. Birindhadevi, N.T.L. Chi, A. Pugazhendhi, Removal of toxic metals from wastewater environment by graphene-based composites: a review on isotherm and kinetic models, recent trends, challenges and future directions, Sci. Total Environ. 840 (2022), 156564, https://doi.org/10.1016/j.scitotenv.2022.156564.

[67] A.I. Kamisan, T.I. Tunku Kudin, A.S. Kamisan, A.F. Che Omar, M.F. Mohamad Taib, O.H. Hassan, A.M.M. Ali, M.Z.A. Yahya, Recent advances on graphene-based materials as cathode materials in lithium-sulfur batteries, Int. J. Hydrogen Energy 47 (2022) 8630–8657, https://doi.org/10.1016/j.ijhydene.2021.12.166.

[68] H.-F. Ju, W.-L. Song, L.-Z. Fan, Rational design of graphene/porous carbon aerogels for high-performance flexible all-solid-state supercapacitors, J. Mater. Chem. 2 (2014) 10895–10903, https://doi.org/10.1039/C4TA00538D.

[69] M. Kotal, J. Kim, J. Oh, I.-K. Oh, Recent progress in multifunctional graphene aerogels, Front. Mater. 3 (2016), https://doi.org/10.3389/fmats.2016.00029.

[70] Y. Xu, G. Shi, X. Duan, Self-assembled three-dimensional graphene macrostructures: synthesis and applications in supercapacitors, Acc. Chem. Res. 48 (2015) 1666–1675, https://doi.org/10.1021/acs.accounts.5b00117.

[71] S. Ye, Y. Liu, J. Feng, Low-density, mechanical compressible, water-induced self-recoverable graphene aerogels for water treatment, ACS Appl. Mater. Interfaces 9 (2017) 22456–22464, https://doi.org/10.1021/acsami.7b04536.

[72] Y.-J. Wan, P.-L. Zhu, S.-H. Yu, R. Sun, C.-P. Wong, W.-H. Liao, Ultralight, super-elastic and volume-preserving cellulose fiber/graphene aerogel for high-performance electromagnetic interference shielding, Carbon 115 (2017) 629–639, https://doi.org/10.1016/j.carbon.2017.01.054.

[73] S. Nardecchia, D. Carriazo, M.L. Ferrer, M.C. Gutiérrez, F. del Monte, Three dimensional macroporous architectures and aerogels built of carbon nanotubes and/or graphene: synthesis and applications, Chem. Soc. Rev. 42 (2013) 794–830, https://doi.org/10.1039/C2CS35353A.

[74] J. Li, J. Li, H. Meng, S. Xie, B. Zhang, L. Li, H. Ma, J. Zhang, M. Yu, Ultra-light, compressible and fire-resistant graphene aerogel as a highly efficient and recyclable absorbent for organic liquids, J. Mater. Chem. A. 2 (2014) 2934, https://doi.org/10.1039/c3ta14725h.

[75] G. Gorgolis, C. Galiotis, Graphene aerogels: a review, 2D Mater. 4 (2017), 032001, https://doi.org/10.1088/2053-1583/aa7883.

[76] J. Mao, J. Iocozzia, J. Huang, K. Meng, Y. Lai, Z. Lin, Graphene aerogels for efficient energy storage and conversion, Energy Environ. Sci. 11 (2018) 772–799, https://doi.org/10.1039/C7EE03031B.

[77] Y. Xu, K. Sheng, C. Li, G. Shi, Self-assembled graphene hydrogel *via* a one-step hydrothermal process, ACS Nano 4 (2010) 4324–4330, https://doi.org/10.1021/nn101187z.

[78] W. Wan, F. Zhang, S. Yu, R. Zhang, Y. Zhou, Hydrothermal formation of graphene aerogel for oil sorption: the role of reducing agent, reaction time and temperature, New J. Chem. 40 (2016) 3040–3046, https://doi.org/10.1039/C5NJ03086B.

[79] Y. Tong, M. He, Y. Zhou, S. Nie, X. Zhong, L. Fan, T. Huang, Q. Liao, Y. Wang, Three-Dimensional hierarchical architecture of the TiO $_2$/Ti $_3$ C $_2$ T $_{x\ /RGO}$ ternary composite aerogel for enhanced electromagnetic wave absorption, ACS Sustain. Chem. Eng. 6 (2018) 8212–8222, https://doi.org/10.1021/acssuschemeng.7b04883.

[80] J. Tang, N. Liang, L. Wang, J. Li, G. Tian, D. Zhang, S. Feng, H. Yue, Three-dimensional nitrogen-doped reduced graphene oxide aerogel decorated with Ni nanoparticles with tunable and unique microwave absorption, Carbon 152 (2019) 575–586, https://doi.org/10.1016/j.carbon.2019.06.049.

[81] R. Shu, Z. Wan, J. Zhang, Y. Wu, Y. Liu, J. Shi, M. Zheng, Facile design of three-dimensional nitrogen-doped reduced graphene oxide/multi-walled carbon nanotube composite foams as lightweight and highly efficient microwave absorbers, ACS Appl. Mater. Interfaces 12 (2020) 4689–4698, https://doi.org/10.1021/acsami.9b16134.

[82] D. Xu, S. Yang, P. Chen, Q. Yu, X. Xiong, J. Wang, Synthesis of magnetic graphene aerogels for microwave absorption by in-situ pyrolysis, Carbon 146 (2019) 301–312, https://doi.org/10.1016/j.carbon.2019.02.005.

[83] I.K. Moon, S. Yoon, K.-Y. Chun, J. Oh, Highly elastic and conductive N-doped monolithic graphene aerogels for multifunctional applications, Adv. Funct. Mater. 25 (2015) 6976–6984, https://doi.org/10.1002/adfm.201502395.

[84] A. Li, C. Zhang, Y.-F. Zhang, Thermal conductivities of PU composites with graphene aerogels reduced by different methods, Composer Part Appl. Sci. Manuf. 103 (2017) 161–167, https://doi.org/10.1016/j.compositesa.2017.10.004.
[85] W. Chen, L. Yan, In situ self-assembly of mild chemical reduction graphene for three-dimensional architectures, Nanoscale 3 (2011) 3132, https://doi.org/10.1039/c1nr10355e.
[86] J. Shen, P. Zhang, L. Song, J. Li, B. Ji, J. Li, L. Chen, Polyethylene glycol supported by phosphorylated polyvinyl alcohol/graphene aerogel as a high thermal stability phase change material, Compos. B Eng. 179 (2019), 107545, https://doi.org/10.1016/j.compositesb.2019.107545.
[87] Q. Guo, S. Chen, Z. Liu, J. Yan, H. Liu, Preparation and performance evaluation of graphene/hydroxypropyl methylcellulose composite aerogel for high viscosity oil adsorption, J. Environ. Chem. Eng. 10 (2022), 108312, https://doi.org/10.1016/j.jece.2022.108312.
[88] K. Ghosh, C.Y. Yue, M.M. Sk, R.K. Jena, S. Bi, Development of a 3D graphene aerogel and 3D porous graphene/MnO 2 @polyaniline hybrid film for all-solid-state flexible asymmetric supercapacitors, Sustain. Energy Fuels 2 (2018) 280–293, https://doi.org/10.1039/C7SE00433H.
[89] X. Jiang, Y. Ma, J. Li, Q. Fan, W. Huang, Self-assembly of reduced graphene oxide into three-dimensional architecture by divalent ion linkage, J. Phys. Chem. C 114 (2010) 22462–22465, https://doi.org/10.1021/jp108081g.
[90] M.A. Worsley, P.J. Pauzauskie, T.Y. Olson, J. Biener, J.H. Satcher, T.F. Baumann, Synthesis of graphene aerogel with high electrical conductivity, J. Am. Chem. Soc. 132 (2010) 14067–14069, https://doi.org/10.1021/ja1072299.
[91] C. Zhu, T.Y.-J. Han, E.B. Duoss, A.M. Golobic, J.D. Kuntz, C.M. Spadaccini, M. A. Worsley, Highly compressible 3D periodic graphene aerogel microlattices, Nat. Commun. 6 (2015) 6962, https://doi.org/10.1038/ncomms7962.
[92] Q. Zhang, F. Zhang, S.P. Medarametla, H. Li, C. Zhou, D. Lin, 3D printing of graphene aerogels, Small 12 (2016) 1702–1708, https://doi.org/10.1002/smll.201503524.
[93] X. Zhou, Y. Li, G. Ma, Q. Ma, Z. Lei, One-step solid-state synthesis of sulfur-reduced graphene oxide composite for lithium-sulfur batteries, J. Alloys Compd. 685 (2016) 216–221, https://doi.org/10.1016/j.jallcom.2016.05.171.
[94] Z. Wang, Y. Dong, H. Li, Z. Zhao, H. Bin Wu, C. Hao, S. Liu, J. Qiu, X.W. Lou, Enhancing lithium–sulphur battery performance by strongly binding the discharge products on amino-functionalized reduced graphene oxide, Nat. Commun. 5 (2014) 5002, https://doi.org/10.1038/ncomms6002.
[95] Y. Zhang, L. Sun, H. Li, T. Tan, J. Li, Porous three-dimensional reduced graphene oxide for high-performance lithium-sulfur batteries, J. Alloys Compd. 739 (2018) 290–297, https://doi.org/10.1016/j.jallcom.2017.12.294.
[96] Y. Mao, G. Li, Y. Guo, Z. Li, C. Liang, X. Peng, Z. Lin, Foldable interpenetrated metal-organic frameworks/carbon nanotubes thin film for lithium–sulfur batteries, Nat. Commun. 8 (2017), 14628, https://doi.org/10.1038/ncomms14628.
[97] G. Hu, C. Xu, Z. Sun, S. Wang, H.-M. Cheng, F. Li, W. Ren, 3D graphene-foam-reduced-graphene-oxide hybrid nested hierarchical networks for high-performance Li-S batteries, Adv. Mater. 28 (2016) 1603–1609, https://doi.org/10.1002/adma.201504765.
[98] J. Lee, S.-K. Park, Y. Piao, N-Doped carbon framework/reduced graphene oxide nanocomposite as a sulfur reservoir for lithium-sulfur batteries, Electrochim. Acta 222 (2016) 1345–1353, https://doi.org/10.1016/j.electacta.2016.11.110.
[99] Y. Hou, J. Li, X. Gao, Z. Wen, C. Yuan, J. Chen, 3D dual-confined sulfur encapsulated in porous carbon nanosheets and wrapped with graphene aerogels as a cathode for advanced lithium sulfur batteries, Nanoscale 8 (2016) 8228–8235, https://doi.org/10.1039/C5NR09037G.
[100] M. Wu, Y. Cui, Y. Fu, Li 2 S nanocrystals confined in free-standing carbon paper for high performance lithium–sulfur batteries, ACS Appl. Mater. Interfaces 7 (2015) 21479–21486, https://doi.org/10.1021/acsami.5b06615.
[101] L. Yin, J. Wang, X. Yu, C.W. Monroe, Y. NuLi, J. Yang, Dual-mode sulfur-based cathode materials for rechargeable Li–S batteries, Chem. Commun. 48 (2012) 7868, https://doi.org/10.1039/c2cc33333c.
[102] F. Nitze, M. Agostini, F. Lundin, A.E.C. Palmqvist, A. Matic, A binder-free sulfur/reduced graphene oxide aerogel as high performance electrode materials for lithium sulfur batteries, Sci. Rep. 6 (2016), 39615, https://doi.org/10.1038/srep39615.
[103] G. Zhou, E. Paek, G.S. Hwang, A. Manthiram, High-performance lithium-sulfur batteries with a self-supported, 3D Li 2 S-doped graphene aerogel cathodes, Adv. Energy Mater. 6 (2016), 1501355, https://doi.org/10.1002/aenm.201501355.
[104] Y. Jiang, M. Lu, X. Ling, Z. Jiao, L. Chen, L. Chen, P. Hu, B. Zhao, One-step hydrothermal synthesis of three-dimensional porous graphene aerogels/sulfur nanocrystals for lithium–sulfur batteries, J. Alloys Compd. 645 (2015) 509–516, https://doi.org/10.1016/j.jallcom.2015.05.125.
[105] B. Li, Q. Xiao, Y. Luo, A modified synthesis process of three-dimensional sulfur/graphene aerogel as binder-free cathode for lithium-sulfur batteries, Mater. Des. 153 (2018) 9–14, https://doi.org/10.1016/j.matdes.2018.04.078.
[106] Z. Wang, C. Xu, L. Chen, J. Si, W. Li, S. Huang, Y. Jiang, Z. Chen, B. Zhao, In-situ lithiation synthesis of nano-sized lithium sulfide/graphene aerogel with covalent bond interaction for inhibiting the polysulfides shuttle of Li-S batteries, Electrochim. Acta 312 (2019) 282–290, https://doi.org/10.1016/j.electacta.2019.04.169.
[107] Z.-Z. Pan, W. Lv, Y.-B. He, Y. Zhao, G. Zhou, L. Dong, S. Niu, C. Zhang, R. Lyu, C. Wang, H. Shi, W. Zhang, F. Kang, H. Nishihara, Q.-H. Yang, A nacre-like carbon nanotube sheet for high performance Li-polysulfide batteries with high sulfur loading, Adv. Sci. 5 (2018), 1800384, https://doi.org/10.1002/advs.201800384.
[108] R. Xu, I. Belharouak, J.C.M. Li, X. Zhang, I. Bloom, J. Bareño, Role of polysulfides in self-healing lithium-sulfur batteries, Adv. Energy Mater. 3 (2013) 833–838, https://doi.org/10.1002/aenm.201200990.
[109] L. Borchardt, H. Althues, S. Kaskel, Carbon nano-composites for lithium–sulfur batteries, Curr. Opin. Green Sustain. Chem. 4 (2017) 64–71, https://doi.org/10.1016/j.cogsc.2017.02.008.
[110] W. Li, H. Yao, K. Yan, G. Zheng, Z. Liang, Y.-M. Chiang, Y. Cui, The synergetic effect of lithium polysulfide and lithium nitrate to prevent lithium dendrite growth, Nat. Commun. 6 (2015) 7436, https://doi.org/10.1038/ncomms8436.
[111] H. Peng, G. Ma, K. Sun, Z. Zhang, J. Li, X. Zhou, Z. Lei, A novel aqueous asymmetric supercapacitor based on petal-like cobalt selenide nanosheets and nitrogen-doped porous carbon networks electrodes, J. Power Sources 297 (2015) 351–358, https://doi.org/10.1016/j.jpowsour.2015.08.025.
[112] H. Pan, J. Chen, R. Cao, V. Murugesan, N.N. Rajput, K.S. Han, K. Persson, L. Estevez, M.H. Engelhard, J.-G. Zhang, K.T. Mueller, Y. Cui, Y. Shao, J. Liu, Non-encapsulation approach for high-performance Li–S batteries through controlled nucleation and growth, Nat. Energy 2 (2017) 813–820, https://doi.org/10.1038/s41560-017-0005-z.
[113] M. Agostini, D.-H. Lim, M. Sadd, J.-Y. Hwang, S. Brutti, J.W. Heo, J.H. Ahn, Y. K. Sun, A. Matic, Rational design of low cost and high energy lithium batteries through tailored fluorine-free electrolyte and nanostructured S/C composite, ChemSusChem 11 (2018) 2981–2986, https://doi.org/10.1002/cssc.201801017.
[114] D.-H. Lim, M. Agostini, F. Nitze, J. Manuel, J.-H. Ahn, A. Matic, Route to sustainable lithium-sulfur batteries with high practical capacity through a fluorine free polysulfide catholyte and self-standing Carbon Nanofiber membranes, Sci. Rep. 7 (2017) 6327, https://doi.org/10.1038/s41598-017-06593-2.
[115] C. Cavallo, M. Agostini, J.P. Genders, M.E. Abdelhamid, A. Matic, A free-standing reduced graphene oxide aerogel as supporting electrode in a fluorine-free Li2S8 catholyte Li-S battery, J. Power Sources 416 (2019) 111–117, https://doi.org/10.1016/j.jpowsour.2019.01.081.
[116] D.H. Wang, D. Xie, T. Yang, Y. Zhong, X.L. Wang, X.H. Xia, C.D. Gu, J.P. Tu, Li 2 S@C composite incorporated into 3D reduced graphene oxide as a cathode material for lithium-sulfur batteries, J. Power Sources 313 (2016) 233–239, https://doi.org/10.1016/j.jpowsour.2016.03.001.
[117] H. Kim, H.-D. Lim, J. Kim, K. Kang, Graphene for advanced Li/S and Li/air batteries, J. Mater. Chem. 2 (2014) 33–47, https://doi.org/10.1039/C3TA12522J.
[118] S.-K. Lee, Y.J. Lee, Y.-K. Sun, Nanostructured lithium sulfide materials for lithium-sulfur batteries, J. Power Sources 323 (2016) 174–188, https://doi.org/10.1016/j.jpowsour.2016.05.037.
[119] M. Agostini, J. Hassoun, J. Liu, M. Jeong, H. Nara, T. Momma, T. Osaka, Y.-K. Sun, B. Scrosati, A lithium-ion sulfur battery based on a carbon-coated lithium-sulfide cathode and an electrodeposited silicon-based anode, ACS Appl. Mater. Interfaces 6 (2014) 10924–10928, https://doi.org/10.1021/am4057166.
[120] X. Li, M. Gao, W. Du, B. Ni, Y. Wu, Y. Liu, C. Shang, Z. Guo, H. Pan, A mechanochemical synthesis of submicron-sized Li 2 S and a mesoporous Li 2 S/C hybrid for high performance lithium/sulfur battery cathodes, J. Mater. Chem. A. 5 (2017) 6471–6482, https://doi.org/10.1039/C7TA00557A.
[121] Y. Jung, B. Kang, Understanding abnormal potential behaviors at the 1st charge in Li 2 S cathode material for rechargeable Li–S batteries, Phys. Chem. Chem. Phys. 18 (2016) 21500–21507, https://doi.org/10.1039/C6CP03146C.
[122] C. Wang, X. Wang, Y. Yang, A. Kushima, J. Chen, Y. Huang, J. Li, Slurryless Li 2 S/reduced graphene oxide cathode paper for high-performance lithium sulfur battery, Nano Lett. 15 (2015) 1796–1802, https://doi.org/10.1021/acs.nanolett.5b00112.
[123] K. Zhang, L. Wang, Z. Hu, F. Cheng, J. Chen, Ultrasmall Li2S nanoparticles anchored in graphene nanosheets for high-energy lithium-ion batteries, Sci. Rep. 4 (2015) 6467, https://doi.org/10.1038/srep06467.
[124] J. Song, Z. Yu, M.L. Gordin, D. Wang, Advanced sulfur cathode enabled by highly crumpled nitrogen-doped graphene sheets for high-energy-density lithium–sulfur batteries, Nano Lett. 16 (2016) 864–870, https://doi.org/10.1021/acs.nanolett.5b03217.
[125] S.-K. Liu, X.-B. Hong, Y.-J. Li, J. Xu, C.-M. Zheng, K. Xie, A nanoporous nitrogen-doped graphene for high performance lithium sulfur batteries, Chin. Chem. Lett. 28 (2017) 412–416, https://doi.org/10.1016/j.cclet.2016.10.038.
[126] J. Xu, D. Su, W. Zhang, W. Bao, G. Wang, A nitrogen–sulfur co-doped porous graphene matrix as a sulfur immobilizer for high performance lithium–sulfur batteries, J. Mater. Chem. A. 4 (2016) 17381–17393, https://doi.org/10.1039/C6TA05878G.
[127] J. Wutthiprom, N. Phattharasupakun, J. Khuntilo, T. Maihom, J. Limtrakul, M. Sawangphruk, Collaborative design of Li–S batteries using 3D N-doped graphene aerogel as a sulfur host and graphitic carbon nitride paper as an interlayer, Sustain. Energy Fuels 1 (2017) 1759–1765, https://doi.org/10.1039/C7SE00291B.
[128] W. Gao, Y. Liu, Y. Zhang, N. Baikalov, A. Konarov, Z. Bakenov, Nitrogen-doped graphitized porous carbon with embedded NiFe alloy nanoparticles to enhance electrochemical performance for lithium-sulfur batteries, J. Alloys Compd. 882 (2021), 160728, https://doi.org/10.1016/j.jallcom.2021.160728.
[129] M. Kaur, M. Kaur, V.K. Sharma, Nitrogen-doped graphene and graphene quantum dots: a review onsynthesis and applications in energy, sensors and environment, Adv. Colloid Interface Sci. 259 (2018) 44–64, https://doi.org/10.1016/j.cis.2018.07.001.
[130] T.-Z. Hou, X. Chen, H.-J. Peng, J.-Q. Huang, B.-Q. Li, Q. Zhang, B. Li, Design principles for heteroatom-doped nanocarbon to achieve strong anchoring of

polysulfides for lithium-sulfur batteries, Small 12 (2016) 3283–3291, https://doi.org/10.1002/smll.201600809.
[131] M. Wang, Q. Liang, J. Han, Y. Tao, D. Liu, C. Zhang, W. Lv, Q.-H. Yang, Catalyzing polysulfide conversion by g-C3N4 in a graphene network for long-life lithium-sulfur batteries, Nano Res. 11 (2018) 3480–3489, https://doi.org/10.1007/s12274-018-2023-y.
[132] L. Ma, H. Fan, K. Fu, S. Lei, Q. Hu, H. Huang, G. He, Protonation of graphitic carbon nitride (g-C 3 N 4) for an electrostatically self-assembling Carbon@g-C 3 N 4 core–shell nanostructure toward high hydrogen evolution, ACS Sustain. Chem. Eng. 5 (2017) 7093–7103, https://doi.org/10.1021/acssuschemeng.7b01312.
[133] H. Tian, H. Fan, J. Ma, Z. Liu, L. Ma, S. Lei, J. Fang, C. Long, Pt-decorated zinc oxide nanorod arrays with graphitic carbon nitride nanosheets for highly efficient dual-functional gas sensing, J. Hazard Mater. 341 (2018) 102–111, https://doi.org/10.1016/j.jhazmat.2017.07.056.
[134] M. Zhang, C. Yu, J. Yang, C. Zhao, Z. Ling, J. Qiu, Nitrogen-doped tubular/porous carbon channels implanted on graphene frameworks for multiple confinement of sulfur and polysulfides, J. Mater. Chem. A. 5 (2017) 10380–10386, https://doi.org/10.1039/C7TA01512G.
[135] S. Niu, W. Lv, C. Zhang, Y. Shi, J. Zhao, B. Li, Q.-H. Yang, F. Kang, One-pot self-assembly of graphene/carbon nanotube/sulfur hybrid with three dimensionally interconnected structure for lithium–sulfur batteries, J. Power Sources 295 (2015) 182–189, https://doi.org/10.1016/j.jpowsour.2015.06.122.
[136] J.-H. Kang, J.-S. Chen, Using ethylenediamine to prepare three dimensional nitrogen-doped graphene aerogel/sulfur composite for lithium-sulfur batteries, Diam. Relat. Mater. 88 (2018) 222–229, https://doi.org/10.1016/j.diamond.2018.07.015.
[137] D. Cheng, P. Wu, J. Wang, X. Tang, T. An, H. Zhou, D. Zhang, T. Fan, Synergetic pore structure optimization and nitrogen doping of 3D porous graphene for high performance lithium sulfur battery, Carbon 143 (2019) 869–877, https://doi.org/10.1016/j.carbon.2018.11.032.
[138] Y. Jia, Y.-S. Zhao, X.-X. Yang, M.-X. Ren, Y.-Q. Wang, B.-Y. Lei, D.-L. Zhao, Sulfur encapsulated in nitrogen-doped graphene aerogel as a cathode material for high performance lithium-sulfur batteries, Int. J. Hydrogen Energy 46 (2021) 7642–7652, https://doi.org/10.1016/j.ijhydene.2020.11.199.
[139] H. Wang, C. Zhang, Z. Liu, L. Wang, P. Han, H. Xu, K. Zhang, S. Dong, J. Yao, G. Cui, Nitrogen-doped graphene nanosheets with excellent lithium storage properties, J. Mater. Chem. 21 (2011) 5430, https://doi.org/10.1039/c1jm00049g.
[140] H. Yan, M. Cheng, B. Zhong, Y. Chen, Three-dimensional nitrogen-doped graphene/sulfur composite for lithium-sulfur battery, Ionics 22 (2016) 1999–2006, https://doi.org/10.1007/s11581-016-1739-5.
[141] H.-Y. Zhou, Z.-Y. Sui, S. Liu, H.-Y. Wang, B.-H. Han, Nanostructured porous carbons derived from nitrogen-doped graphene nanoribbon aerogels for lithium–sulfur batteries, J. Colloid Interface Sci. 541 (2019) 204–212, https://doi.org/10.1016/j.jcis.2019.01.067.
[142] L. Chen, R. Du, J. Zhu, Y. Mao, C. Xue, N. Zhang, Y. Hou, J. Zhang, T. Yi, Three-Dimensional nitrogen-doped graphene nanoribbons aerogel as a highly efficient catalyst for the oxygen reduction reaction, Small 11 (2015) 1423–1429, https://doi.org/10.1002/smll.201402472.
[143] D.V. Kosynkin, A.L. Higginbotham, A. Sinitskii, J.R. Lomeda, A. Dimiev, B. K. Price, J.M. Tour, Longitudinal unzipping of carbon nanotubes to form graphene nanoribbons, Nature 458 (2009) 872–876, https://doi.org/10.1038/nature07872.
[144] L.-C. Yin, J. Liang, G.-M. Zhou, F. Li, R. Saito, H.-M. Cheng, Understanding the interactions between lithium polysulfides and N-doped graphene using density functional theory calculations, Nano Energy 25 (2016) 203–210, https://doi.org/10.1016/j.nanoen.2016.04.053.
[145] L. Yang, S. Jiang, Y. Zhao, L. Zhu, S. Chen, X. Wang, Q. Wu, J. Ma, Y. Ma, Z. Hu, Boron-doped carbon nanotubes as metal-free electrocatalysts for the oxygen reduction reaction, Angew. Chem. Int. Ed. 50 (2011) 7132–7135, https://doi.org/10.1002/anie.201101287.
[146] Y. Xie, Z. Meng, T. Cai, W.-Q. Han, Effect of boron-doping on the graphene aerogel used as cathode for the lithium–sulfur battery, ACS Appl. Mater. Interfaces 7 (2015) 25202–25210, https://doi.org/10.1021/acsami.5b08129.
[147] X. Gu, C. Tong, C. Lai, J. Qiu, X. Huang, W. Yang, B. Wen, L. Liu, Y. Hou, S. Zhang, A porous nitrogen and phosphorous dual doped graphene blocking layer for high performance Li–S batteries, J. Mater. Chem. A. 3 (2015) 16670–16678, https://doi.org/10.1039/C5TA04255K.
[148] X. Ma, G. Ning, C. Qi, C. Xu, J. Gao, Phosphorus and nitrogen dual-doped few-layered porous graphene: a high-performance anode material for lithium-ion batteries, ACS Appl. Mater. Interfaces 6 (2014) 14415–14422, https://doi.org/10.1021/am503692g.
[149] C.-J. Tong, H. Zhang, Y.-N. Zhang, H. Liu, L.-M. Liu, New manifold two-dimensional single-layer structures of zinc-blende compounds, J. Mater. Chem. 2 (2014), 17971, https://doi.org/10.1039/C4TA03944K. –17978.
[150] H.L. Zhuang, A.K. Singh, R.G. Hennig, Computational discovery of single-layer III-V materials, Phys. Rev. B 87 (2013), 165415, https://doi.org/10.1103/PhysRevB.87.165415.
[151] Z. Yang, Z. Yao, G. Li, G. Fang, H. Nie, Z. Liu, X. Zhou, X. Chen, S. Huang, Sulfur-doped graphene as an efficient metal-free cathode catalyst for oxygen reduction, ACS Nano 6 (2012) 205–211, https://doi.org/10.1021/nn203393d.
[152] Q. Zhang, Y. Wang, Z.W. Seh, Z. Fu, R. Zhang, Y. Cui, Understanding the anchoring effect of two-dimensional layered materials for lithium–sulfur batteries, Nano Lett. 15 (2015) 3780–3786, https://doi.org/10.1021/acs.nanolett.5b00367.
[153] J. Tan, D. Li, Y. Liu, P. Zhang, Z. Qu, Y. Yan, H. Hu, H. Cheng, J. Zhang, M. Dong, C. Wang, J. Fan, Z. Li, Z. Guo, M. Liu, A self-supported 3D aerogel network lithium–sulfur battery cathode: sulfur spheres wrapped with phosphorus doped graphene and bridged with carbon nanofibers, J. Mater. Chem. A. 8 (2020) 7980–7990, https://doi.org/10.1039/D0TA00284D.
[154] J. Ren, L. Xia, Y. Zhou, Q. Zheng, J. Liao, D. Lin, A reduced graphene oxide/nitrogen, phosphorus doped porous carbon hybrid framework as sulfur host for high performance lithium-sulfur batteries, Carbon 140 (2018) 30–40, https://doi.org/10.1016/j.carbon.2018.08.026.
[155] X. Pu, G. Yang, C. Yu, Liquid-type cathode enabled by 3D sponge-like carbon nanotubes for high energy density and long cycling life of Li-S batteries, Adv. Mater. 26 (2014) 7456–7461, https://doi.org/10.1002/adma.201403337.
[156] J.L. Gómez-Urbano, J.L. Gómez-Cámer, C. Botas, T. Rojo, D. Carriazo, Graphene oxide-carbon nanotubes aerogels with high sulfur loadings suitable as binder-free cathodes for high performance lithium sulfur batteries, J. Power Sources 412 (2019) 408–415, https://doi.org/10.1016/j.jpowsour.2018.11.077.
[157] Y. Fu, Y.-S. Su, A. Manthiram, Highly reversible lithium/dissolved polysulfide batteries with carbon nanotube electrodes, Angew. Chem. Int. Ed. 52 (2013) 6930–6935, https://doi.org/10.1002/anie.201301250.
[158] N. Baikalov, N. Serik, S. Kalybekkyzy, I. Kurmanbayeva, Z. Bakenov, A. Mentbayeva, High mass-loading sulfur-composite cathode for lithium-sulfur batteries, Front. Energy Res. 8 (2020) 207, https://doi.org/10.3389/fenrg.2020.00207.
[159] X. Li, X. Pu, S. Han, M. Liu, C. Du, C. Jiang, X. Huang, T. Liu, W. Hu, Enhanced performances of Li/polysulfide batteries with 3D reduced graphene oxide/carbon nanotube hybrid aerogel as the polysulfide host, Nano Energy 30 (2016) 193–199, https://doi.org/10.1016/j.nanoen.2016.10.015.
[160] J. He, Y. Chen, W. Lv, K. Wen, C. Xu, W. Zhang, W. Qin, W. He, Three-Dimensional CNT/graphene–Li 2 S aerogel as freestanding cathode for high-performance Li–S batteries, ACS Energy Lett. 1 (2016) 820–826, https://doi.org/10.1021/acsenergylett.6b00272.
[161] H. Tan, J. Tang, J. Henzie, Y. Li, X. Xu, T. Chen, Z. Wang, J. Wang, Y. Ide, Y. Bando, Y. Yamauchi, Assembly of hollow carbon nanospheres on graphene nanosheets and creation of iron–nitrogen-doped porous carbon for oxygen reduction, ACS Nano 12 (2018) 5674–5683, https://doi.org/10.1021/acsnano.8b01502.
[162] J. He, W. Lv, Y. Chen, J. Xiong, K. Wen, C. Xu, W. Zhang, Y. Li, W. Qin, W. He, Direct impregnation of SeS 2 into a MOF-derived 3D nanoporous Co–N–C architecture towards superior rechargeable lithium batteries, J. Mater. Chem. A. 6 (2018) 10466–10473, https://doi.org/10.1039/C8TA02434K.
[163] J. He, L. Luo, Y. Chen, A. Manthiram, Yolk–shelled C@Fe 3 O 4 nanoboxes as efficient sulfur hosts for high-performance lithium–sulfur batteries, Adv. Mater. 29 (2017), 1702707, https://doi.org/10.1002/adma.201702707.
[164] J. He, Y. Chen, W. Lv, K. Wen, C. Xu, W. Zhang, Y. Li, W. Qin, W. He, From metal–organic framework to Li 2 S@C–Co–N nanoporous architecture: a high-capacity cathode for lithium–sulfur batteries, ACS Nano 10 (2016) 10981–10987, https://doi.org/10.1021/acsnano.6b05696.
[165] N. Wang, J. Wang, J. Zhao, J. Wang, J. Pan, J. Huang, Synthesis of porous-carbon@reduced graphene oxide with superior electrochemical behaviors for lithium-sulfur batteries, J. Alloys Compd. 851 (2021), 156832, https://doi.org/10.1016/j.jallcom.2020.156832.
[166] R. Wang, Z. Chen, Y. Sun, C. Chang, C. Ding, R. Wu, Three-dimensional graphene network-supported Co, N-codoped porous carbon nanocages as free-standing polysulfides mediator for lithium-sulfur batteries, Chem. Eng. J. 399 (2020), 125686, https://doi.org/10.1016/j.cej.2020.125686.
[167] H.-J. Peng, Z.-W. Zhang, J.-Q. Huang, G. Zhang, J. Xie, W.-T. Xu, J.-L. Shi, X. Chen, X.-B. Cheng, Q. Zhang, A cooperative interface for highly efficient lithium-sulfur batteries, Adv. Mater. 28 (2016) 9551–9558, https://doi.org/10.1002/adma.201603401.
[168] X. Liang, C.Y. Kwok, F. Lodi-Marzano, Q. Pang, M. Cuisinier, H. Huang, C.J. Hart, D. Houtarde, K. Kaup, H. Sommer, T. Brezesinski, J. Janek, L.F. Nazar, Tuning transition metal oxide-sulfur interactions for long life lithium sulfur batteries: the "Goldilocks" principle, Adv. Energy Mater. 6 (2016), 1501636, https://doi.org/10.1002/aenm.201501636.
[169] H.-J. Peng, J.-Q. Huang, X.-B. Cheng, Q. Zhang, Review on high-loading and high-energy lithium-sulfur batteries, Adv. Energy Mater. 7 (2017), 1700260, https://doi.org/10.1002/aenm.201700260.
[170] J.-Q. Huang, J. Huang, W.G. Chong, J. Cui, S. Yao, B. Huang, J.-K. Kim, Graphene/RuO2 nanocrystal composites as sulfur host for lithium-sulfur batteries, J. Energy Chem. 35 (2019) 204–211, https://doi.org/10.1016/j.jechem.2019.03.017.
[171] X. Wang, G. Li, J. Li, Y. Zhang, A. Wook, A. Yu, Z. Chen, Structural and chemical synergistic encapsulation of polysulfides enables ultralong-life lithium–sulfur batteries, Energy Environ. Sci. 9 (2016) 2533–2538, https://doi.org/10.1039/C6EE00194G.
[172] X. Tao, J. Wang, C. Liu, H. Wang, H. Yao, G. Zheng, Z.W. Seh, Q. Cai, W. Li, G. Zhou, C. Zu, Y. Cui, Balancing surface adsorption and diffusion of lithium-polysulfides on nonconductive oxides for lithium–sulfur battery design, Nat. Commun. 7 (2016), 11203, https://doi.org/10.1038/ncomms11203.
[173] M. Wang, S. Tan, S. Kan, Y. Wu, S. Sang, K. Liu, H. Liu, In-situ assembly of TiO2 with high exposure of (001) facets on three-dimensional porous graphene aerogel for lithium-sulfur battery, J. Energy Chem. 49 (2020) 316–322, https://doi.org/10.1016/j.jechem.2020.03.011.
[174] Y. Chen, S. Choi, D. Su, X. Gao, G. Wang, Self-standing sulfur cathodes enabled by 3D hierarchically porous titanium monoxide-graphene composite film for high-

performance lithium-sulfur batteries, Nano Energy 47 (2018) 331–339, https://doi.org/10.1016/j.nanoen.2018.03.008.
[175] X. Tao, J. Wang, Z. Ying, Q. Cai, G. Zheng, Y. Gan, H. Huang, Y. Xia, C. Liang, W. Zhang, Y. Cui, Strong sulfur binding with conducting magnéli-phase Ti n O 2 n –1 nanomaterials for improving lithium–sulfur batteries, Nano Lett. 14 (2014) 5288–5294, https://doi.org/10.1021/nl502331f.
[176] J. Wang, C. Fu, X. Wang, Y. Yao, M. Sun, L. Wang, T. Liu, Three-dimensional hierarchical porous TiO2/graphene aerogels as promising anchoring materials for lithium−sulfur batteries, Electrochim. Acta 292 (2018) 568–574, https://doi.org/10.1016/j.electacta.2018.09.109.
[177] S. Tan, Z. Yang, H. Yuan, J. Zhang, Y. Yang, H. Liu, MnO2-decorated graphene aerogel with dual-polymer interpenetrating network as an efficient hybrid host for Li-S batteries, J. Alloys Compd. 791 (2019) 483–489, https://doi.org/10.1016/j.jallcom.2019.03.337.
[179] X. Liang, C. Hart, Q. Pang, A. Garsuch, T. Weiss, L.F. Nazar, A highly efficient polysulfide mediator for lithium–sulfur batteries, Nat. Commun. 6 (2015) 5682, https://doi.org/10.1038/ncomms6682.
[180] S. Rehman, T. Tang, Z. Ali, X. Huang, Y. Hou, Integrated design of MnO 2 @carbon hollow nanoboxes to synergistically encapsulate polysulfides for empowering lithium sulfur batteries, Small 13 (2017), 1700087, https://doi.org/10.1002/smll.201700087.
[181] E. Peled, M. Goor, I. Schektman, T. Mukra, Y. Shoval, D. Golodnitsky, The effect of binders on the performance and degradation of the lithium/sulfur battery assembled in the discharged state, J. Electrochem. Soc. 164 (2017), https://doi.org/10.1149/2.0161701jes. A5001–A5007.
[182] G. Ai, Y. Dai, Y. Ye, W. Mao, Z. Wang, H. Zhao, Y. Chen, J. Zhu, Y. Fu, V. Battaglia, J. Guo, V. Srinivasan, G. Liu, Investigation of surface effects through the application of the functional binders in lithium sulfur batteries, Nano Energy 16 (2015) 28–37, https://doi.org/10.1016/j.nanoen.2015.05.036.
[183] Q. Wei, Y. Zhang, Y. Wang, W. Chai, M. Yang, Measurement and modeling of the effect of composition ratios on the properties of poly(vinyl alcohol)/poly(vinyl pyrrolidone) membranes, Mater. Des. 103 (2016) 249–258, https://doi.org/10.1016/j.matdes.2016.04.087.
[184] M. Bercea, S. Morariu, M. Teodorescu, Rheological investigation of poly(vinyl alcohol)/poly(N-vinyl pyrrolidone) mixtures in aqueous solution and hydrogel state, J. Polym. Res. 23 (2016) 142, https://doi.org/10.1007/s10965-016-1040-3.
[185] Y. Yang, Y. Yu, G. Ma, J. Nan, H. Chen, Z. Zhang, W. Lin, High-performance lithium−sulfur batteries fabricated from a three-dimensional porous reduced graphene oxide/La2O3 microboards/sulfur aerogel, Ceram. Int. 45 (2019) 9017–9024, https://doi.org/10.1016/j.ceramint.2019.01.235.
[186] J. Zhang, Y. Shi, Y. Ding, W. Zhang, G. Yu, In situ reactive synthesis of polypyrrole-MnO 2 coaxial nanotubes as sulfur hosts for high-performance lithium–sulfur battery, Nano Lett. 16 (2016) 7276–7281, https://doi.org/10.1021/acs.nanolett.6b03849.
[187] X. Yao, J. Xu, Z. Hong, G. Li, X. Wang, F. Lu, W. Wang, H. Liu, C. Liang, Z. Lin, W. Wang, Metal/graphene composites with strong metal–S bondings for sulfur immobilization in Li–S batteries, J. Phys. Chem. C 122 (2018) 3263–3272, https://doi.org/10.1021/acs.jpcc.7b12063.
[188] Q. Pang, L.F. Nazar, Long-Life and high-areal-capacity Li–S batteries enabled by a light-weight polar host with intrinsic polysulfide adsorption, ACS Nano 10 (2016) 4111–4118, https://doi.org/10.1021/acsnano.5b07347.
[189] S. Wang, J. Liao, X. Yang, J. Liang, Q. Sun, J. Liang, F. Zhao, A. Koo, F. Kong, Y. Yao, X. Gao, M. Wu, S.-Z. Yang, R. Li, X. Sun, Designing a highly efficient polysulfide conversion catalyst with paramontroseite for high-performance and long-life lithium-sulfur batteries, Nano Energy 57 (2019) 230–240, https://doi.org/10.1016/j.nanoen.2018.12.020.
[190] Y. Zhong, D. Chao, S. Deng, J. Zhan, R. Fang, Y. Xia, Y. Wang, X. Wang, X. Xia, J. Tu, Confining sulfur in integrated composite scaffold with highly porous carbon fibers/vanadium nitride arrays for high-performance lithium-sulfur batteries, Adv. Funct. Mater. 28 (2018), 1706391, https://doi.org/10.1002/adfm.201706391.
[191] U. Zubair, S. Bianco, J. Amici, C. Francia, S. Bodoardo, Probing the interaction mechanism of heterostructured VOxNy nanoparticles supported in nitrogen-doped reduced graphene oxide aerogel as an efficient polysulfide electrocatalyst for stable sulfur cathodes, J. Power Sources 461 (2020), 228144, https://doi.org/10.1016/j.jpowsour.2020.228144.
[192] H. Yu, F. Zi, X. Hu, Y. Nie, Y. Chen, H. Cheng, Adsorption of gold from thiosulfate solutions with chemically modified activated carbon, Adsorpt. Sci. Technol. 36 (2018) 408–428, https://doi.org/10.1177/0263617417698864.
[193] Y. Rao, L.-M. Zhang, X. Shang, B. Dong, Y.-R. Liu, S.-S. Lu, J.-Q. Chi, Y.-M. Chai, C.-G. Liu, Vanadium sulfides interwoven nanoflowers based on in-situ sulfurization of vanadium oxides octahedron on nickel foam for efficient hydrogen evolution, Appl. Surf. Sci. 423 (2017) 1090–1096, https://doi.org/10.1016/j.apsusc.2017.06.218.
[194] Y. Zhou, P. Liu, F. Jiang, J. Tian, H. Cui, J. Yang, Vanadium sulfide sub-microspheres: a new near-infrared-driven photocatalyst, J. Colloid Interface Sci. 498 (2017) 442–448, https://doi.org/10.1016/j.jcis.2017.03.081.
[195] J. Xu, T. Lawson, H. Fan, D. Su, G. Wang, Updated metal compounds (MOFs, S, OH, N, C) used as cathode materials for lithium–sulfur batteries, Adv. Energy Mater. 8 (2018), 1702607, https://doi.org/10.1002/aenm.201702607.
[196] Z. Cui, C. Zu, W. Zhou, A. Manthiram, J.B. Goodenough, Mesoporous titanium nitride-enabled highly stable lithium-sulfur batteries, Adv. Mater. 28 (2016) 6926–6931, https://doi.org/10.1002/adma.201601382.
[197] Z. Hao, L. Yuan, C. Chen, J. Xiang, Y. Li, Z. Huang, P. Hu, Y. Huang, TiN as a simple and efficient polysulfide immobilizer for lithium–sulfur batteries, J. Mater. Chem. A. 4 (2016) 17711–17717, https://doi.org/10.1039/C6TA07411A.
[198] Q. Cheng, Z. Yin, Z. Pan, X. Zhong, H. Rao, Lightweight free-standing 3D nitrogen-doped graphene/TiN aerogels with ultrahigh sulfur loading for high energy density Li–S batteries, ACS Appl. Energy Mater. 4 (2021) 7599–7610, https://doi.org/10.1021/acsaem.1c00880.
[199] D.-R. Deng, T.-H. An, Y.-J. Li, Q.-H. Wu, M.-S. Zheng, Q.-F. Dong, Hollow porous titanium nitride tubes as a cathode electrode for extremely stable Li–S batteries, J. Mater. Chem. A. 4 (2016) 16184–16190, https://doi.org/10.1039/C6TA07221F.
[200] Q. Cheng, Z. Pan, H. Rao, X. Zhong, Free-standing 3D nitrogen-doped graphene/Co4N aerogels with ultrahigh sulfur loading for high volumetric energy density Li-S batteries, J. Alloys Compd. 901 (2022), 163625, https://doi.org/10.1016/j.jallcom.2022.163625.
[201] H. Zhang, D. Tian, Z. Zhao, X. Liu, Y.-N. Hou, Y. Tang, J. Liang, Z. Zhang, X. Wang, J. Qiu, Cobalt nitride nanoparticles embedded in porous carbon nanosheet arrays propelling polysulfides conversion for highly stable lithium–sulfur batteries, Energy Storage Mater. 21 (2019) 210–218, https://doi.org/10.1016/j.ensm.2018.12.005.
[202] Y. Yue, N. Liu, Y. Ma, S. Wang, W. Liu, C. Luo, H. Zhang, F. Cheng, J. Rao, X. Hu, J. Su, Y. Gao, Highly self-healable 3D microsupercapacitor with MXene–graphene composite aerogel, ACS Nano 12 (2018) 4224–4232, https://doi.org/10.1021/acsnano.7b07528.
[203] X. Zhang, R. Lv, A. Wang, W. Guo, X. Liu, J. Luo, MXene aerogel scaffolds for high-rate lithium metal anodes, Angew. Chem. Int. Ed. 57 (2018) 15028–15033, https://doi.org/10.1002/anie.201808714.
[204] X. Guo, J. Zhang, J. Song, W. Wu, H. Liu, G. Wang, MXene encapsulated titanium oxide nanospheres for ultra-stable and fast sodium storage, Energy Storage Mater. 14 (2018) 306–313, https://doi.org/10.1016/j.ensm.2018.05.010.
[205] B. Anasori, M.R. Lukatskaya, Y. Gogotsi, 2D metal carbides and nitrides (MXenes) for energy storage, Nat. Rev. Mater. 2 (2017), 16098, https://doi.org/10.1038/natrevmats.2016.98.
[206] J. Song, X. Guo, J. Zhang, Y. Chen, C. Zhang, L. Luo, F. Wang, G. Wang, Rational design of free-standing 3D porous MXene/rGO hybrid aerogels as polysulfide reservoirs for high-energy lithium–sulfur batteries, J. Mater. Chem. A. 7 (2019) 6507–6513, https://doi.org/10.1039/C9TA00212J.
[207] W. Bao, L. Liu, C. Wang, S. Choi, D. Wang, G. Wang, Facile synthesis of crumpled nitrogen-doped MXene nanosheets as a new sulfur host for lithium-sulfur batteries, Adv. Energy Mater. 8 (2018), 1702485, https://doi.org/10.1002/aenm.201702485.
[208] X. Liang, Y. Rangom, C.Y. Kwok, Q. Pang, L.F. Nazar, Interwoven MXene nanosheet/carbon-nanotube composites as Li-S cathode hosts, Adv. Mater. 29 (2017), 1603040, https://doi.org/10.1002/adma.201603040.
[209] Y. Dong, S. Zheng, J. Qin, X. Zhao, H. Shi, X. Wang, J. Chen, Z.-S. Wu, All-MXene-based integrated electrode constructed by Ti 3 C 2 nanoribbon framework host and nanosheet interlayer for high-energy-density Li–S batteries, ACS Nano 12 (2018) 2381–2388, https://doi.org/10.1021/acsnano.7b07672.
[210] H. Tang, W. Li, L. Pan, C.P. Cullen, Y. Liu, A. Pakdel, D. Long, J. Yang, N. McEvoy, G.S. Duesberg, V. Nicolosi, C.J. Zhang, In situ formed protective barrier enabled by Sulfur@Titanium carbide (MXene) ink for achieving high-capacity, long lifetime Li-S batteries, Adv. Sci. 5 (2018), 1800502, https://doi.org/10.1002/advs.201800502.
[211] Y. Liu, M. Zhang, Y. Gao, J. Guo, Regulate the reaction kinetic rate of lithium-sulfur battery by rational designing of TEMPO-oxidized cellulose nanofibers/rGO porous aerogel with monolayer MXene coating, J. Alloys Compd. 898 (2022), 162821, https://doi.org/10.1016/j.jallcom.2021.162821.
[212] Z. Yuan, H.-J. Peng, T.-Z. Hou, J.-Q. Huang, C.-M. Chen, D.-W. Wang, X.-B. Cheng, F. Wei, Q. Zhang, Powering lithium–sulfur battery performance by propelling polysulfide redox at sulfiphilic hosts, Nano Lett. 16 (2016) 519–527, https://doi.org/10.1021/acs.nanolett.5b04166.
[213] Y. Lu, X. Li, J. Liang, L. Hu, Y. Zhu, Y. Qian, A simple melting-diffusing-reacting strategy to fabricate S/NiS 2 –C for lithium–sulfur batteries, Nanoscale 8 (2016) 17616–17622, https://doi.org/10.1039/C6NR05626A.
[214] Z. Liu, X. Zheng, S. Luo, S. Xu, N. Yuan, J. Ding, High performance Li–S battery based on amorphous NiS 2 as the host material for the S cathode, J. Mater. Chem. A. 4 (2016) 13395–13399, https://doi.org/10.1039/C6TA05635K.
[215] Z. Li, S. Zhang, J. Zhang, M. Xu, R. Tatara, K. Dokko, M. Watanabe, Three-Dimensionally hierarchical Ni/Ni 3 S 2/S cathode for lithium–sulfur battery, ACS Appl. Mater. Interfaces 9 (2017) 38477–38485, https://doi.org/10.1021/acsami.7b11065.
[216] Z. Li, R. Xu, S. Deng, X. Su, W. Wu, S. Liu, M. Wu, MnS decorated N/S codoped 3D graphene which used as cathode of the lithium-sulfur battery, Appl. Surf. Sci. 433 (2018) 10–15, https://doi.org/10.1016/j.apsusc.2017.10.050.
[217] C.-M. Chen, Q. Zhang, M.-G. Yang, C.-H. Huang, Y.-G. Yang, M.-Z. Wang, Structural evolution during annealing of thermally reduced graphene nanosheets for application in supercapacitors, Carbon 50 (2012) 3572–3584, https://doi.org/10.1016/j.carbon.2012.03.029.
[218] X. Chen, H.-J. Peng, R. Zhang, T.-Z. Hou, J.-Q. Huang, B. Li, Q. Zhang, An analogous periodic law for strong anchoring of polysulfides on polar hosts in lithium sulfur batteries: S- or Li-binding on first-row transition-metal sulfides? ACS Energy Lett. 2 (2017) 795–801, https://doi.org/10.1021/acsenergylett.7b00164.
[219] X. Li, Z. Pan, Z. Li, X. Wang, B. Saravanakumar, Y. Zhong, L. Xing, M. Xu, C. Guo, W. Li, Coral-like reduced graphene oxide/tungsten sulfide hybrid as a cathode

host of high performance lithium-sulfur battery, J. Power Sources 420 (2019) 22–28, https://doi.org/10.1016/j.jpowsour.2019.02.089.
[220] L. Tan, X. Li, Z. Wang, H. Guo, J. Wang, Lightweight reduced graphene oxide@MoS 2 interlayer as polysulfide barrier for high-performance lithium–sulfur batteries, ACS Appl. Mater. Interfaces 10 (2018) 3707–3713, https://doi.org/10.1021/acsami.7b18645.
[221] Y. Wei, Z. Kong, Y. Pan, Y. Cao, D. Long, J. Wang, W. Qiao, L. Ling, Sulfur film sandwiched between few-layered MoS 2 electrocatalysts and conductive reduced graphene oxide as a robust cathode for advanced lithium–sulfur batteries, J. Mater. Chem. A. 6 (2018) 5899–5909, https://doi.org/10.1039/C8TA00222C.
[222] F. Pei, L. Lin, D. Ou, Z. Zheng, S. Mo, X. Fang, N. Zheng, Self-supporting sulfur cathodes enabled by two-dimensional carbon yolk-shell nanosheets for high-energy-density lithium-sulfur batteries, Nat. Commun. 8 (2017) 482, https://doi.org/10.1038/s41467-017-00575-8.
[223] School of material and chemical engineering, henan provincial key laboratory of surface interface science, zhengzhou university of light Industry, zhengzhou 450001, PR China, H. Fang, nanostructured manganese oxide films for high performance supercapacitors, Int. J. Electrochem. Sci. (2018) 8736–8744, https://doi.org/10.20964/2018.09.21.
[224] Y. Hou, Y. Ren, S. Zhang, K. Wang, F. Yu, T. Zhu, 3D S@MoS2@reduced graphene oxide aerogels cathode for high-rate lithium-sulfur batteries, J. Alloys Compd. 852 (2021), 157011, https://doi.org/10.1016/j.jallcom.2020.157011.
[225] Y. Li, J. Li, J. Yuan, Y. Zhao, J. Zhang, H. Liu, F. Wang, J. Tang, J. Song, 3D CoS2/rGO aerogel as trapping-catalyst sulfur host to promote polysulfide conversion for stable Li-S batteries, J. Alloys Compd. 873 (2021), 159780, https://doi.org/10.1016/j.jallcom.2021.159780.
[226] A. Sarkar, A.K. Chakraborty, S. Bera, S. Krishnamurthy, Novel hydrothermal synthesis of CoS 2/MWCNT nanohybrid electrode for supercapacitor: a systematic investigation on the influence of MWCNT, J. Phys. Chem. C 122 (2018) 18237–18246, https://doi.org/10.1021/acs.jpcc.8b04137.
[227] J. Shen, X. Xu, J. Liu, Z. Liu, F. Li, R. Hu, J. Liu, X. Hou, Y. Feng, Y. Yu, M. Zhu, Mechanistic understanding of metal phosphide host for sulfur cathode in high-energy-density lithium–sulfur batteries, ACS Nano 13 (2019) 8986–8996, https://doi.org/10.1021/acsnano.9b02903.
[228] S. Huang, Y.V. Lim, X. Zhang, Y. Wang, Y. Zheng, D. Kong, M. Ding, S.A. Yang, H. Y. Yang, Regulating the polysulfide redox conversion by iron phosphide nanocrystals for high-rate and ultrastable lithium-sulfur battery, Nano Energy 51 (2018) 340–348, https://doi.org/10.1016/j.nanoen.2018.06.052.
[229] Y. Chen, S. Liu, X. Yuan, X. Hu, W. Ye, A. Abdul Razzaq, Y. Lian, M. Chen, X. Zhao, Y. Peng, J.-H. Choi, J.-H. Ahn, Z. Deng, rGO-CNT aerogel embedding iron phosphide nanocubes for high-performance Li-polysulfide batteries, Carbon 167 (2020) 446–454, https://doi.org/10.1016/j.carbon.2020.05.066.
[230] Y. Zhong, L. Yin, P. He, W. Liu, Z. Wu, H. Wang, Surface chemistry in cobalt phosphide-stabilized lithium–sulfur batteries, J. Am. Chem. Soc. 140 (2018) 1455–1459, https://doi.org/10.1021/jacs.7b11434.
[231] Y. Zhang, R. Wang, W. Tang, L. Zhan, S. Zhao, Q. Kang, Y. Wang, S. Yang, Efficient polysulfide barrier of a graphene aerogel–carbon nanofibers–Ni network for high-energy-density lithium–sulfur batteries with ultrahigh sulfur content, J. Mater. Chem. A. 6 (2018) 20926–20938, https://doi.org/10.1039/C8TA08048H.
[232] P. Arora, Z.(John, Zhang, Battery separators, Chem. Rev. 104 (2004) 4419–4462, https://doi.org/10.1021/cr020738u.
[233] C. Li, R. Liu, Y. Xiao, F. Cao, H. Zhang, Recent progress of separators in lithium-sulfur batteries, Energy Storage Mater. 40 (2021) 439–460, https://doi.org/10.1016/j.ensm.2021.05.034.
[234] S.-H. Chung, A. Manthiram, Bifunctional separator with a light-weight carbon-coating for dynamically and statically stable lithium-sulfur batteries, Adv. Funct. Mater. 24 (2014) 5299–5306, https://doi.org/10.1002/adfm.201400845.
[235] J.-Q. Huang, Q. Zhang, F. Wei, Multi-functional separator/interlayer system for high-stable lithium-sulfur batteries: progress and prospects, Energy Storage Mater. 1 (2015) 127–145, https://doi.org/10.1016/j.ensm.2015.09.008.
[236] J. Park, B.-C. Yu, J.S. Park, J.W. Choi, C. Kim, Y.-E. Sung, J.B. Goodenough, Tungsten disulfide catalysts supported on a carbon cloth interlayer for high performance Li-S battery, Adv. Energy Mater. 7 (2017), 1602567, https://doi.org/10.1002/aenm.201602567.
[237] W. Hua, Z. Yang, H. Nie, Z. Li, J. Yang, Z. Guo, C. Ruan, X. Chen, S. Huang, Polysulfide-scission reagents for the suppression of the shuttle effect in lithium–sulfur batteries, ACS Nano 11 (2017) 2209–2218, https://doi.org/10.1021/acsnano.6b08627.
[238] S. Tan, Y. Wu, S. Kan, M. Bu, Y. Liu, L. Yang, Y. Yang, H. Liu, A combination of MnO2-decorated graphene aerogel modified separator and I/N codoped graphene aerogel sulfur host to synergistically promote Li–S battery performance, Electrochim. Acta 348 (2020), 136173, https://doi.org/10.1016/j.electacta.2020.136173.
[239] Y.C. Jeong, J.H. Kim, S. Nam, C.R. Park, S.J. Yang, Rational design of nanostructured functional interlayer/separator for advanced Li-S batteries, Adv. Funct. Mater. 28 (2018), 1707411, https://doi.org/10.1002/adfm.201707411.
[240] J.-Q. Huang, Q. Zhang, H.-J. Peng, X.-Y. Liu, W.-Z. Qian, F. Wei, Ionic shield for polysulfides towards highly-stable lithium–sulfur batteries, Energy Environ. Sci. 7 (2014) 347–353, https://doi.org/10.1039/C3EE42223B.
[241] H. Yao, K. Yan, W. Li, G. Zheng, D. Kong, Z.W. Seh, V.K. Narasimhan, Z. Liang, Y. Cui, Improved lithium–sulfur batteries with a conductive coating on the separator to prevent the accumulation of inactive S-related species at the cathode–separator interface, Energy Environ. Sci. 7 (2014) 3381–3390, https://doi.org/10.1039/C4EE01377H.
[242] S.-H. Chung, A. Manthiram, High-performance Li–S batteries with an ultra-lightweight MWCNT-coated separator, J. Phys. Chem. Lett. 5 (2014) 1978–1983, https://doi.org/10.1021/jz5006913.
[243] J.-Q. Huang, T.-Z. Zhuang, Q. Zhang, H.-J. Peng, C.-M. Chen, F. Wei, Permselective graphene oxide membrane for highly stable and anti-self-discharge lithium–sulfur batteries, ACS Nano 9 (2015) 3002–3011, https://doi.org/10.1021/nn507178a.
[244] Z. Xiao, Z. Yang, L. Wang, H. Nie, M. Zhong, Q. Lai, X. Xu, L. Zhang, S. Huang, A lightweight TiO 2/graphene interlayer, applied as a highly effective polysulfide absorbent for fast, long-life lithium-sulfur batteries, Adv. Mater. 27 (2015) 2891–2898, https://doi.org/10.1002/adma.201405637.
[245] X. Liang, C. Hart, Q. Pang, A. Garsuch, T. Weiss, L.F. Nazar, A highly efficient polysulfide mediator for lithium–sulfur batteries, Nat. Commun. 6 (2015) 5682, https://doi.org/10.1038/ncomms6682.
[246] J. Wutthiprom, N. Phattharasupakun, M. Sawangphruk, Designing an interlayer of reduced graphene oxide aerogel and nitrogen-rich graphitic carbon nitride by a layer-by-layer coating for high-performance lithium sulfur batteries, Carbon 139 (2018) 945–953, https://doi.org/10.1016/j.carbon.2018.08.008.
[247] Z.A. Ghazi, X. He, A.M. Khattak, N.A. Khan, B. Liang, A. Iqbal, J. Wang, H. Sin, L. Li, Z. Tang, MoS 2/celgard separator as efficient polysulfide barrier for long-life lithium-sulfur batteries, Adv. Mater. 29 (2017), 1606817, https://doi.org/10.1002/adma.201606817.
[248] G. Babu, N. Masurkar, H. Al Salem, L.M.R. Arava, Transition metal dichalcogenide atomic layers for lithium polysulfides electrocatalysis, J. Am. Chem. Soc. 139 (2017) 171–178, https://doi.org/10.1021/jacs.6b08681.
[249] H. Shi, X. Zhao, Z.-S. Wu, Y. Dong, P. Lu, J. Chen, W. Ren, H.-M. Cheng, X. Bao, Free-standing integrated cathode derived from 3D graphene/carbon nanotube aerogels serving as binder-free sulfur host and interlayer for ultrahigh volumetric-energy-density lithium sulfur batteries, Nano Energy 60 (2019) 743–751, https://doi.org/10.1016/j.nanoen.2019.04.006.